Stable carbon isotopic studies of microbial lipids from distinct geochemical marine environments

Dissertation zur Erlangung des Doktorgrades der
Naturwissenschaften
Dr. rer. nat.

Am Fachbereich Geowissenschaften
der Universität Bremen

vorgelegt von
Qing-Zeng Zhu

Bremen
Dezember 2019

Die vorliegende Arbeit wurde in der Zeit von November 2015 bis Dezember 2019 in der Arbeitsgruppe Organische Geochemie am MARUM - Zentrum für Marine Umweltwissenschaften und dem Fachbereich Geowissenschaften der Universität Bremen angefertigt.

1. Gutachter: Prof. Dr. Kai-Uwe Hinrichs

2. Gutachter: Prof. Dr. Volker Thiel

Tag des Promotionskolloquiums: 27. Januar 2019

Versicherung an Eides Statt / Affirmation in lieu of an oath

gem. § 5 Abs. 5 der Promotionsordnung vom 18.06.2018 /
according to § 5 (5) of the Doctoral Degree Rules and Regulations of 18 June, 2018

Ich / I,

Vorname / First Name: Zhu

Name / Name: Qing-Zeng

Anschrift / Address: Room 1223, Luisental 29, 28359, Bremen

Matr.-Nr / student ID no. : 3060586

versichere an Eides Statt durch meine Unterschrift, dass ich die vorliegende Dissertation selbständig und ohne fremde Hilfe angefertigt und alle Stellen, die ich wörtlich dem Sinne nach aus Veröffentlichungen entnommen habe, als solche kenntlich gemacht habe, mich auch keiner anderen als der angegebenen Literatur oder sonstiger Hilfsmittel bedient habe und die zu Prüfungszwecken beigelegte elektronische Version (PDF) der Dissertation mit der abgegebenen gedruckten Version identisch ist. / With my signature I affirm in lieu of an oath that I prepared the submitted dissertation independently and without illicit assistance from third parties, that I appropriately referenced any text or content from other sources, that I used only literature and resources listed in the dissertation, and that the electronic (PDF) and printed versions of the dissertation are identical.

Ich versichere an Eides Statt, dass ich die vorgenannten Angaben nach bestem Wissen und Gewissen gemacht habe und dass die Angaben der Wahrheit entsprechen und ich nichts verschwiegen habe. / I affirm in lieu of an oath that the information provided herein to the best of my knowledge is true and complete.

Die Strafbarkeit einer falschen eidesstattlichen Versicherung ist mir bekannt, namentlich die Strafandrohung gemäß § 156 StGB bis zu drei Jahren Freiheitsstrafe oder Geldstrafe bei vorsätzlicher Begehung der Tat bzw. gemäß § 161 Abs. 1 StGB bis zu einem Jahr Freiheitsstrafe oder Geldstrafe bei fahrlässiger Begehung. / I am aware that a false affidavit is a criminal offence which is punishable by law in accordance with § 156 of the German Criminal Code (StGB) with up to three years imprisonment or a fine in case of intention, or in accordance with § 161 (1) of the German Criminal Code with up to one year imprisonment or a fine in case of negligence.

_____ _____

Ort / Place, Datum / Date Unterschrift / Signature

Contents

Abstract

Microorganisms participate extensively in shaping the marine biosphere and driving biogeochemical cycles of carbon and other elements. The investigation of microbial membrane lipids provides a culture-independent approach to study microbial adaptions to environmental stressors such as high pressure and energy limitation. In addition, sedimentary microbial lipids are widely used as sensitive indicators of environmental conditions in paleoenvironmental and biogeochemical studies. Nonetheless, systematic isotopic investigations of microbial lipids to constrain their sources, modes of production, and turnover remain fragmentary. In order to decipher the information encoded in sedimentary archaeal and bacterial lipids in different marine depositional environments, I conducted carbon isotopic analysis of marine environmental samples (Chapter III and IV) and laboratory-based stable isotope probing (SIP) experiments (Chapter V).

Chapter III provides fundamental constraints on archaeal activity, sources of archaeal lipids, and preservation signatures in diverse marine sediments. This is, to my knowledge, the first systematic comparison of stable carbon isotopic compositions of archaeal core lipids (CLs) and intact polar lipids (IPLs). Results from lipid analysis are interpreted in the context of geochemical data in contrasting depositional regimes, including a transect from the Rhone River delta into the western Mediterranean Sea, the anoxic Black Sea, Marmara Sea, and sapropel layers in the Eastern Mediterranean Sea. Mass balance calculation along the transect of the Western Mediterranean Sea proved that terrestrial input of archaea into marine sediments can be substantial (up to 42%) and suggests caution when reconstructing such inputs based on existing molecular proxies, such as BIT (Branched isoprenoid tetraether index). Similar $\delta^{13}C$ values of core and intact polar crenarchaeol strongly suggest that the alkyl moieties are not synthesized *de novo*, thus indicating that intact polar crenarchaeol is either a fossil relic from planktonic archaea or a product of lipid recycling by benthic archaea. By contrast, an average offset in $\delta^{13}C$ values of 2.6‰ between core and intact polar caldarchaeol indicates active in-situ activity of benthic archaea. No matter whether present as IPL or CL, the relatively strong ^{13}C-depletion of archaeol relative to both total organic carbon and dissolved inorganic carbon is consistent with mixtures of functional sources of sedimentary chemolithoautotrophic, methanotrophic and heterotrophic archaea.

To further constrain the sources and turnover of sedimentary archaeal lipids, we compared the stable carbon isotopic compositions of archaeal IPLs and CLs through the oxic, suboxic and anoxic water column and in high resolution within an 8-m deep sediment core in the Black Sea **(Chapter IV)**. The comparison between the water column and surface samples suggests that archaea residing in the lower suboxic zone are the main source of lipids found in surface sediments, including a large fraction of IPLs. The isotopic offset between core and intact caldarchaeol indicates sedimentary in-situ production by benthic archaea. Based on a two endmember mixing model, an average of 34% sedimentary intact polar caldarchaeol is likely produced by benthic archaea. In addition, the negative deviation of core caldarchaeol $\delta^{13}C$ values with depth is consistent with the addition of hydrolytic products from the ^{13}C-depleted IPL pool. Two independent isotope mass balance calculations suggested that on average 35% and 18% of CL-caldarchaeol are derived from IPL degradation in sediment.

In addition to the analysis of environmental samples, laboratory-based SIP provides us another distinct perspective to understand the microbial-mediated processes in marine sediments, for example, anaerobic oxidation of methane (AOM). AOM is performed by consortia of anaerobic methanotrophic archaea (ANME) and sulfate-reducing bacteria (SRB). Their enrichment cultures have been increasingly purified but still contain additional community members, even after years of repeated dilution and inoculation. In order to investigate the potential heterotrophic activity of the microorganisms coexisting with AOM consortia, I performed an L-leucine-3-^{13}C (^{13}C-leu) labeling study on a mesophilic AOM enrichment culture **(Chapter V)**. Our results showed that most ^{13}C-Leu incorporation was observed in bacterial fatty acids, especially iso and anteiso-branched $C_{15:0}$ and $C_{17:0}$, but very limited in archaeal ether lipids. Interestingly, these incorporation patterns were independent of the addition of methane to the enrichments, suggesting the ancillary heterotopic bacteria (e.g. Anaerolineae and Spirochaetes) are the main producers of these ^{13}C-labeled lipids rather than AOM consortia. These ancillary heterotopic bacteria probably thrive on the amino acids derived from AOM necromass and likely explain the common absence of AOM lipid signals in sedimentary records.

This thesis highlights the presence of various archaeal lipid inputs from terrestrial, planktonic and sedimentary sources into marine sediments. New lipids are continuously produced and degraded by microorganisms in the active subseafloor biosphere. The incubation experiment suggests that heterotrophic bacteria may play a pivotal role in necromass turnover in marine sediments.

Zusammenfassung

Mikroorganismen sind maßgeblich an der Gestaltung der marinen Biosphäre beteiligt und sind die treibende Kraft hinter dem biogeochemischen Kreislauf von Kohlenstoff und weiteren essentiellen Elementen. Die Untersuchung mikrobieller Membranlipide ermöglicht einen kulturunabhängigen Ansatz zur Analyse mikrobieller Anpassungen an Umweltfaktoren wie Druck und Energielimitierung. Darüber hinaus ist die Verwendung von in Sedimenten überlieferten mikrobiellen Lipidbiomarkern als empfindliche Indikatoren sowohl gegenwärtiger als auch vergangener Umweltbedingungen in biogeochemischen und paläoökologischen Studien weit verbreitet. Systematische Isotopenstudien zu ihren Quellen, zu Synthese und Umsatz sind jedoch weiterhin lückenhaft. Um die in sedimentären Lipiden von Archaeen und Bakterien gespeicherten Informationen aufzuschlüsseln, wurden in der vorliegenden Dissertation Analysen zur Kohlenstoffisotopie von marinen Umweltproben (Kapitel III und IV) und laborbasierte Inkubationsexperimente mit stabilen Isotopenmarkern (‚Stable Isotope Probing' (SIP), Kapitel V) durchgeführt.

Kapitel III beinhaltet grundlegende Ausführungen zur Aktivität von Archaeen, sowie den Quellen ihrer Etherlipide und deren Erhaltungspotential in verschiedenen marinen Sedimenten. Nach jetzigem Kenntnisstand ist dies der erste systematische Vergleich der stabilen Kohlenstoffisotopie von Kernlipiden (CL) und intakten polaren Lipiden (IPL). Die Ergebnisse der Lipidanalysen werden im Kontext geochemischer Daten von kontrastierenden Ablagerungsräumen, einschließlich eines Transekts vom Rhône-Delta in das westliche Mittelmeer, des anoxischen Schwarzen Meeres, des Marmarameeres und der Sapropelschichten im östlichen Mittelmeer, interpretiert. Die Berechnung einer Massenbilanz von Etherlipiden entlang des westlichen Mittelmeeres hat gezeigt, dass der terrestrische Eintrag von Archaeen in marine Sedimente erheblich sein kann (bis zu 42%), und deutet an, dass bei der Rekonstruktion solcher Einträge auf Grundlage vorhandener molekularer Proxys wie BIT (Branched Isoprenoid Tetraether Index) Vorsicht geboten ist. Ähnliche $\delta^{13}C$-Werte bei den CLs und IPLs von Crenarchaeol deuten stark darauf hin, dass deren Alkylreste nicht de novo synthetisiert werden, woraus sich schließen lässt, dass das intakte Crenarchaeol entweder ein fossiles Relikt von planktonischen Archaeen oder ein Produkt des Lipidrecyclings durch benthische Archaeen ist. Im Gegensatz dazu zeigt eine durchschnittliche Abweichung von 2.6‰ zwischen den $\delta^{13}C$-Werten von CL und IPL des Caldarchaeols eine in situ-Aktivität

benthischer Archaeen an. Unabhängig davon ob es als IPL oder CL vorliegt, deutet die relativ starke ^{13}C-Abreicherung von Archaeol im Verhältnis sowohl zum gesamten organischen Kohlenstoffpool als auch zum gelösten anorganischen Kohlenstoff, auf eine Herkunft aus verschiedenen benthischen Quellen bestehend aus chemolithoautotrophen, methanotrophen und heterotrophen Archaeengemeinschaften hin.

Zur weiteren Eingrenzung der Quellen und des Umsatzes sedimentärer Archaeenlipide verglichen wir die stabile Isotopenzusammensetzung des Kohlenstoffs von archaeellen IPLs und Cls entlang der oxischen, suboxischen und anoxischen Wassersäule, sowie in einem räumlich und zeitlich hochauflösenden 8 m langen Sedimentkern aus dem Schwarzen Meer (Kapitel IV). Der Vergleich zwischen den Proben aus der Wassersäule und den Oberflächensedimenten legt nahe, dass Archaeengemeinschaften aus der unteren suboxischen Zone die Hauptquelle für den Eintrag von Etherlipiden, einschließlich eines Großteils der IPLs, in die oberflächennahen Sedimente sind. Die Abweichungen in der Kohlenstoffisotopie zwischen Kern- und intaktem Caldarchaeol deuten auf eine sedimentäre In-situ-Produktion durch benthische Archaeen hin. Basierend auf einem Mischungsmodell mit zwei Endgliedern ist anzunehmen, dass im Durchschnitt 34% des intakten polaren Caldarchaeols im Sediment von benthischen Archaeen produziert wird. Außerdem ist eine mit der Tiefe zunehmende negative Abweichung in den δ^{13}C-Werten der Caldarchaeol-Kernlipide konsistent mit einer Beimischung von hydrolytischen Abbauprodukten aus dem an ^{13}C verarmten IPL-Pool. Zwei unabhängige Berechnungen der Isotopenmassenbilanz ergaben, dass durchschnittlich 35% und 18% des CL-Caldarchaeols aus dem IPL-Abbau im Sediment stammen.

Neben der Analyse von Umweltproben bietet uns die laborbasierte stabile Isotopenbeprobung (SIP) eine weitere Perspektive, um mikrobiell gesteuerte Prozesse in marinen Sedimenten, beispielsweise die anaerobe Oxidation von Methan (AOM), besser zu verstehen. Die AOM ist ein Stoffwechselprozess, der von einem Konsortium aus anaeroben methanotrophen Archaeen (ANME) und sulfatreduzierenden Bakterien (SRB) durchgeführt wird. Obwohl zunehmend reine Anreicherungskulturen dieser mikrobiellen Gemeinschaften gewonnen werden konnten, enthalten aber auch diese noch nach Jahren wiederholter Verdünnung und Inokulation zusätzliche funktionelle Gruppen von Mikroorganismen. Um potenziell heterotrophe Aktivitäten dieser mit AOM-Konsortien koexistierenden Mikroorganismen zu untersuchen,

führte ich eine Markierungsstudie an einer mesophilen AOM-Anreicherungskultur mit L-leucin-3-^{13}C (^{13}C-leu) als zugegebenes Substrat durch (Kapitel V). Unsere Ergebnisse zeigten, dass ein hoher Einbau von ^{13}C-Leu in bakterielle Fettsäuren, insbesondere iso- und anteiso-verzweigte $C_{15:0}$ und $C_{17:0}$ Fettsäuren, zu beobachten war, wohingegen nur sehr geringe Mengen dieses Substrates in die Etherlipide von Archaeen inkorporiert wurden. Interessanterweise erfolgte der Einbau des markierten Substrates unabhängig von einer Zugabe von Methan zu den Anreicherungskulturen, was darauf hindeutet, dass nicht die AOM-Konsortien sondern weitere heterotrophe Bakterien (z. B. Anaerolineae und Spirochaetes) die Hauptproduzenten dieser ^{13}C-markierten Lipide darstellen. Diese heterotrophen Bakteriengemeinschaften verstoffwechseln demnach wahrscheinlich Aminosäuren die durch den Abbau der AOM-Nekromasse freigesetzt werden und erklären möglicherweise das häufige Fehlen von AOM-typischen Lipidsignalen in Aufzeichnungen sedimentärer Ablagerungen.

Diese Arbeit zeigt anhand der Untersuchung stabiler Kohlenstoffisotope den Einfluss unterschiedlicher Einträge aus terrestrischen, planktonischen und sedimentären Quellen auf die Verteilung archaeeller Etherlipide in marinen Sedimenten auf. In der aktiven Biosphäre unterhalb des Meeresbodens finden kontinuierlich die Biosynthese und der Abbau von Lipiden durch Mikroorganismen statt. Die Ergebnisse des Inkubationsexperimentes legen die Vermutung nahe, dass heterotrophe Bakterien eine zentrale Rolle beim Umsatz von Biomasse in marinen Sedimenten spielen könnten.

Acknowledgments

Just like a butterfly, Ph.D. is an adventure of metamorphosis which breaks free from the frame and builds a bridge for the future. Standing at the last stop of the adventure and looking back, I sincerely thank everyone who helped me, pushed me, and encouraged me. Kai, thank you for your supervision. You opened the door of organic chemistry to explore the unknown deep biosphere. Most importantly, you give me complete freedom and support to pursue my interest topic and at the same time keep guiding me and inspiring me with your talent and experience. A special thanks to you, Marcus, what I appreciated is not only your help in science but more on encouraging me to be a communicator to connect China and the world, to break people's stereotypes. I also would like to thank Martin Könneke and Gunter Wegener who agreed to join my thesis committee and at the same time guided me on microbiological experiments. All of my lab work would not have been possible without the assistance of Xavier, Jenny, Heidi, and Julius. Thanks, Evert for solving all the IT problems as well as teaching me German. Travis, Kevin, and Verena thank you for your contribution to my projects and manuscripts as coauthors. Thanks to my Hiwis: Kasha and Johannes, with your help I can finish the job on time. I would also like to address my gratitude to my friends and colleagues who shared experiences and thoughts. They are Weichao, Igor, Sahra, Lukas, Shuchai, Min, Stani, Niro, Susanne, Bernhard, Florence, Sandra, and Rebecca. The working atmosphere has been excellent and enjoyable in AG. Hinrichs. I also enjoyed very much and benefited a lot from the collaboration with scientists from other groups or institutes, Xiuran, David. I would not be able to carry out my research without the generous financial supports from the CSC. GLOMAR is acknowledged for providing travel grants and organizing interesting courses. I also would like to thank my previous master supervisor for their encouragement. They are Prof. Qing Sun and Prof. Guoqiang Chu. Special thanks go to my Chinese friends in Bremen who always entertained me: Cenling, Dongchen, Chuanxu, Yumeng, Yanyan, and Lewen. In the end, I would like to thank Charlotte, who supports me all the time when I was writing this thesis. My tremendous respect and appreciation are for my Dad (Guang-Li Zhu) and Sister (Qing-Yan Zhu) who are always there for me.

List of abbreviations

1G	Monoglycosidic
2G	Diglycosidic
3G	Triglycosidic
AOA	Ammonia oxidizing archaea
Anammox	anaerobic oxidation of ammonium
ANME	Anaerobic methane-oxidizing archaea
AOM	Anaerobic oxidation of methane
BDGT	Butanetriol dibiphytanyl glycerol tetraether
Br-GDGT	Branched glycerol dibiphytanyl glycerol tetraether
CIE	Carbon isotope excursions
CLs	Core lipids
cmbsf	centimeter below the seafloor
Cren	Crenarchaeol
DCM	Dichloromethane
DIC	Dissolved inorganic carbon
DOM	Dissolved organic matter
ESI-MS	Electrospray ionization mass spectrometry
Eq	Equation
FID	Flame ionization detector
GC	Gas chromatography
GDGT 0-4	Glycerol dibiphytanyl glycerol tetraether with 0 to 4 pentacyclic rings
GlcDGD	glucosyl diphytanylglyceroldiether
GTGT	Glycerol trialkyl glycerol tetraether
HCl	Hydrochloric acid
HPH	Hexose-phosphohexose
HPLC	High performance liquid chromatography
IPL	Intact polar lipid
ky	thousand years
Mbsl	Meter below the sea level

MCG	Miscellaneous crenarchaeotal group
MeOH	Methanol
My	million years
MZ	Methanogenic zone
NP	Normal phase
OH-group	Hydroxyl-group
OH-AR	Hydroxyarchaeol
OH-GDGT	Hydroxylated glycerol dibiphytanyl glycerol tetraether
PC	Phosphatidylcholine
PDGT	Pentantriol dibiphytanyl glycerol tetraether
PDME	Phosphatidyldimethylethanolamine
PE	Phosphatidylethanolamine
PG	Phosphatidylglycerol
PH	Phosphohexose
PI	Phosphatidylinositol
(r)RNA	(ribosomal) Ribonucleic acid
RP	Reverse phase
SIP	Stable isotope probing
SMTZ	Sulfate methane transition zone
SPM	Suspended particulate matter
SRB	Sulfate reducing Bacteria
SRZ	Sulfate reduction zone
SST	Sea surface temperature
TEX_{86}	Tetraether index of tetraethers consisting of 86 carbon atoms
TLE	Total lipid extract
Uns	Unsaturated
yr	Year

Chapter I

Introduction

I.1 Microbial life in the ocean and underlying sediments

I.1.1 Microorganisms in marine environments

Life on Earth is divided into three domains including Eukarya, Bacteria, and Archaea, with the latter two belonging to unicellular prokaryotic groups (Woese and Fox, 1977; Woese et al., 1990). These microorganisms participate extensively in driving elemental cycles and shaping the marine biosphere (Falkowski et al., 1998; Galloway et al., 2004; Azam and Malfatti, 2007). With new techniques being increasingly developed, a far more complex microbial community in the ocean and subseafloor unveils itself even though high proportions of them remain uncultured (Steen et al., 2019). Bacteria were first observed several centuries ago and since then have been systematically studied. They exhibit an extremely wide variety of metabolic types in marine environments. Some species of cyanobacteria, green sulfur bacteria, and purple bacteria derive energy from light using photosynthesis (Campbell et al., 1998; Bryant and Frigaard, 2006). They are important contributors to primary production. Many bacteria grow as heterotrophs such as Spirochaetes and Chloroflexi bacterium (Nunoura et al., 2013; Kümmel et al., 2015). Some bacteria are involved in nitrification such as ammonium oxidizing bacteria (AOB) and nitrite oxidizing bacteria (Schmid et al., 2007; Pachiadaki et al., 2017). Sulfate reducing bacteria are largely involved in the organic mineralization in sediments (Oremland and Taylor, 1978). Compared to bacteria, archaea remain much less investigated. With the advances of technologies in molecular phylogenetics, the classification of archaea is becoming a rapidly evolving field (Hug et al., 2016; Spang et al., 2017). Culture-independent genomics (16S rRNA, genome sequences, etc.) has revealed the vast diversity existing among archaea, including superphylum Euryarchaeota, TACK (Thaumarchaeota, Aigarchaeota, Crenarchaeota, and Korarchaeota), Asgard (Lokiarchaeota, Thorarchaeota, Odinarchaeota, and Heimdallarchaeota), and DPANN (Diapherotrites, Parvarchaeota, Aenigmarchaeota, Nanoarchaeota, and Nanohaloarchaeota). Recent studies revealed additional phyla to the TACK superphylum, such as Bathyarchaeota. Bathyarchaeota (formerly known as the Miscellaneous Crenarchaeotal Group, MCG) is extraordinarily widespread in anoxic sediments and host a relatively high abundance of archaeal communities (Zhou et al., 2018). Asgard archaea are placed as the closest prokaryotic relatives of eukaryotes phylogenetically (Spang

et al., 2015; Eme et al., 2017). All the new discoveries and findings clearly remind people that microorganisms in marine environments are far more diverse and complex than expected before.

I.1.2 Microbial-driven biogeochemical cycles

Carbon and nutrient cycling are regulated by microbial life in different geochemical zones of ocean and subseafloor. The **epipelagic zone** is located in the uppermost layer of the ocean which is exposed to intense sunlight. Almost 50% of the global primary production occurs in the ocean, particularly in the epipelagic zone (Falkowski et al., 1998). The photosynthetic activity (by cyanobacteria and eukaryotic algae) produces most of the organic carbon in the ocean (Platt et al., 1983; Kolber et al., 2000). However, the majority of organic matter produced in the marine photic zone is remineralized to CO_2 by heterotrophic bacteria and archaea (Orsi et al., 2016). For example, Marine Group II resides mainly in the marine photic zone and genome analysis showed that they are motile photoheterotrophs (Iverson et al., 2012; Lincoln et al., 2014; Rinke et al., 2019). The balance between heterotrophy and autotrophy plays a key role in regulating the atmospheric CO_2 concentration which has a huge impact on climate. In addition to the mineralization of the organic matter, ca. 20% was exported in the form of particulate and dissolved organic matter to the deep ocean (Ducklow et al., 2001; Hansell et al., 2009).

Mesopelagic and bathypelagic zones are found below the epipelagic zone. They together provide one of the largest contiguous habitats for microbes on Earth. The knowledge about microbial diversity and the response of microbes to changes in the carbon and energy source is limited (Aristegui et al., 2009). Generally, microorganisms in this habitat are assumed dominantly degrading the sinking organic matter from the photic zone (Del Giorgio and Duarte, 2002). This process in return resupplies inorganic nutrients to the photic layer. However, this may not be the case (Karl et al., 1984; Karner et al., 2001; Herndl et al., 2005; Swan et al., 2011). Studies revealed that autotrophic Thaumarchaeota dominates prokaryotic cell numbers in the mesopelagic zone of the Pacific Ocean (Karner et al., 2001). They oxidize low concentration of ammonia to nitrite (rate-limiting step of nitrification) and are well adapted to the oligotrophic conditions commonly found in the open and deep ocean (Stahl and de la Torre, 2012; Könneke et al., 2014). Interestingly, they may transform the relatively labile carbon formed by degradation of organic matter into a more refractory form (Hugler and Sievert, 2011).

In fact, the characteristic membrane molecules of Thaumarchaeota can accumulate in the sediments in geological timescales, as far as Cretaceous (Kuypers et al., 2001). This means the carbon fixed by Thaumarchaeota may escape remineralization. However, some studies suggest their contribution to primary production is generally small due to small cell size (Schattenhofer et al., 2009). Moreover, archaeal nitrification may be insufficient to support the measured inorganic carbon fixation rates (Varela et al., 2011). Thus, there must be unidentified microbial lineages and energy sources responsible for a significant fraction of carbon fixation in the dark ocean (Karl et al., 1984; Swan et al., 2011; Varela et al., 2011). Recently, oxygen minimum zones (OMZ) received increasing attention as they are expected to increase in response to climatic warming and enhanced water stratification (Keeling et al., 2010; Doney et al., 2011; Lam and Kuypers, 2011; Breitburg et al., 2018). OMZs are either located enclosed between oxygenated water layers (upwelling regions, e.g., Baltic Sea) or at transition from oxic to anoxic marine bottom waters (e.g., Black Sea). OMZ was traditionally thought to be dominated by heterotrophic activities such as aerobic respiration and denitrification coupled to oxidation of organic materials until the discovery of anaerobic oxidation of ammonium (Anammox) (Kuypers et al., 2003; Dalsgaard et al., 2005; Hugler and Sievert, 2011). Anammox is an autotrophic process in which carbon is fixed by reductive acetyl-coenzyme A pathway (Wood-Ljungdahl pathway, WL) (Schouten et al., 2004). The estimation of carbon fixation by WL pathway reached up to 3.5 Tg C y^{-1}, almost 0.7% of primary production in the ocean (Raven, 2009). In sum, mesopelagic and bathypelagic zones are active habitat where both heterotrophs and autotrophs together regulating carbon cycling.

Despite high global marine primary production (~55 Pg C y^{-1}), most organic matter is remineralized in the water column and only 2-3 Pg C y^{-1} reaches the **seafloor** (Middelburg, 2019). All the organic materials reaching to seafloor are exposed to degradation by benthic microorganisms. Marine sediment serves as the largest organic carbon reservoir (Hedges and Keil, 1995) and one of the largest microbial habitats on Earth (Whitman et al., 1998; Parkes et al., 2014). With increasing data gathered through ocean drilling programs in the past two decades, the current estimate of the global subseafloor cell number in sediments is around 2.9 $\times 10^{29}$ cells (Kallmeyer et al., 2012; Hoshino and Inagaki, 2019), a downsize of two orders of magnitude than previous estimates (Whitman et al., 1998; Lipp et al., 2008). The current estimation of cell numbers equals to 4 Pg of biomass carbon, corresponding to 0.18-3.6% of the total living biomass on Earth (Kallmeyer et al., 2012; Hoshino and Inagaki, 2019). Despite

extensive research of microbial biomass in the subseafloor, archaea remain mysterious in the perspective of abundance and distribution. Recent global quantification of 16S rRNA genes in 221 diverse sediment core samples revealed that archaeal cells constitute 37.3% of the total microbial cells (Hoshino and Inagaki, 2019). The authors also postulated that the archaea at ocean margin constitute 40% of total cells, three times more than open-ocean sites (Hoshino and Inagaki, 2019). This means archaea possibly play a comparable role like bacteria in organic matter degradation. Organic carbon biodegradation processes quickly occur in sediments and only a small fraction eventually escapes mineralization (Middelburg, 2019). Diverse sedimentary microorganisms are responsible for the oxidation of organic matter by utilizing a variety of electron acceptors diffusing into sediments from the seawater. Due to the enzymatic catalysis in living organisms, the redox reactions in marine environments are accelerated by orders of magnitude (Jørgensen, 2000; Offre et al., 2013). This process has long been supported by geochemical evidence (Froelich et al., 1979; Canfield and Thamdrup, 2009). The main terminal electron-accepting processes (Fig. I.1) are in order of aerobic respiration, nitrate reduction, manganese reduction, iron reduction, organoclastic sulfate reduction, and methanogenesis (Froelich et al., 1979; Canfield and Thamdrup, 2009). Organic matter can also be mineralized by fermentation. This process produces small organic metabolites such as formate, acetate, lactate, butyrate, propionate, etc. which can further support sulfate reduction or methane formation.

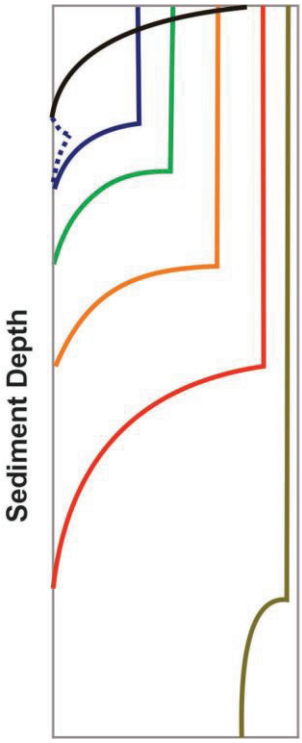

Reactions Stoichiometry	ΔG (kJ/mol)
$O_2 + \frac{1}{2}C_2H_3O_2^- \rightarrow HCO_3^- + \frac{1}{2}H^+$	-402
$\frac{4}{5}NO_3^- + \frac{1}{2}C_2H_3O_2^- + \frac{3}{5}H^+ \rightarrow \frac{2}{5}N_2 + HCO_3^- + \frac{1}{5}H_2O$	-359
$2MnO_2 + \frac{1}{2}C_2H_3O_2^- + \frac{7}{2}H^+ \rightarrow 2Mn^{2+} + HCO_3^- + 2H_2O$	-385
$4FeOOH + \frac{1}{2}C_2H_3O_2^- + 15/2H^+ \rightarrow 4Fe^{2+} + HCO_3^- + 6H_2O$	-241
$\frac{1}{2}SO_4^{2-} + \frac{1}{2}C_2H_3O_2^- + \frac{1}{2}H^+ \rightarrow \frac{1}{2}H_2S + HCO_3^-$	-43.8
$\frac{1}{2}H_2O + \frac{1}{2}C_2H_3O_2^- \rightarrow \frac{1}{2}CH_4 + \frac{1}{2}HCO_3^-$	-19.9

Fig. I.1. Terminal electron-accepting processes in sediment (modified after Froelich et al., 1979; Canfield and Thamdrup, 2009). (b) Simplified oxidation reactions of sedimentary organic matter with different electron acceptors and associated Gibbs free energy yield (ΔG; Froelich et al., 1979).

Based on the redox difference in marine sediments, the main biogeochemical zones (Fig. I.2) can be divided into sulfate reduction zone (SRZ), sulfate-methane transition zone (SMTZ), and methanogenic zone (MGZ) (Jørgensen and Kasten, 2006; Mitterer, 2010). Different biogeochemical zones consist of different microbial compositions and metabolic activities. Sulfate-reducing bacteria (SRB) outcompete methanogens for a common organic substrate until all sulfates are depleted. Consequently, methanogenesis in marine sediments occurs only after almost all sulfate has been reduced (Jørgensen and Kaster, 2006). This relationship results in the MGZ underlying the SRZ. Anaerobic oxidation of methane (AOM) is carried out by syntrophic associations between sulfate-reducing bacteria and methane-oxidizing archaea (Hinrichs and Boetius, 2002) at the diffusion-controlled interface between the SRZ and MGZ, which is the so-called sulfate-methane transition zone (SMTZ, Fig. I.2). In typical marine sediments, AOM mediating organisms can remove CH_4 efficiently due to the relatively slow upward transport of CH_4 (Iversen and Jorgensen, 1985). AOM is a major geochemical process that functions as an important sink in oceanic methane geochemistry considering the enormous volume of marine sediments (Reeburgh, 2007). The carbon cycling within the SMTZ

influences the geochemical gradients (Fig. I.2A, CH_4, SO_4^{2-}) and stable carbon isotopic profiles (Fig. I.2B CH_4 and DIC). Depleted stable carbon isotopic compositions of both CH_4 and DIC (see Fig. I.2B) provided carbon source for the distinct ^{13}C-depleted bacterial and archaeal lipids (Elvert et al., 1999; Hinrichs et al., 1999; Blumenberg et al., 2004).

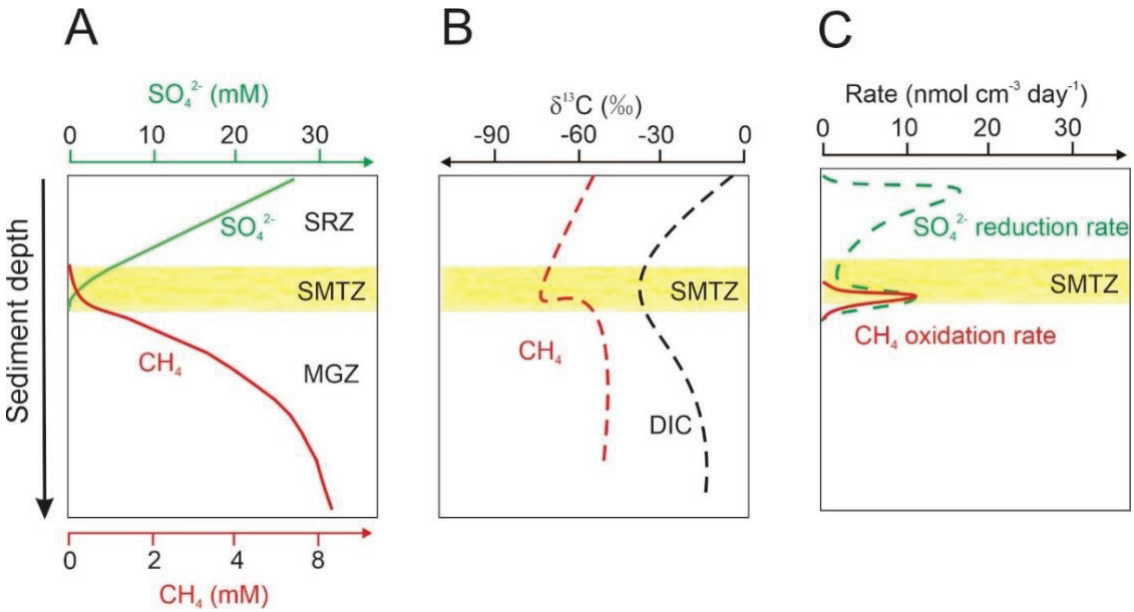

Fig. I.2. Distribution of geochemical zones and geochemical profiles in marine sediment (A) Concentration profiles of SO_4^{2-}, CH_4; (B) $\delta^{13}C$ of DIC and CH_4; (C) rates of SO_4^{2-} reduction and CH_4 oxidation; SRZ: sulfate reduction zone, SMTZ: sulfate-methane transition zone, MGZ: methanogenic zone. Figures are modified or redrawn from (Iversen and Jorgensen, 1985; Reeburgh, 2007; Kellermann, 2012)

I.2 Microbial lipids and their turnover in sediments

I.2.1 Microbial lipids

The microbial membrane serves as a biological semi-permeable barrier that protects intracellular components from the extracellular environment, mediates cellular transport and transmits cellular signals (Madigan et al., 1997). The principal components of the membrane are lipids, proteins, and carbohydrates. The structure of the membrane can be described by the Fluid Mosaic Model (Nicolson, 2014). In brief, amphiphilic lipid molecules act as the fabric of the membrane. Integral proteins are integrated into the fabric with their hydrophobic components interacting with the hydrophobic region of the phospholipid bilayer. Carbohydrates are normally found on the exterior surface where they are bound either to

proteins or lipids, forming glycoproteins or glycolipids, respectively (Nicolson, 2014). In order to maintain the cell integrity, microbial membrane fluidity is carefully regulated by adapting the lipid compositions to external variations in temperature, salinity, pressure, pH or other environmental factors (Hazel and Williams, 1990). All microbial membrane lipids shared a similar structure: core lipid (CL) bounded to hydrophilic headgroup to form the intact polar lipids (IPL) (Fig. I.3). The CL is comprised of a glycerol backbone with two attached hydrophobic side chains. IPLs assemble into 2D sheets with hydrophilic headgroups facing either cytoplasm or cell exterior while in between are the hydrophobic chains. The difference in the structure of polar headgroups determines their physical properties and biological functions (Fig. I.3). For instance, size can directly influence the packing and organization and consequently for the physical and chemical properties of the membrane (Dowhan, 1997). The different ionic characters (anionic and zwitterionic) of polar head groups help microbes adapt to physiological pH range as well as maintain the optimal activity of major integral proteins. Zwitterionic head groups include Phosphatidylethanolamine (PE), phosphatidyl-(N)-methylethanolamine (PME), phosphatidyl-(N,N)-dimethylethanolamine (PDME), and phosphatidylcholine (PC), while anionic groups include phosphatidylglycerol (PG), diphosphatidylglycerol (DPG), and phosphatidyl inositol (PI).

However, there are distinctions between archaeal and bacterial lipids. Archaeal lipids consist of isoprenoid alcohols that are ether-linked to glycerol, contrasting to the bacterial lipids which are dominantly composed of fatty acids esterified to glycerol moiety. Chemically the ether bonds are more resistant to hydrolysis than ester bonds. Moreover, the stereochemistry of the archaeal glycerol moiety is enantiomer to the glycerol moiety found in bacteria. The archaeal lipids are built on a backbone of sn-glycerol-1 while bacteria use sn-glycerol-3 (Kate, 1993). This suggests that archaea probably use different enzymes for synthesizing lipids compared to bacteria. Most bacterial membrane lipids have core diacylglycerol structure with two fatty acids having either straight or branched chains with variable length and degrees of unsaturation. The patterns could help bacteria adapt to different external environments. For example, a high degree of unsaturation keeps the membrane fluidity at low temperature and the high content of branched-chain fatty acids protects the cell integrity under the low pH environment (Kaneda, 1991). Archaeal membrane lipids can be divided into two major types, archaeols and GDGTs (Glycerol dibiphytanyl glycerol tetraethers, Fig. I.3). Archaeols consist of a glycerol ether-linked to two C-20 isoprenoid chains and form a bilayer structure; GDGT consists of a glycerol

ether-linked to two C-40 isoprenoid chains and forms a monolayer (Koga and Morii, 2007; Villanueva et al., 2014). GDGTs can contain from 0 to 8 cyclopentane rings which are important to maintain membrane function and cell homeostasis under extreme environmental conditions (Knappy et al., 2012). For example, higher temperatures and lower pH can force more ring syntheses (Uda et al., 2001; Macalady et al., 2004; Chong, 2010; Knappy et al., 2012). The comparison between microbial phylogeny and lipid distribution patterns reveals that most lipids are not characteristic of a phylogenetic group (Schouten et al., 2013; Villanueva et al., 2014). Only several lipids so far have been constrained for their sources. For example, crenarchaeol, a GDGT containing four cyclopentane moieties and one cyclohexane moiety, has been found so far exclusively in Thaumarchaeota (Schouten et al., 2008; Pitcher et al., 2011; Sinninghe Damsté et al., 2012). Archaeol with hydroxylated side chains (sn-2 hydroxyarchaeol) is distinct for methanogenic and methanotrophic archaea (Koga et al., 1993; Hinrichs et al., 1999).

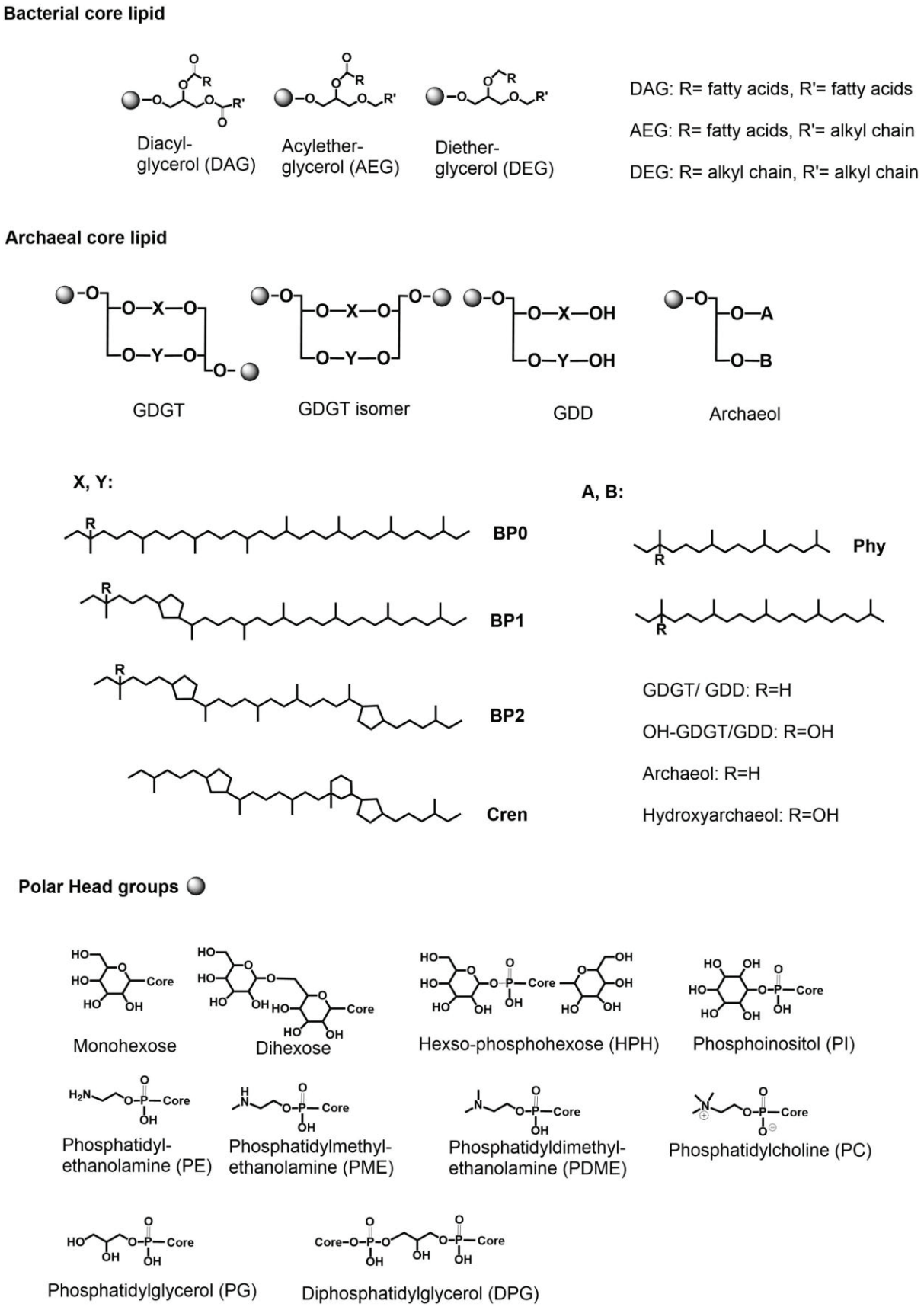

Fig. I.3. Structures of bacterial and archaeal core lipids and associated polar head groups found in the marine environment.

I.2.2 Microbial lipid turnover

Lipid turnover has impact on the interpretation of paleoenvironmental proxies as well as estimates of the living biomass in sediments. Low organic matter (OM) sediments under aerobic conditions facilitate lipids degradation into CO_2 (Harvey et al., 1986). Anaerobic and high OM could support the preservation of lipids because the OM (e.g. humic substances) matrix may protect the lipid from the microbial availability. Harvey et al. (1986) suggested that there are two lipid pools, a readily available pool (Pool-A) and a tightly bound pool (Pool-B). The lipids in Pool-A are exposed to microorganisms and will be first degraded while the lipids in Pool-B are adsorbed to the OM matrix. The lipids in Pool-B would be slowly released and degraded when the lipids in Pool-A are depleted. The authors also found that IPLs with glycosidic head groups show higher stability against degradation than IPLs with phosphoester head groups (Harvey et al., 1986). Nonetheless, Logemann et al. (2011) found that degradation rates have no difference among different head groups (phosphoester-bound head groups vs glycosidic head groups) but among the bond types between glycerol unit and alkyl moieties. No matter which degradation mechanism is taking place, the IPLs from bacteria seem to have a higher turnover rate than IPLs from archaea (Xie et al., 2013). The quantitative estimate of microbial IPLs turnover has been investigated both in incubation experiments or modeling (Lipp and Hinrichs, 2009; Schouten et al., 2010; Logemann et al., 2011; Xie et al., 2013). Even though the estimated turnover time is highly variable, the consensus is that a remarkable amount of archaeal IPLs can resist degradation on the scale of hundreds of thousand years, being 1-2 orders of magnitude longer than those of bacterial IPLs. Later, TEX_{86} paleotemperature based on core and IPL GDGTs proved that 1G-GDGT is as stable as CL-GDGTs and be preserved in marine sediments over geological timescales (Lengger et al., 2013; 2014). Within the glycosidic IPLs, 2G-GDGTs are more indicative of living biomass than 1G-GDGTs (Evans et al., 2019). Compared to abundant glycosidic IPLs, hexose-phospho-hexose (HPH) crenarchaeol does not exist in adequate quantities in deeply buried sediments and thus probably has higher lability (Lengger et al., 2014). All the studies listed above indicate that likely only a small portion of IPL-GDGTs present in deeply buried sediments is part of cell membranes of active archaea. Estimating the living biomass in subseafloor by extracting the useful information from lipids is still challenging.

The subseafloor is believed to be highly energy limited. Recycling of fossil molecules (e.g. lipids) becomes a potential strategy for microbes in coping with conditions of energy starvation by minimizing energy expenditures for growth and maintenance (Takano et al., 2010; Lin et al., 2013; Dippold and Kuzyakov, 2016; Lipsewers et al., 2018; Thomas et al., 2019). Long-term SIP incubation studies of archaea showed glycerol and head groups are preferentially labeled while alkyl moiety is less labeled (Takano et al., 2010; Lin et al., 2013; Evans et al., 2019). Based on this observation, it suggested that lipid recycling maybe a strategic mechanism for microbes to save energy in the infertile marine sediments. Furthermore, the lipid recycling process becomes increasingly slower with increasing depth due to lower energy availability (Lin et al., 2013). Heterotrophic bacteria are even found to build isoprenoid wax ester by recycling the lipids of putatively better-adapted archaea in deep Dead Sea sediments (Thomas et al., 2019). This mechanism illustrates a new pathway of carbon transformation adapting to extreme environments characterized by long-term isolation and minimal energetic resources. Even though these strategies keep being found, a reasonable quantification of lipid recycling in subseafloor has so far been hardly achieved.

I.3 Microbial metabolism and lipid isotopic compositions

I.3.1 Microbial metabolism

Microorganisms are generally grouped based on the metabolic strategies for gaining energy and carbon sources (Fig. I. 4). The optional energy can be either sunlight or reduced chemical compounds, which drive phototrophic or chemotrophic lifestyles, respectively. Chemotrophs are further subdivided into chemoautotrophs or chemoheterotrophs depending on the carbon source, either from inorganic or organic origin. Another way to subdivide chemotrophs is depending on the energy source, lithotrophs obtaining energy from inorganic compounds and organotrophs obtaining energy from organic compounds. Mixotrophy is a more widespread phenomenon when compared to autotrophy and heterotrophy (Eiler, 2006). Mixotrophic microbes use several metabolic strategies simultaneously. They can incorporate organic carbon into biomass with inorganic chemicals as energy sources (Madigan et al., 1997). Meanwhile, they can also switch strategy by assimilating simple organic compounds (e.g., acetate, succinate, or propionate, etc.) in addition to the fixation of CO_2 (Hugler and Sievert, 2011).

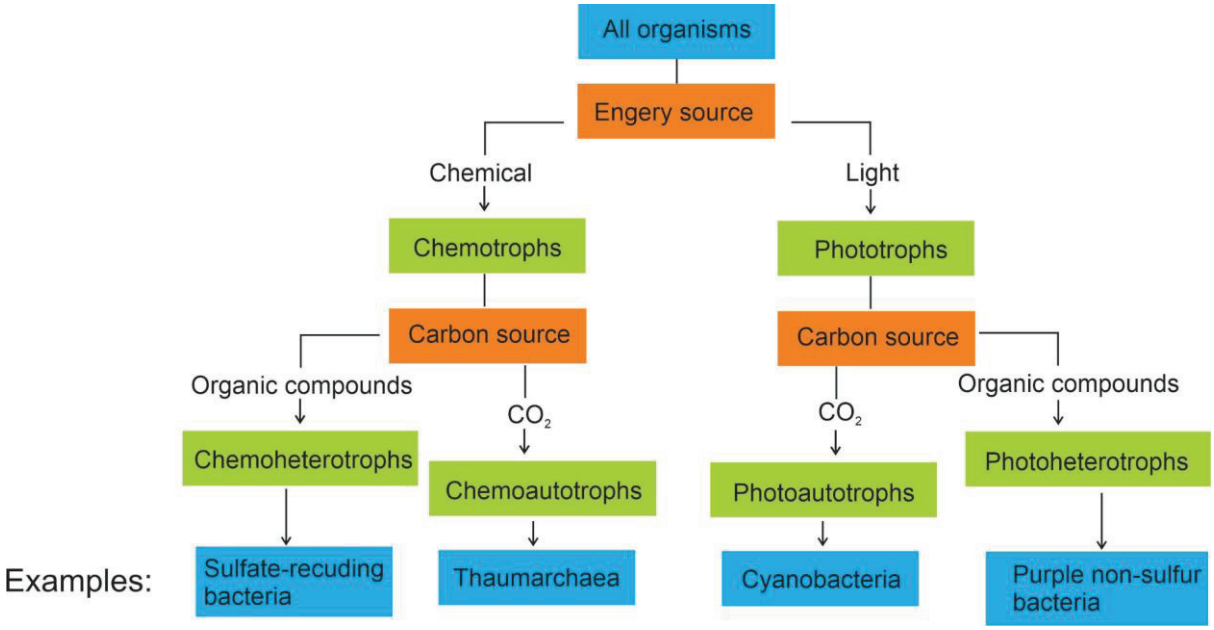

Fig. I.4. Classification of microorganisms based on carbon and energy sources

Carbon fixation is the most important biosynthetic process on Earth, enabling autotrophs to synthesize biomass from inorganic carbon at the expense of energy generated by light or chemical reactions. The biomass synthesized by CO_2 fixation (especially photosynthesis) provides the food web foundation for the entire earth system. Autotrophs assimilate inorganic carbon (CO_2, HCO_3^-, etc.) into cellular building blocks by reducing CO_2 (oxidation number = +4) to cellular C (oxidation number = 0) with a requirement of energy input. Six different CO_2 fixation mechanisms have been found so far in microbial communities, including reductive pentose phosphate cycle (Calvin-Benson-Bassham cycle, CBB), reductive tricarboxylic acid cycle (rTCA), reductive acetyl-coenzyme A pathway (also called Wood-Ljungdahl pathway, WL), 3-Hydroxypropionate bicycle (3-HP), 3-Hydroxypropionate/4-hydroxybutyrate cycle (3-HP/4-HP), and Dicarboxylate-hydroxybutyrate cycle (DC/4-HB). Multiple factors determine which pathways to use in the microbial communities, such as O_2 concentration, metal availability, C1 compounds, energy demands, CO_2 species (CO_2, HCO_3^-, etc.) as well as co-assimilation of organic molecules (Berg et al., 2010a).

The CBB cycle is widely operated in plants, algae, cyanobacteria, etc. This pathway contains a key enzyme, ribulose 1,5-bisphosphate carboxylase–oxygenase (RubisCO), participating in the first step of CO_2 reduction (Bassham et al., 1954). This pathway has been found in some bacteria but not in archaea.

The rTCA cycle involves enzymes that are sensitive to oxygen and is therefore found only in anaerobes or in aerobes growing at low oxygen concentrations (Buchanan and Arnon, 1990). This cycle is found in green sulfur bacteria and some proteobacteria but not in Archaea. The citric acid cycle is the process where organic molecules are oxidized to CO_2 by heterotrophs. rTCA is the reversed process where CO_2 is fixed to organic carbon.

The reductive acetyl-CoA pathway or Wood–Ljungdahl (WL) pathway is not a circle pathway (Hugler and Sievert, 2011). It is often found in some Gram-positive bacteria (Proteobacteria, Planctomycetes, Spirochaetes) and Euryarchaeota (methanogens) (Ragsdale and Pierce, 2008; Hugler and Sievert, 2011). This pathway contains two CO_2 molecules that are reduced to CO and methyl group, and then these two reduced groups are bound to Acetyl-CoA. Acetyl-CoA and carbon monoxide dehydrogenase are the two key enzymes in this pathway. WL is a favorable autotrophic carbon fixation pathway which is restricted to strictly anaerobic microorganisms.

The 3-HP bicycle occurs in some green nonsulfur bacteria of family Chloroflexaceae (Zarzycki et al., 2009) but has not been found elsewhere. Different from the cycles described above, 3-HP use HCO_3^- instead of CO_2. The solubility of HCO_3^- in slightly alkaline water is much higher than that of CO_2, autotrophs might benefit from using HCO_3^- instead of CO_2. Besides it is a two-cycle pathway, the fixation of two HCO_3^- and formation of glyoxylate operating as the first cycle and the assimilation of glyoxylate as the second cycle.

The 3-HP/4-HB cycle operates in autotrophic thermoacidophilic members of the crenarchaeal order Sulfolobales (Metallosphaera sedula, Stygiolobus azoricus) and Thaumarchaeota (Nitrosopumilus maritimus) (Berg et al., 2007; Berg et al., 2010a; Könneke et al., 2014). This cycle can be subdivided into two parts. The first half is the reaction sequence from Acetyl-CoA to succinyl-CoA which is the same as 3-HP bicycle. The second half is the regeneration of Acetyl-CoA from succinyl-CoA. Recently, ammonia-oxidizing Thaumarchaeota were proven to use a modified 3-HP/4-HB cycle which is more energy-efficient (5 ATP required for one pyruvate production) (Könneke et al., 2014). Comparative phylogenetic analysis of proteins of this pathway suggests that 3-HP/4-HB cycle emerged independently in Crenarchaeota and Thaumarchaeota. Moreover, 4-hydroxybutyryl-CoA dehydratase (key enzyme in 3-HP/4-HB) sequences were widely found in the Global Ocean Sampling database and ranked only secondly after Rubisco in CBB (Berg et al., 2010a). All the evidence so far indicates 3-HP/4-HB is an important pathway in global-scale carbon cycling.

The DC/4-HB occurs in the anaerobic crenarchaeal orders Thermoproteales and Desulfurococcales (Huber et al., 2008; Berg et al., 2010b). In this cycle, CO_2 fixation is operated by pyruvate synthase and phosphoenolpyruvate carboxylase. Some enzymes are shared among DC/4HB, rTCA, and 3-HP/4-HB pathway (Hugler and Sievert, 2011).

I.3.2 Stable carbon isotopic composition of lipids in different microbes

The determination of $\delta^{13}C$ values provides abundant information for the characterization of the modern and reconstruction of past biogeochemical environments (Hayes et al., 1990; Hayes, 2001; Hayes, 2004; Biddle et al., 2006; Elling et al., 2019). Lipid biomarker isotopic composition provides an explicit and powerful tool inferring prokaryotic metabolism (Biddle et al., 2006; Berg et al., 2010a; Hugler and Sievert, 2011; Pearson et al., 2019). $^{12}C/^{13}C$ ratio depends on multiple environmental variables such as substrate isotopic composition, substrate limitation, the isotopic fractionation associated with enzymatic carbon assimilation, temperature, and pressure, etc.

Table I.1 Carbon source, isotopic fractionation, environment (sensitivity to O_2), and distribution of different autotrophic pathways (Summons et al., 1998; House et al., 2003; Londry et al., 2008; Berg et al., 2010a; Penger et al., 2012; Pearson et al., 2019). The fractionation did not take substrate limitation into consideration; $\varepsilon = \delta^{13}C$ (carbon source) - $\delta^{13}C$ (lipid or biomass).

Pathway	Carbon source	ε (‰)	Environment	Distribution
WL	CO_2	> 30	anoxic	Bacteria and Archaea
CBB	CO_2	20 ~ 30	oxic	Bacteria and Eukaryotes
rTCA	CO_2	2 ~ 12	anoxic / suboxic	Bacteria
3-HP	HCO_3^-	13	oxic	Bacteria
3-HP/4-HB	HCO_3^-	0 ~ 20	oxic	Archaea
DC/4-HB	HCO_3^-	0 ~ 3.8	anoxic	Archaea

Autotrophic microorganisms preferentially incorporate light carbon (^{12}C) into their biomass. Hence the biomass is normally more ^{13}C-depleted than source carbon ($\varepsilon = \delta^{13}C_{\text{Carbon source}} - \delta^{13}C_{\text{lipid or biomass}} > 0$, Table I.1 and Fig. I.5). Different carbon fixation pathways may leave distinct isotopic signatures (House et al., 2003; Schouten et al., 2004; Berg et al., 2010a; Pearson et al., 2019). Thaumarchaeota utilize 3-HP/4-HB biochemical pathway (Berg et al., 2007; Könneke et al., 2014) for carbon fixation in which HCO_3^- is exclusively involved in

biomass synthesis. The carbon isotopic fractionation between DIC and Thaumarchaeota-derived crenarchaeol (ε) is 19.7 ± 0.5‰ (Könneke et al., 2012), which is consistent with sedimentary records (Pearson et al., 2016). Even though Sulfolobales share the same carbon fixation way with Thaumarchaeota, they have a significant difference in carbon isotopic fractionation, with an average ε value of 3‰ (van der Meer et al., 2001; House et al., 2003; Jennings et al., 2014; Pearson et al., 2019). Pearson et al. (2019) systematically studied the cause of this difference and attributed the primary cause of different ε values to carbonic anhydrase. Methanogens and methanotrophs use the WL pathway which creates relatively large carbon isotopic fractionations between substrate and biomass (Table I.1 and Fig. I.5). The ε values of methanogens depend on the type and concentration of substrates (Summons et al., 1998; Londry et al., 2008; Bradley et al., 2009). Of all the substrates (unlimited) used by Methanosarcina barkeri, for example, methanol resulted in the most ^{13}C-depleted methane and lipids (ε value up to 52‰) while acetate yielded the least ^{13}C-depleted lipids (ε≈5‰) (Londry et al., 2008). The growth under CO_2/H_2 creates fractionation between 5 to 27‰ (House et al., 2003). Limited substrate will cause a smaller depletion of methane and lipids and smaller ε values (Bradley et al., 2009). Methanotrophs produce strongly depleted lipids (up to -107‰) with a fractionation reaching up to 80‰ (Orphan et al., 2002). It is worth noting that isotopic fractionation between lipids and substrate is a growth-dependent process (House et al., 2003). Thus the isotopic data should be interpreted with the knowledge of substrate concentration, energy availability, and pressure, etc. (Takai et al., 2008; Nguyen et al., 2019).

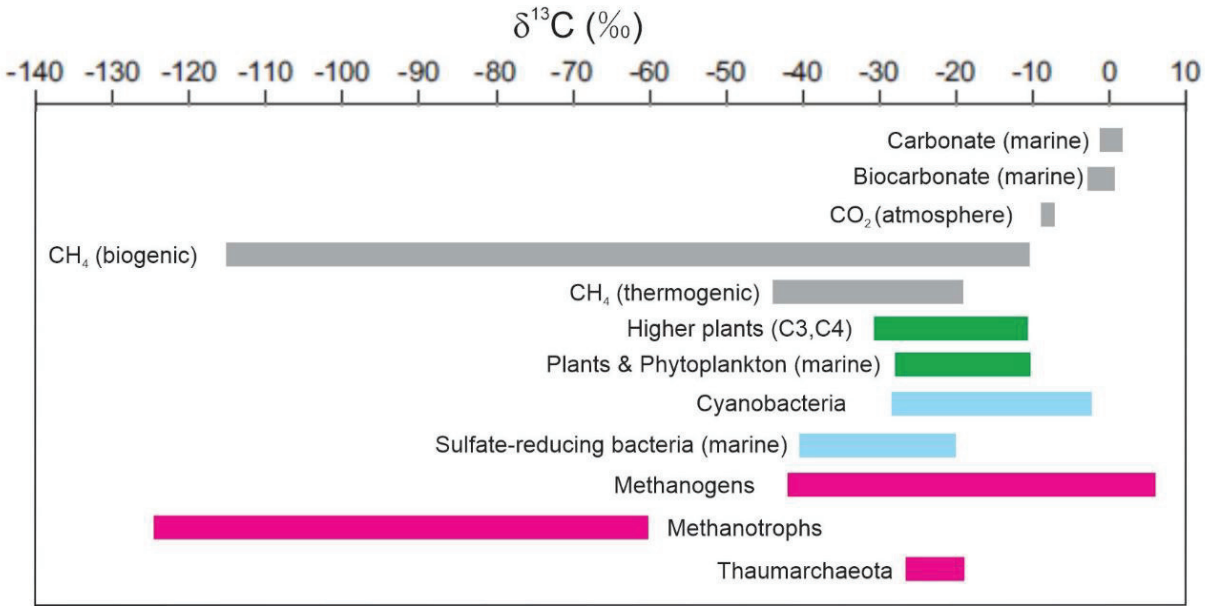

Fig. I.5. The ranges of $\delta^{13}C$ in selected archaeal (pink), bacterial (sky blue), and eukaryotic (green) groups as well as possible carbon substrates (gray). Figure adapted from Becker et al. (2015), Gaines et al. (2009), and Blumenberg (2010).

Compared to autotrophs, heterotrophic bacteria and archaea display a different carbon uptake strategy but basically following the source isotopic compositions, namely the "you are what you eat isotopically" theory (Kohn, 1999). However, different compounds are processed within the cell to different degrees. Ultimately biomass or lipid carbon isotopic composition may be slightly different from the original substrate compounds. Identifying direct sources will further improve our understanding of their metabolism. Heterotrophic microorganisms are believed to play an important role in the carbon cycling of marine subseafloor. Anaerolineae, members of the phylum *Chloroflexi,* are characterized by a chemoorganotrophic lifestyle on the basis of carbohydrates and amino acid degradation under strictly anaerobic conditions (Rosenkranz et al., 2013; Liang et al., 2016; Swiatczak et al., 2017). So far, several pure cultures belonging to this bacterial family have been isolated and iso and anteiso C_{15} and C_{17} are their major cellular fatty acids (Yamada et al., 2006). Spirochaetes, another heterotrophic candidate group, are obligate fermenters that metabolize proteins and carbohydrates (Paster, 2010) and are specifically consuming detrital biomass in anoxic hydrocarbon-rich habitats (Dong et al., 2018). Heterotrophic archaea are widely spread in the subseafloor as well (Biddle et al., 2006; Lloyd et al., 2013; Yu et al., 2017). A combination of rRNA, cell biomass and lipid isotopic analysis

found that high amount of organic matter is likely fueling a heterotrophic lifestyle of archaea, including Bathyarchaeota and Marine Benthic Group-B (Biddle et al., 2006). Based on the physiological and genomic evidence, Bathyarchaeota apply acetyl-coenzyme A-centralized heterotrophic pathways to anaerobically utilize detrital proteins, lipids, carbohydrate, etc (Zhou et al., 2018). To sum up, heterotrophic bacteria and archaea play a pivotal role in shaping the OM pool in sediments.

I.4 Microbial lipid analysis

Microbial lipid analysis in this thesis was performed on samples obtained from the Mediterranean, Black Sea, and Marmara Sea marine sediments, Black Sea water column, as well as cultures of AOM consortia. All the samples were extracted by a modified Bligh and Dyer protocol (Sturt et al., 2004). For identification and quantification, total lipid extract (TLE) was either measured directly by high performance liquid chromatography coupled to mass spectrometry (HPLC–MS) or further treated with different pretreatment (e.g., fraction separation, cleavage reactions, derivatization) before GC (gas chromatography)-based analysis. The following is a brief introduction of techniques relevant to the thesis.

I.4.1 GC- and LC-based methods

The GC-based analysis is one of the most developed techniques in organic geochemistry. It integrates separation, detection and quantification of individual compounds in complex marine sediment extracts. Sample pretreatments (column separation, compounds derivatization) are sometimes necessary for detection and quantification. The target compounds have to be easily heated up into gaseous phase (boiling point less than 430 °C). Detection of compounds is mainly achieved by multiple detectors, with flame ionization detection (FID), mass spectrometry (MS), isotope ratio mass spectrometry (IRMS) as the most common ones. FID provides C quantities of target compounds indiscriminate of the type of compounds. MS-based detection provides rich information on molecular structure. The most common compounds in GC analysis are alkanes, fatty acids, and alcohols including sterols and hopanols (Volkman et al., 1998). Compared to GC, LC-based methods are more suitable for high molecular weight compounds such as IPLs. Hopmans et al. (2000) established HPLC–APCI (atmospheric pressure chemical ionization)-MS method for direct analysis of core GDGTs (Hopmans et al.,

2000). The development of HPLC–ESI (electrospray ionization)-MS facilitated the direct analysis of IPL phospho- and glycolipids (Rütters et al., 2002; Sturt et al., 2004). Since then extended methods were possible due to the availability of alternative stationary phases, such as hydrophilic interaction liquid chromatography (HILIC) or reversed phase (RP), resulting in either more complete separation or synchronous analysis of IPLs and CLs (Wörmer et al., 2013; Zhu et al., 2013).

I.4.2 Isotope analysis of GDGTs and fatty acids

Conventionally, isotope measurements are made on the C_{40} biphytane (BP) skeletons of GDGTs, rather than on the complete structures (Langworthy, 1977; Jahn et al., 2004). This approach loses some information from whole GDGT molecules. High temperature GC-methods (HTGC, up to 430 °C) can be applied to the analysis of the whole core GDGT molecules (Nichols et al., 1993; Weijers et al., 2006; Pancost et al., 2008). Very recently, HTGC coupled to time-of-flight mass spectrometry or IRMS has been employed to produce spectra of GDGTs and isotopic analysis from an archaeal culture as well as environmental samples (Lengger et al., 2018). Another protocol to circumvent chemical pretreatment, Spooling Wire Microcombustion (SWiM)-IRMS method has been established for the direct measurement of whole core GDGT molecules with precision and accuracy of ±0.25‰ (1σ) (Pearson et al., 2016). However, this method requires high sample purification by orthogonal dimensions of HPLC, no mention that it is not commercialized yet and requires demanding maintenance skills. Based on the evaluation, ether cleavage is still the commonly used method for isotopic analysis of GDGTs and thus was chosen in this thesis. Bacterial fatty acids were measured by GC-IRMS in the form of fatty acid methyl esters (FAMES) after saponification of the TLE and derivatization with BF_3 (Elvert et al., 2003).

I.4.3 Stable isotope probing (SIP)

In this thesis, we used SIP culture on the AOM enrichment. SIP is a cultivation independent approach which is performed on microbial community from environments. The culture is spiked with a substrate containing heavy stable isotopes (e.g., ^{13}C or ^{2}H), which is assimilated by distinct populations. Finally, the labeled biomolecules (e.g., lipids, carbohydrates, protein, RNA, DNA) are qualitatively and quantitatively detected by isotope-sensitive analytical

instrument (Boschker et al., 1998; Manefield et al., 2002; Harsha et al., 2008; Jehmlich et al., 2016; Wegener et al., 2016a). The advantage of isotope tracer methods is that they can reveal growth rates that reflect population biosynthetic activity regardless of whether the population is expanding, at steady state, or declining. Isotopic enrichments thus can provide a measurement of biosynthetic turnover that is independent of total biomass (Kopf et al., 2016). Dual-SIP (^{13}C and ^{2}H) is also implemented to estimate the auto- and heterotrophic carbon fixation (Wegener et al., 2016a). Recently, position-specific labeling is popular in the ecological study in overcoming the disadvantage from uniformly isotope-labeled compounds which cannot provide a clear framework for tracing microbial biosynthetic pathways (Scandellari et al., 2009; Fischer and Kuzyakov, 2010). The most commonly used molecules are position-specific glucose and amino acids (Apostel et al., 2013; 2015). For example, the functional groups of the amino acids are utilized differently. The carboxylic carbon is preferentially decomposed to CO_2 while the alkyl carbon tends to be incorporated into biomass (Apostel et al., 2013; Aepfler et al., 2019). This is crucial in understanding the carbon source and flow driven by microorganisms in incubation experiments.

Chapter II

Scope and Outline

This Ph.D. thesis is under the interdisciplinary project "Deep subsurface Archaea: carbon cycle, life strategies, and role in sedimentary ecosystems" (DARCLIFE) which was granted by the European Research Council (ERC, Advanced Grant DARCLIFE; principal investigator, K.-U.H.). The DARCLIFE project included two cruises (Zabel et al., 2011; Heuer et al., 2014), FS Meteor cruise M84-1 (DARCSEAS) and FS Poseidon cruise POS450 (DARCSEAS II). The aim of this project was to understand how benthic archaea are distributed and adapted to energy-limited marine sedimentary systems and constrain their role in the deep biosphere carbon cycling. Already at the beginning of this Ph.D. project, a large amount of data, methods, and publications were available thanks to the excellent work of project members. In particular, advanced HPLC–MS-based methods for intact polar lipid analysis have been built to discover new biomarkers and investigate the biological origin and fate of microbial lipids in a variety of environments (Liu et al., 2012; Wörmer et al., 2013; Zhu et al., 2013). Moreover, extensive work on the same studying sites as mine provided abundant information to support my Ph.D. study (Schmidt et al., 2017; Becker et al., 2018; Zhuang et al., 2018; Coffinet et al., 2019; Evans et al., 2019). Within the framework of DARCLIFE, this thesis focused on decrypting the messages from the isotopic composition of microbial membrane lipids in different environmental samples and archaeal enrichment cultures.

Sedimentary microbial lipids are widely used in paleoenvironmental and biogeochemical studies. Core lipids preserved in the sedimentary record normally reflect the environmental conditions of the time when archaeal community members have existed. However, the degradation kinetics of sedimentary IPLs are not well constrained and possibly influence the core lipid pool, further affect the sound interpretation of lipid-based paleoenvironmental proxies (e.g. TEX_{86}). In addition, the sources of sedimentary IPLs are also in debate because the subseafloor provides a habitat for a vast number of active microbes who may also produce new IPLs. The challenge of exploring benthic microbes also comes from their relatively low activity and abundance in the deep marine biosphere. To overcome these difficulties, my Ph.D. project employed the isotopic approach to investigate the biological origin and fate of microbial lipids in the marine environment.

II.1 Objectives

This Ph.D. project investigated the fate of microbial lipids and characterize the archaeal and bacterial life in different marine environments by using lipid isotopic analysis as well as SIP incubation. This thesis is divided into two parts: In the first part (Chapters III and IV), I provide a comprehensive study on extracting information encoded in the isotopic compositions of archaeal lipids from different sedimentary environments. In the second part (Chapter V), I investigated heterotrophic activities in AOM enrichments by using SIP incubation. This thesis is guided by the following objectives and experiment designs.

1. **To constrain the archaeal activity and sedimentary lipid input and preservation signatures in different marine environments (Chapter III).**
   Sedimentary archaeal lipids are widely used as sensitive indicators of environmental conditions in paleoenvironmental and biogeochemical studies. I performed a systematic study targeting $\delta^{13}C$ compositions of archaeal CL and IPL combined with geochemical information in contrasting depositional regimes including a transect from the Rhone River delta into the western Mediterranean Sea, the anaerobic Black Sea, the salinity-influenced Marmara Sea, and sapropel layers in the Eastern Mediterranean Sea (N=44).

2. **To further constrain the sources and turnover of archaeal lipids in Black Sea (Chapter IV)**
   I compared the stable carbon isotopes of archaeal IPLs and CLs in high resolution through the water column (N=5) and within an 8-m long sediment core (N=28) of the Black Sea. This is the first report of IPL isotopic compositions in the marine water column. The lipid isotopic records will provide information about original sources and turnover of IPLs in sediments.

3. **To investigate the importance of heterotrophic microorganisms thriving on the amino acids released from AOM necromass (Chapter V).**
   Cultures dominated by AOM consortia have been frequently obtained but they contain still additional community members, even after years of repeated dilution and inoculation. It has been suggested that these bacteria thrive on AOM necromass. To study the potential heterotrophic activity of community members, I performed a

position-specific SIP study in a mesophilic AOM culture dominated by ANME-1 archaea and its partner bacteria (Seep SRB2 and HotSeep-1).

II.2 Contribution to publications

Stable carbon isotopic compositions of archaeal lipids as a gauge to constrain terrestrial, planktonic, and benthic sources (Chapter III)

Qing-Zeng Zhu, Marcus Elvert, Travis B. Meador, Kevin W. Becker, Verena B. Heuer, Kai-Uwe Hinrichs

MARUM - Center for Marine Environmental Sciences and Department of Geosciences, University of Bremen, Germany

In preparation for *Geochimica et Cosmochimica Acta*

Q.-Z.Z, K.-U.H, and M.E designed the project; Q.-Z.Z performed lab work; Q.-Z.Z analyzed the data; K.B.W and T.B.M analyzed intact polar lipids in sediments; Q.-Z.Z, K.-U.H, and M.E wrote the manuscript with contributions from the co-authors, especially T.B.M and K.B.W.

Isotope geochemistry of archaeal lipids in the Black Sea and underlying sediments constrains their sources and turnover (Chapter IV)

Qing-Zeng Zhu, Marcus Elvert, Travis B. Meador, Kevin W. Becker, Jan M. Schröder, Verena B. Heuer, Matthias Zabel, Kai-Uwe Hinrichs

MARUM - Center for Marine Environmental Sciences and Department of Geosciences, University of Bremen, Germany

In preparation for *Geochimica et Cosmochimica Acta*

Q.-Z.Z, K.-U.H, and M.E designed the project; Q.-Z.Z performed lab work; Q.-Z.Z analyzed the data; J.M.S, K.W and T.M analyzed intact polar lipids in sediments; Q.-Z.Z and K.-U.H wrote the manuscript with contributions from the co-authors.

Microbial heterotrophy in enrichment cultures dominated by anaerobic methane-oxidizing consortia (Chapter V)

Qing-Zeng Zhu[1*], Gunter Wegener[1,2], Kai-Uwe Hinrichs[1], Marcus Elvert[1]

[1]MARUM - Center for Marine Environmental Sciences and Department of Geosciences, University of Bremen, Germany

[2]Max-Planck Institute for Marine Microbiology, 28359 Bremen, Germany.

In preparation for *Environmental Microbiology*

Q.-Z.Z and M.E designed the project; Q.-Z.Z and G.W performed lab work; Q.-Z.Z analyzed the data; Q.-Z.Z and M.E wrote the manuscript with contributions from the co-authors.

Chapter III

Stable carbon isotopic compositions of archaeal lipids as a gauge to constrain terrestrial, planktonic, and benthic sources

Qing-Zeng Zhu, Marcus Elvert, Travis B. Meador, Kevin W. Becker, Verena B. Heuer, Kai-Uwe Hinrichs

MARUM Center for Marine Environmental Sciences and Department of Geosciences, University of Bremen, Germany

Abstract

Sedimentary archaeal lipids are widely used as sensitive indicators of environmental conditions in paleoenvironmental and biogeochemical studies. The principal sources of archaeal lipids in marine sediments are planktonic archaea, benthic archaea and lipids from allochthonous sources such as soils. However, their relative contributions to the lipid pool in sediments have not been well constrained. In order to provide insights into the relative contributions of these sources and possibly identify signals derived from sedimentary activity, we performed a systematic survey of stable carbon isotopic compositions ($\delta^{13}C$) of core and intact archaeal lipids (i.e., archaeol, caldarchaeol and crenarchaeol) via analyses of their (bi)phytanyl moieties in diverse marine sediments. The analyzed sample set consists of 44 samples from the Mediterranean and adjacent Seas with largely varying sources of organic matter. Complementary geochemical data enabled to associate lipid distributions and carbon isotopic signatures to redox conditions. The $\delta^{13}C$ of crenarchaeol ranges from -19.1 to -28.6‰ and -18.1 to -27.4‰ for its core and intact form, respectively. The $\delta^{13}C$ values of core and intact crenarchaeol were highly similar in all samples, suggesting that that intact crenarchaeol is either a fossil relic from planktonic archaea or a product of lipid recycling by benthic archaea rather than being synthesized *de novo*. Core and intact caldarchaeol have $\delta^{13}C$ ranges from -19.4 to -32.0‰ and -20.9 to -37.0‰, respectively. In contrast to crenarchaeol, intact caldarchaeol was on average 2.6‰ more ^{13}C-depleted than its core counterpart, indicative of in-situ production of intact caldarchaeol by benthic archaea. Core and intact archaeol present the largest ranges in $\delta^{13}C$ from -21.6 to -42.1‰ and -22.7 to -58.9‰, respectively. No matter whether present as intact or core forms, the relatively strong ^{13}C-depletion of archaeol relative

to total organic carbon as well as dissolved inorganic carbon is consistent with mixtures of functional sources of sedimentary chemolithoautotrophic, methanotrophic and heterotrophic archaea. Both crenarchaeol as well as caldarchaeol showed significant ^{13}C-depletion towards the terrestrial endmember sites in the vicinity of the Rhône River delta by up to 9‰ and 12‰, respectively. Mass balance estimates suggest that soil contribution of crenarchaeol to marine sediment can reach up to 43%. This indicates that terrestrial input of archaeal lipids including their intact froms to marine sediments can be substantial and suggests caution when reconstructing such inputs based on existing molecular proxies. The isotopic analysis of core and intact archaeal lipids in our study highlights the in-situ lipid production by sedimentary archaea and provides a potential way to estimate the various archaeal lipid inputs from terrestrial, planktonic and sedimentary sources into marine sediments.

Introduction

Archaea, as one of three domains of life in addition to Bacteria and Eukaryota (Woese et al., 1990), play a pivotal role in the cycling of carbon and nutrients in marine environments (Biddle et al., 2006; Lipp et al., 2008), where their habitable zone extends from surface waters to 2.5 km below the seafloor (Inagaki et al., 2015; Trembath-Reichert et al., 2017). Membrane lipids of archaea are sensitive indicators of environmental conditions and have been widely used in paleoenvironmental and biogeochemical studies (Hinrichs et al., 1999; Elvert et al., 2000; Schouten et al., 2002; Biddle et al., 2006; Coffinet et al., 2019). Archaeal membranes primarily comprise glycerol phytanyl diethers (archaeol) and isoprenoid glycerol dibiphytanyl glycerol tetraethers (iGDGTs; e.g. caldarchaeol and crenarchaeol), both of which being ubiquitous components in marine sediments (Schouten et al., 2002; Koga and Nakano, 2008). Archaeol is a typical compound found in a wide range of Euryarchaeota including the methanogens, while caldarchaeol is the most common iGDGT in sediments. The archaeal lipids preserved in sediments are contributed by three principal sources, allochthonous input from soil, deposition from the overlying water column, and in-situ production within the sediment (Biddle et al., 2006; Schouten et al., 2013; Pearson et al., 2016). The majority of archaeal lipids reaching marine sediments are presumed to be primarily sourced from planktonic Thaumarchaeota (Sinninghe Damsté et al., 2002; Pearson et al., 2016), possibly also from Euryarchaeota (Lincoln et al., 2014). Exogenous GDGT from soil could also be very important in estuaries and location affected by riverine input. The in-situ production from benthic archaea could

possibly contribute to the lipid pool in the sediments, such as Bathyarchaeota (Biddle et al., 2006; Takano et al., 2010; Yu et al., 2018), methanogens (Brassell et al., 1981; Zhuang et al., 2016), as well as members of the recently defined, ubiquitous DPANN archaea (Castelle et al., 2018; Lipsewers et al., 2018). Due to their multiple microbial sources and overwhelming contributions to archaeal lipid pools (Pearson and Ingalls, 2013; Schouten et al., 2013; Sollai et al., 2019), archaeol and caldarchaeol are potentially useful as biomarkers that integrate bulk archaeal activity in sediments. On the contrary, crenarchaeol is taxonomically more specific and exclusively produced by chemoautotrophic, ammonia-oxidizing Thaumarchaeota (Pitcher et al., 2011; Sinninghe Damsté et al., 2012; Elling et al., 2017), which directly use bicarbonate as carbon source (Berg et al., 2007; Könneke et al., 2014). Of all the archaeal lipids preserved in sediments, those which do not possess a polar headgroup (i.e., core lipids, CL) have been considered as remnants of decayed cells (i.e., molecular fossils) thus providing information of past microbial communities and environmental conditions. In contrast, intact polar lipids (IPLs), i.e., archaeal ether lipids with headgroups, are nowadays thought to provide signals from both extant and decayed archaeal members of the deep biosphere and exogenous input (Schouten et al., 2010; Logemann et al., 2011; Lin et al., 2013; Xie et al., 2013). In addition, various sedimentary biogeochemical processes can impact the IPLs differently (Biddle et al., 2006; Meador et al., 2015).

Given the wealth of potential IPL sources and uncertainties regarding their fate in sediments, stable carbon isotopic ($\delta^{13}C$) analysis provides a promising way to unravel the microbial metabolic details and possibly can even differentiate their source organisms (Biddle et al., 2006; Schubotz et al., 2011). For example, based on the rRNA and IPL isotopic analysis, Biddle et al. (2006) suggested that heterotrophic archaea are dominant in the subseafloor. Schubotz et al. (2011) measured isotopic compositions of archaeal IPLs with different polar head groups to track the carbon flow in cold seep systems. In order to constrain the potentially differing sources of three major archaeal lipids both among different depositional settings and within the pool of core lipids (CL) versus IPLs as well as to identify potential sedimentary sources, a systematic comparison of $\delta^{13}C$ values of archaeal CL and IPL is promising but has not been carried out to date. In order to fill this gap, we determined the $\delta^{13}C$ values of the main archaeal core lipids (i.e., archaeol, caldarchaeol and crenarchaeol) and their corresponding intact derivatives combined with geochemical information in contrasting depositional regimes from

the Mediterranean and adjacent Seas. We investigated 44 sediment samples and compared $\delta^{13}C$ values of phytanes (Phy) and biphytanes (BPs) released from separated CL and IPL fractions. Samples were collected from different sedimentary regimes, including a transect from the Rhône River delta into the western Mediterranean Sea, Black Sea, Marmara Sea, and the Eastern Mediterranean Sea. A rich set of complementary geochemical data provides a robust contextual framework for the interpretation of archaeal lipid $\delta^{13}C$ values with respect to sedimentary input as well as in relation to the main marine biogeochemical reactions of sulfate reduction, anaerobic oxidation of methane and methanogenesis.

Materials and methods

Samples Collection. Sediment samples were retrieved using gravity and multi-corers during two expeditions of the DARCLIFE project (Deep subsurface Archaea: carbon cycle, life strategies, and role in sedimentary ecosystems; Fig. S1) (Zabel et al., 2011; Heuer et al., 2014). The samples from the Eastern Mediterranean Sea (GeoB15103), the Marmara Sea (GeoB15104), and the Black Sea (GeoB15105) were collected during *RV* Meteor cruise M84/1 in February 2011 (Zabel et al., 2011). Samples from the Western Mediterranean Sea (GeoB17302, GeoB17306, GeoB17307, GeoB17308) were collected during *RV* Poseidon cruise POS450 in April 2013 (Heuer et al., 2014). The sampling sites represent diverse settings including anoxic to oxic and slightly brackish to saline geochemical regimes, marine and terrestrial sediment sources, organic-rich and organic-lean sediments, as well as eutrophic and oligotrophic environments. For example, the four sites from Western Mediterranean Sea formed a terrestrial to marine transect. GeoB17306 and GeoB17307 represent the pro-delta in the proximity to the mouth of the River Rhône at a water depth of 30 m and 52 m, respectively. GeoB17308 was on the shelf, 6.3 NM west of the mouth of the River Rhône, in a water depth of 62 m. GeoB17302 is located along the preferential material transport pathway close to the northern slope of the upper Cap de Creus canyon at a water depth of 746 m (Palanques et al., 2006). After recovery, the samples were immediately frozen and stored at -80 °C until further treatment. All sediment cores are archived in the MARUM GeoB Core Repository with supporting data archived in PANGAEA-Data Publisher for Earth & Environmental Science and in a related publication (Schmidt et al., 2017).

Bulk sediment analyses and pore water analysis. Analysis of total organic carbon (TOC) content and isotopic compositions of sediment samples as well as methane and sulfate concentrations in pore water samples are described in detail by Schmidt et al. (2017). In brief, TOC content and $\delta^{13}C$ of TOC were analyzed after decalcification with 10% HCl of freeze-dried and homogenized sediment samples on a Thermo Scientific Flash 2000 elemental analyzer connected to a Thermo Delta V Plus IRMS (Thermo Fisher Scientific, Bremen, Germany). Reported TOC and corresponding $\delta^{13}C$ values represent mean values of duplicate analyses. The 1σ precision averaged over all samples was 0.1‰. Concentration of methane was measured on board (Zabel et al., 2011; Heuer et al., 2014). 3 mL of wet sediment was incubated at 60 °C for 20 min in a gas-tight glass vial. The methane concertation in the headspace was analyzed by a gas chromatograph equipped with a flame ionization detector (GC-FID, Thermo Fisher Scientific). Based on the partial pressure and headspace volume, the total amount of released methane was quantified and normalized to the pore-water volume of sediments. SO_4^{2-} was measured by ion chromatography (Metrohm Compact IC, ASupp5 column, conductivity detection after chemical suppression) following the protocols described by Lloyd et al. (2011). The $\delta^{13}C$ of dissolved inorganic carbon (DIC) in pore water was analyzed using a gas bench coupled to a Finnigan MAT 252 mass spectrometer (Thermo Fisher Scientific). Samples were prepared according to (Heuer et al., 2009), such that 100 µl of phosphoric acid were transferred to glass tubes which were subsequently sealed with butyl septa and plastic caps and purged with helium. The liquid sample was injected into the purged tubes by using a syringe. Samples were allowed to degas CO_2 from the acidified aqueous matrix for five hours before the determination of $\delta^{13}C$ of the gas phase. The precision of the analysis was less than 0.1‰ (1σ).

Lipid extraction. Freeze-dried sediment samples were extracted using a modified Bligh and Dyer method (Sturt et al., 2004). In Brief, samples were ultrasonically extracted with a mixture of DCM/MeOH/buffer (1:2:0,8; v: v: v), with a phosphate buffer at pH 7.4 for the first two steps and a trichloroacetic acid one at pH 2.0 for another two steps. The samples were extracted in two final steps with DCM/MeOH (5:1). After all extraction steps, the centrifuged supernatants were combined in a separatory funnel. The ratio of DCM/MeOH/buffer of 1:1:0.8 (v: v: v) solvent composition was adjusted by adding DCM and MilliQ water. The water phase was washed three times with DCM and then combined with the original organic phase. The

combined organic phase was washed three times with MilliQ water and gently evaporated to dryness under a stream of nitrogen and stored at -20 °C until analysis.

Lipid analysis. Archaeal lipids were analyzed by injecting an aliquot of the total lipid extract (TLE) on a Dionex Ultimate 3000 ultra-high performance liquid chromatography (UPLC) system connected to a Bruker maXis Ultra-High Resolution quadrupole time-of-flight tandem mass spectrometer (MS) with electrospray ionization (ESI). ion source operating in positive mode (Bruker Daltonik, Bremen, Germany). The MS was set to a resolving power of 27,000 at *m/z* 1222. Each analysis was mass-calibrated by loop injections of a calibration standard and correction by lock mass, leading to a mass accuracy of typically less than 1 ppm (cf.Wörmer et al., 2013; Zhu et al., 2013). Ion source and other MS parameters were optimized by infusion of standards (GDGT-0, 1G-GDGT-0, 2G-GDGT-0) into the eluent flow from the UPLC system using a T-piece. The branched isoprenoid tetraether index (BIT, Eq. 1) was calculated and serve as a proxy for the relative abundance of terrestrial OM based on the different origins of lipids (Hopmans et al., 2004).

$$\text{BIT index} = \frac{([\text{GDGT}-\text{I}]+[\text{GDGT}-\text{II}]+[\text{GDGT}-\text{III}])}{([\text{GDGT}-\text{I}]+[\text{GDGT}-\text{II}]+[\text{GDGT}-\text{III}]+[\text{Crenarchaeol}])} \quad \text{Eq. 1}$$

Separation of core and intact polar lipids. Aliquots of total lipid extract (TLE) samples were separated into apolar (containing CL) and polar (containing IPLs) fractions using preparative high-performance liquid chromatography (HPLC, Meador et al., 2014). In detail, an Inertsil Diol column (5µm, 150×10mm, GL Sciences Inc., Tokyo, Japan) was connected to an Agilent 1200 series HPLC equipped with an Agilent 1200 series fraction collector. The eluent flow was split with a ratio of 100:1 and introduced to an Agilent 6130 Single Quadrupole mass spectrometer to monitor GDGT ions (Meador et al., 2015). The flow rate was set to 3 mL min^{-1} and the eluent gradient was: 100% A to 10% B in 5 min, to 85% in 1 min, hold at 85% B for 9 min, then column re-equilibration with 100% A for 6 min, where eluent A was composed of n-hexane/2-propanol (85:15, v: v) and eluent B was 2-propanol/MilliQ water (90:10, v: v). The fraction collection time windows are from 0.1 to 5 min for the apolar fraction and from 5 to 15 min for the polar fraction. Aliquots of sample fractions were reanalyzed on the analytical

column on HPLC-qTOF-MS (Bruker, Bremen, Germany) to check the separation and purity (Wörmer et al., 2013). The carryover rate of core GDGT into IPL fraction was less than 5% of intact GDGT and thus the interference of fossil lipids with the intact lipids was minimal.

Ether cleavage and $\delta^{13}C$ analysis. Di- and tetraether lipids in fraction CL and IPL were chemically treated to convert them into their hydrocarbon derivatives (Fig. S2), Phytanes (Phy) and biphytanes (BP) by using ether cleavage (Jahn et al., 2004). In brief, 300 µl 1.0 M BBr_3 was added to individual lipid under a stream of argon. The vials were sealed and heated to 60 °C for 2 h. The resulting bromides were reduced to hydrocarbons by adding 1 ml Super-Hydride solution (1.0 M lithium triethylborohydride in tetrahydrofuran, Sigma Aldrich) under a stream of argon. Carbon stable isotopic compositions of ether cleavage derivatives were determined by gas chromatography isotope ratio mass spectrometry (GC-IRMS). Briefly, the samples were injected into the Trace GC Ultra (Thermo Finnigan) equipped with a Restek Rxi-5ms column (30m×250µm×0.25µm, Restek, Bad Homburg, Germany) coupled to a Delta V Plus IRMS via GC IsoLink connected to a ConFlow IV interface (Thermo Fisher Scientific GmbH, Bremen, Germany). The initial GC oven temperature was held at 60 °C for 1 min, increased to 150 °C at a rate of 10 °C min^{-1}, then raised to 310 °C at a rate of 4 °C min^{-1} and held at 310 °C for 40 min. The carrier gas was helium with a constant flow rate of 1.0 ml min^{-1}. The injector temperature was set at 290 °C. The oxidation oven of the combustion interface was operated at 940 °C. The precision of the duplicate analysis was ≤0.5‰ (1σ). All isotopic values are reported in the delta notation as $\delta^{13}C$ relative to the Vienna PeeDee Belemnite (VPDB) Standard.

Results

Environmental and geochemical conditions

The geochemical and environmental conditions at the sampling sites are described in detail in Schmidt et al. (Schmidt et al., 2017). In brief, sediments were sampled from different sediment depths ranging from the surface down to a maximum of 6.35 m bsf (below seafloor), including diverse environmental and geochemical conditions. The coring sites (GeoB17306-8) at Western Mediterranean Sea have high sedimentation rates (Marion et al., 2010) and are largely

affected by terrestrial organic matter input (Rhône River). Due to the high sedimentation rates, the collected sediments from the Western Mediterranean Sea are relatively young (less than 1.7 ky, Table S1), have a high TOC content, and comparably negative $\delta^{13}C_{TOC}$ values (Fig. 1, Table S1). In contrast, the Eastern Mediterranean is an ultra-oligotrophic marine basin with low primary productivity and thus low sedimentation rates. The 5.67 m core collected from Eastern Mediterranean Sea covered the past 173 ky containing alternating periods of inherently different depositional regimes. Organic-carbon-poor sediments (TOC content of < 0.5 wt%) are periodically interspersed with dark, organic-rich layers (up to 4.3 wt%), known as sapropels. The sapropel samples in this study were also sampled from Marmara Sea (S1) and Black Sea (S1) in addition to Eastern Mediterranean Sea (S1, S3, S5, S6). Moreover, lacustrine sediments were also collected below the Sapropel layer of Marmara Sea and Black Sea cores. At each sampling location, three types of geochemical zonations were classified based on the profiles of CH_4 and SO_4^{2-} concentrations as well as $\delta^{13}C$ of dissolved inorganic carbon ($\delta^{13}C_{DIC}$) (Figs. S3 to S9). Main geochemical zonations are SRZ (sulfate reduction zone; n = 27), SMTZ (sulfate-methane transition zone; n = 8), and MGZ (methanogenesis zone; n = 9; Fig. 1, 2). Here we present the lipid isotopic data in the order of marine to terrestrial-affected sedimentation, which can be identified by the $\delta^{13}C_{TOC}$ values (Fig. 1 and Fig. 2).

Archaeal lipid composition

GDGT-0 and Crenarchaeol are the dominant tetraether components in CLs. The CL-GDGTs detected in the samples mainly include GDGT-0 to -4 and crenarchaeol. The concentrations of CL-GDGTs ranged from 33.6 to 58000 ng/g sed dw (Table S2). Phytane (Phy) is primarily derived from archaeol and partly from OH-archaeol, and methoxy (MeO) -archaeol (Sprott et al., 1993; Elvert et al., 1999; Hinrichs et al., 2000). The concentrations of CL-archaeol ranged from 0.4 to 551.3 ng/g sed dw. The detected IPL-GDGTs in this study consist of monohexose (MH)-, dihexose (DH)-, trihexose (TH), and hexose-phosphohexose (HPH)-GDGTs. IPL-GDGTs ranged from 6.7 to 5200 ng/g sed dw. IPL-archaeols mainly occur as MH- and DH- archaeol and ranged from 0.5 to 449.9 ng/g sed dw. The terrestrial-affected Western Mediterranean Sea and oligotrophic horizons from Eastern Mediterranean Sea have relatively low GDGT concentrations while the sapropel horizons from the Eastern Mediterranean Sea have the highest concentrations.

Archaeal lipid stable carbon isotopic composition

The stable carbon isotopic composition of most archaeal lipids cannot be measured directly by conventional GC methods because they are non-volatile high molecular weight compounds. Measurements thus rely on the analysis of the GC-amenable products of the ether cleavage reaction (BPs and Phy, see Fig. S2 for structures). BP0 could be derived from multiple sources, such as GDGT-0, -1 as well as BDGTs (butanetriol dialkyl glycerol tetraethers). Crenarchaeol possesses one biphytane moiety containing two cyclopentane moieties and a cyclohexane moiety (hereafter BPcren, see Fig. S2) (Sinninghe Damsté et al., 2002). $\delta^{13}C_{CL\text{-}BP0}$ varied from -19.4‰ to -20.7‰ in sapropel horizons and -22.1‰ to -25.6‰ in oligotrophic horizons in the Eastern Mediterranean Sea sediments (GeoB15103, Fig. 1). The corresponding $\delta^{13}C_{IPL\text{-}BP0}$ values ranged from -22.2‰ to -23.7‰ in sapropel horizons and -22.3‰ to -26.3‰ in oligotrophic horizons. $\delta^{13}C_{IPL\text{-}BP0}$ values from oligotrophic samples were similar to $\delta^{13}C_{CL\text{-}BP0}$, however, the $\delta^{13}C_{IPL\text{-}BP0}$ value was on average 3‰ more negative than $\delta^{13}C_{CL\text{-}BP0}$ in sapropel horizons. In samples from the Marmara Sea (GeoB15104), $\delta^{13}C_{CL\text{-}BP0}$ and $\delta^{13}C_{IPL\text{-}BP0}$ varied from -19.9‰ to -23.3‰ and -21.0‰ to -25.0‰, respectively. $\delta^{13}C_{IPL\text{-}BP0}$ values are more negative than $\delta^{13}C_{CL\text{-}BP0}$ throughout the core with an average 1.5‰ offset. $\delta^{13}C_{CL\text{-}BP0}$ in the Black Sea (GeoB15105) ranged from -21.1‰ to -24.3‰, with an average of -22.4‰. $\delta^{13}C_{IPL\text{-}BP0}$ ranged from -21.7‰ to -26.4‰, with an average of -24.4‰. A ca. 2‰ offset between $\delta^{13}C_{IPL\text{-}BP0}$ and $\delta^{13}C_{CL\text{-}BP0}$ was also observed in Black Sea. In sediments collected along a transect from the Rhône River Delta to the Cap de Creus Canyon (GeoB17302, GeoB17306, GeoB17307, GeoB17308), $\delta^{13}C_{CL\text{-}BP0}$ varied from -19.9‰ to -32.0‰, with most negative $\delta^{13}C$ values detected in the terrestrial-influenced Rhône River Delta samples. Similarly, $\delta^{13}C_{IPL\text{-}BP0}$ varied from -20.9‰ to -37‰ along the transect in the western Mediterranean Sea. The offset between $\delta^{13}C_{IPL\text{-}BP0}$ and $\delta^{13}C_{CL\text{-}BP0}$ was 2.6 ‰ on average and differed among three geochemical zones (Table 1). The offset was largest in sediments from the SMTZ with an average offset of 4‰ ±1.8, while the SRZ and MGZ had smaller offsets with average values of 1.9‰ and 1.2‰, respectively.

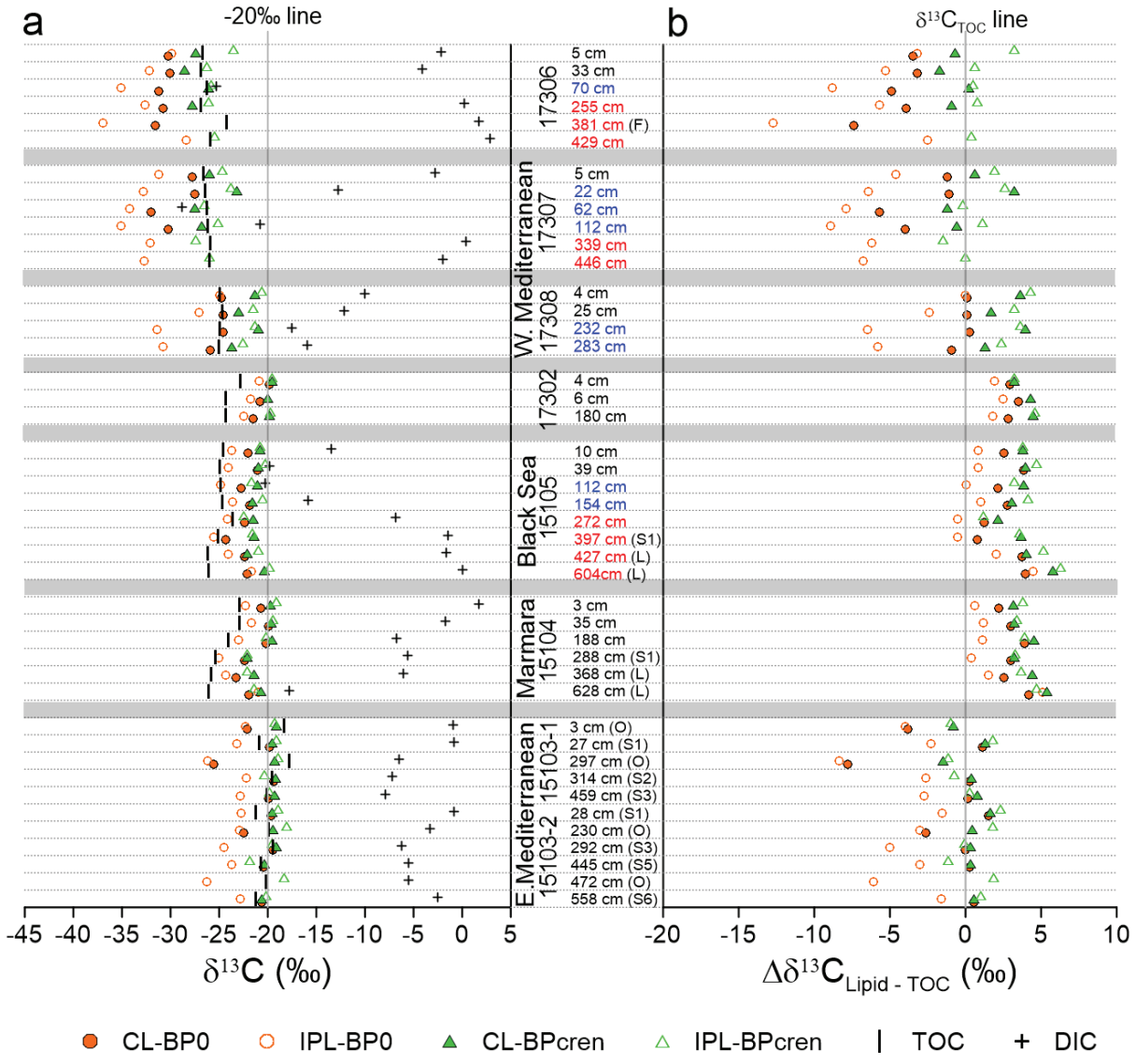

Fig. 1. Downcore profiles of (a) stable carbon isotopic compositions of CL and IPL GDGTs, $\delta^{13}C_{DIC}$, and $\delta^{13}C_{TOC}$ and (b) $\Delta\delta^{13}C_{Lipid\text{-}TOC}$ from the East and West Mediterranean Sea, Marmara Sea, and Black Sea. The lipid isotopic compositions are in the form of $\delta^{13}C$ values of biphytanes (BP0 and BPcren) released from archaeal CL and IPL GDGTs. $\Delta\delta^{13}C_{Lipid\text{-}TOC}$ is defined as the difference between $\delta^{13}C$ values of biphytanes and $\delta^{13}C_{TOC}$. Different geochemical zones are indicated by the color of the depth number with black representing samples from the sulfate reduction zone, blue samples from the sulfate-methane transition zone, and red samples from the methanogenic zone. F: flood event; L: lake sediments; S: sapropel; O: deposition under oligotrophic conditions. The grey shaded bars are used to separate sample sites.

Table 1. Average values of $\delta^{13}C_{DIC}$, $\delta^{13}C_{CL\text{-}BP0}$, $\delta^{13}C_{IPL\text{-}BP0}$, and $\Delta\delta^{13}C_{BP0}$ in the three biogeochemical zones.

Zonation	$\delta^{13}C_{DIC}$	$\delta^{13}C_{CL\text{-}BP0}$	$\delta^{13}C_{IPL\text{-}BP0}$	$\Delta\delta^{13}C_{BP0}$
SRZ (n = 26)	-6.2 ± 5.3	-22.3 ± 3.1	-24.3 ± 2.9	-1.9 ± 1.4
SMTZ (n =8)	-19.6 ± 5.3	-27.0 ± 3.9	-31.0 ± 4.5	-4.0 ± 1.8
MGZ (n = 5)	-0.7 ± 2.8	-25.6 ± 4.4	-27.6 ± 5.1	-1.2 ± 1.9

In samples from the Eastern Mediterranean, Marmara, and Black Seas, $\delta^{13}C_{CL\text{-}BPcren}$ and $\delta^{13}C_{IPL\text{-}BPcren}$ values were highly similar and showed a relatively narrow range from -18.1‰ to -22.4‰ with only minor downcore variations (Fig. 1). Along the terrestrial to marine transect in the Western Mediterranean Sea, $\delta^{13}C_{CL\text{-}BPcren}$ and $\delta^{13}C_{IPL\text{-}BPcren}$ also followed similar trends but values showed a wider range from -19.6‰ and -28.6‰. Similar to BP0, the most negative BPcren $\delta^{13}C$ values for both core and intact pools were found in the terrestrial-influenced Rhône River Delta. However, downcore $\delta^{13}C$ values of crenarchaeol were invariant at the different sites and thus not affected by geochemical zones.

The isotopic compositions of BP1 and BP2 could only be obtained from a few samples from the Eastern Mediterranean, Marmara, and Black Seas (Table S3), but not in any of the samples from the Western Mediterranean because they were below the detection limit of our instrument. Where available, the stable carbon isotopic composition of BP1 and BP2 was highly similar for both intact and core lipid pools and little downcore variations or variations between sites were observed. The $\delta^{13}C$ values ranged from -17.4‰ to 23.0‰ and were similar to BPcren.

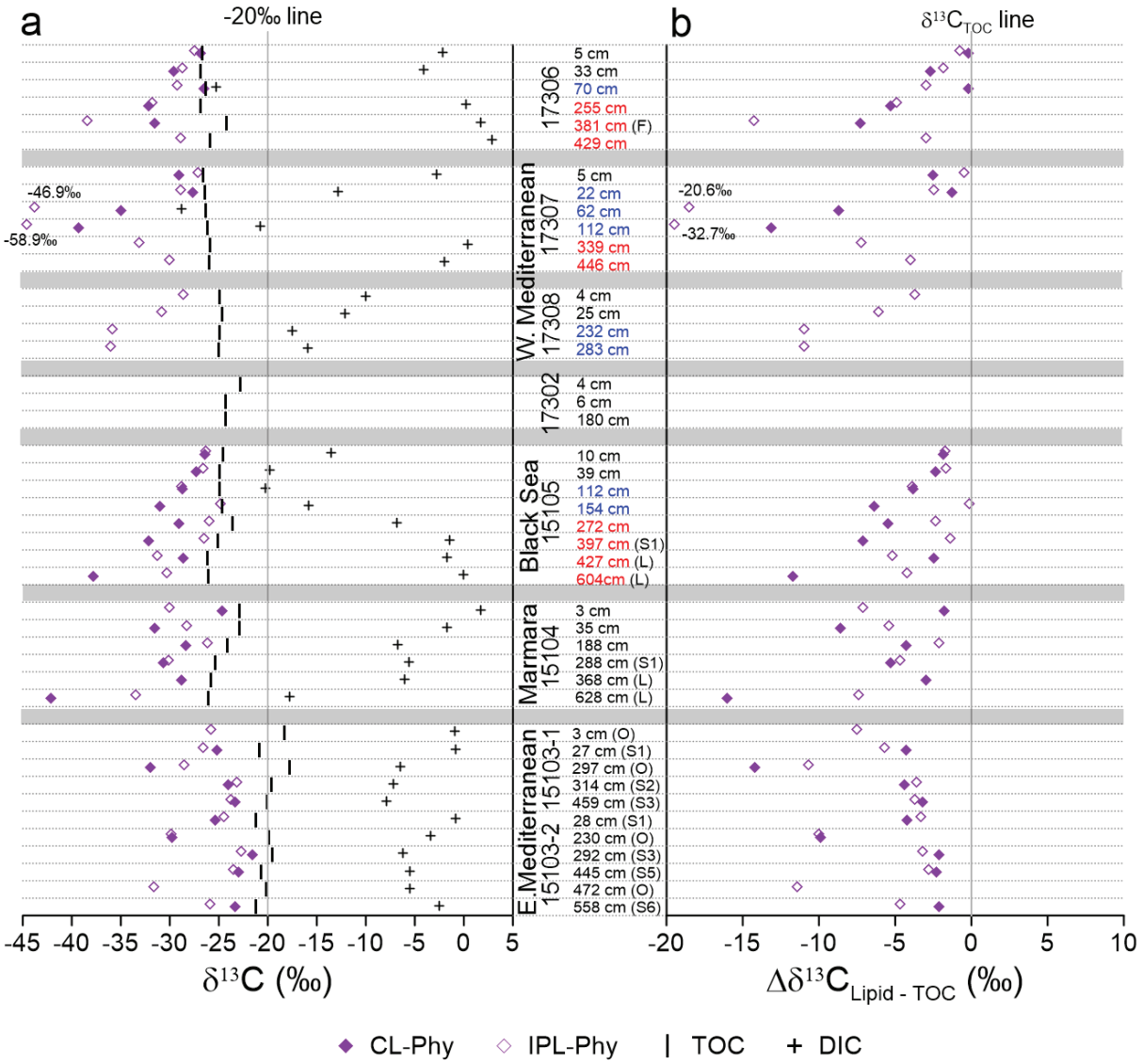

Fig. 2. Downcore profiles of (a) stable carbon isotopic compositions of CL and IPL archaeol, $\delta^{13}C_{DIC}$, and $\delta^{13}C_{TOC}$ and (b) $\Delta\delta^{13}C_{Lipid\text{-}TOC}$ from the East and West Mediterranean Sea, Marmara Sea, and Black Sea. The lipid isotopic compositions are in the form of $\delta^{13}C$ values of phytane (Phy) released from archaeal CL and IPL archaeol. $\Delta\delta^{13}C_{Lipid\text{-}TOC}$ is defined as the difference between $\delta^{13}C$ values of phytane and $\delta^{13}C_{TOC}$. Different geochemical zones are indicated by the color of the depth number with black representing samples from the sulfate reduction zone, blue samples from the sulfate-methane transition zone, and red samples from the methanogenic zone. F: flood event; L: lake sediments; S: sapropel; O: deposition under oligotrophic conditions. The grey shaded bars are used to separate sample sites.

The stable carbon isotopic composition of the core and intact archaeol-derived phytanes could be obtained from almost all samples (Fig. 2) except Cap de Creus Canyon (GeoB17302) and

some samples from Gulf of Lion. In general, the $\delta^{13}C_{CL\text{-}Phy}$ and $\delta^{13}C_{IPL\text{-}Phy}$ showed a wide range between -21.6‰ and -58.9‰ with lowest values for $\delta^{13}C_{IPL\text{-}Phy}$ in samples from the SMTZ in the distal Rhône River Delta. In the Western Mediterranean Sea, $\delta^{13}C_{CL\text{-}Phy}$ varied from -26.9‰ to -39.3‰ and $\delta^{13}C_{IPL\text{-}Phy}$ from -27.5‰ to -58.9‰. In the Eastern Mediterranean, $\delta^{13}C_{CL\text{-}Phy}$ and $\delta^{13}C_{IPL\text{-}Phy}$ values were between -21.6‰ and -32.0‰, with the lower values typically occurring in the organic-poor horizons. Samples from the Marmara Sea and the Black Sea showed $\delta^{13}C_{CL\text{-}Phy}$ values varying from -24.7‰ to -42.1‰ and -26.4‰ to -37.8‰, respectively, which were overall more negative than $\delta^{13}C_{IPL\text{-}Phy}$ with values ranging from -26.2‰ to -33.5‰ and -24.8‰ to -31.3‰, respectively.

Discussion

Isotopic offset between caldarchaeol CL and IPLs indicate sedimentary archaeal activity

After cell death, the polar headgroup of archaeal IPLs is eventually cleaved off to form CLs (Sturt et al., 2004; Lipp et al., 2008; Liu et al., 2011). Recent studies have demonstrated that for archaeal glycosidic IPLs this degradation step may require geological timescales (Schouten et al., 2010; Xie et al., 2013). We sought to elucidate the relative contributions of allochthonous fossil input versus in-situ IPL production by active sedimentary archaea by comparing the $\delta^{13}C$ values of CL and IPLs in different depositional settings. In general, $\delta^{13}C$ of lipids depends on the $\delta^{13}C$ of the carbon source used for cell growth as well as the carbon fixation pathway. For example, in the SRZ, sulfate reduction is coupled to OM fermentation, which results in the availability of low-molecular-weight organic compounds such as formate and acetate; these compounds may stimulate the growth of heterotrophic bacteria and archaea (Sørensen et al., 1981; Heuer et al., 2009). Lipids produced from these carbon sources will show $\delta^{13}C$ values similar to $\delta^{13}C_{TOC}$. The most striking isotopic excursion is expected to be observed in SMTZ due to the metabolism of ^{13}C-depleted methane and intense assimilation of DIC produced thereof via the anaerobic oxidation of methane (AOM) (Wegener et al., 2008; Kellermann et al., 2012; Meador et al., 2015). However, it has been shown that archaea not related to AOM are active in SMTZ (Biddle et al., 2006; Sorensen and Teske, 2006; Yoshinaga et al., 2015). Such post-depositional productions have the potential to alter the isotopic compositions of the IPL pool, and due to their degradation or *de novo* production of CLs (Evans et al., 2019) also the CL pool. The magnitude of isotopic change of the archaeal CL pool induced by IPL

degradation depends on the size of the CL pool as well as degradation rate of IPLs. We found that caldarchaeol-based IPLs were depleted in ^{13}C relative to the corresponding CL caldarchaeol on average by 2.6‰. This isotopic difference ($\Delta\delta^{13}C_{BP0} = \delta^{13}C_{IPL\text{-}BP0} - \delta^{13}C_{CL\text{-}BP0}$) indicates that the archaeal sources of caldarchaeol CL and IPLs are different, most probably due to the contribution of active sedimentary archaea to the latter pool.

To further investigate the factors that determine $\Delta\delta^{13}C_{BP0}$, we performed a principal component analysis (PCA, Fig. 3) of the lipid isotopic patterns and other geochemical data, including TOC content, $\delta^{13}C_{TOC}$, $\delta^{13}C_{DIC}$, NH_4^+, IPL/(IPL + CL), and sediment age (Table S1). Five principal components (PC) explained > 90% of the variance. PC1 explained most variances of $\delta^{13}C_{TOC}$, NH_4^+, IPL/(IPL + CL), and age. These variables are strongly related to the influence of the high terrestrial input and high microbial activity in Rhône River deltaic sediments. $\Delta\delta^{13}C_{BP0}$ has the highest loading on PC2 where the loading of TOC content is also high. Further comparison showed the good correlation of $\Delta\delta^{13}C_{BP0}$ with TOC in sediments from the SRZ (Fig. 4; $R^2 = 0.42$, $p < 0.01$). This relationship is consistent with a dependency of in-situ production of caldarchaeol from TOC concentration; this caldarchaeol is ^{13}C depleted relative to that sourced from marine Thaumarchaeota. Moreover, the dependency of TOC in the SRZ suggests that heterotrophic activity is primarily responsible for caldarchaeol production. Our finding is thus consistent with previous studies that invoked organic matter mineralization by benthic archaea (Biddle et al., 2006), which is further supported by strong correlation between TOC content and the abundance of sedimentary Bathyarchaeota ((Biddle et al., 2006; Yu et al., 2017) formerly known as Miscellaneous Crenarchaeotal Group, MCG), i.e., one of the most prominent groups of benthic archaea in marine sediments around the world.

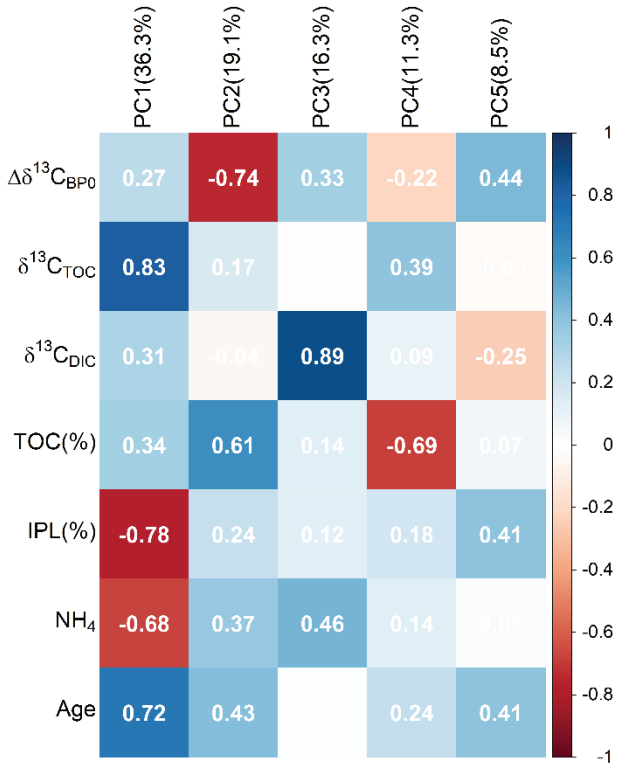

Fig. 3. The contribution of each variable to different principal components of PCA analysis. Five principal components explain > 90% of the variance among $\Delta\delta^{13}C_{BP0}$ (= $\delta^{13}C_{IPL\text{-}BP0}$ - $\delta^{13}C_{CL\text{-}BP0}$), TOC content, $\delta^{13}C_{TOC}$, $\delta^{13}C_{DIC}$, NH_4^+ concentration, IPL content, and age. The PCA analysis was performed by using FactoMineR package in R. The numbers in the plot mean the correlation, [-1, 0) means negatively related; (0, 1] means positively related. 0 means non-related.

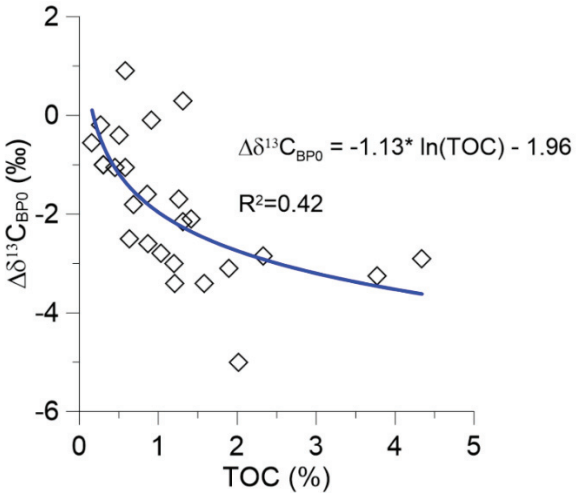

Fig.4. Relationship of TOC content to $\Delta\delta^{13}C_{BP0}$ in samples from the SRZ (n = 26, $\delta^{13}C_{CL\text{-}BP0}$ is not available in GeoB15103-2-472cm).

$\delta^{13}C_{DIC}$ values are much more negative in the SMTZ than in horizons around it (Table 1). This is caused by the production of ^{13}C-depleted DIC by anaerobic methane-oxidizing archaea (ANME) (Yoshinaga et al., 2014; Wegener et al., 2016b). Compared to the average $\Delta\delta^{13}C_{BP0}$ of -1.9‰ from SRZ, SMTZ has an average $\Delta\delta^{13}C_{BP0}$ value of -4‰ (Table 1). This higher offset is consistent with the input of IPLs from AOM-related archaeal communities. However, the relatively small ^{13}C-depletion of caldarchaeol IPL suggests only a minor contribution of IPLs by methanotrophic archaea in our sample set. If we assume that biphytane lipids of methanotrophic archaea have $\delta^{13}C$ values of -92‰ (Michaelis et al., 2002), a 2‰ deviation in $\delta^{13}C$ from a planktonic archaeal end member in $\delta^{13}C_{BP0}$ of -20‰ will be reached by a small contribution of BP0 from archaeal methanotrophs of only 2.8%. When looking in sediments of the MGZ, both $\delta^{13}C_{IPL\text{-}BP0}$ and $\delta^{13}C_{CL\text{-}BP0}$ values are more positive than those in the corresponding SMTZ. In addition, $\Delta\delta^{13}C_{BP0}$ was -1.2‰ on average and this value is larger than SMTZ (-4.0‰, Table 1). If we assume the fluxes of sulfate and methane have remained in a steady state, the depth of the SMTZ should be constant and moving steadily with sedimentation. The deeper sediment which used to belong to SMTZ in history but now is regarded as MGZ does not preserve the ^{13}C-depleted archaeal lipids. Our data thus suggest that ^{13}C-depleted archaeal lipids from the SMTZ are degraded more quickly than the time required for deposition of 200 cm of sediment, or roughly within 5.3 to 15.4 years in the Rhône River Delta based on the sedimentation rates (Miralles et al., 2005; Schmidt et al., 2017).

Soil input instead of in-situ production drives the stable carbon isotopic compositions of crenarchaeol

Crenarchaeol is presumably exclusively derived from Thaumarchaeota, which inhabit both the marine water column and terrestrial soils (Sinninghe Damsté et al., 2012; Stahl and de la Torre, 2012; Elling et al., 2017). The isotopic compositions of crenarchaeol did not significantly differ between the CL and IPL pool (t-test between $\delta^{13}C_{CL\text{-}BPcren}$ and $\delta^{13}C_{IPL\text{-}BPcren}$; $P = 0.89$). Furthermore, $\delta^{13}C_{IPL\text{-}BPcren}$ did not track the large variations of in-situ $\delta^{13}C_{DIC}$. This indicates that the biphytane moieties of intact crenarchaeol are not newly synthesized and are remnants of former sedimentary input. There are two possible explanations: they either represent fossil IPLs (Schouten et al., 2010; Xie et al., 2013) or are products of crenarchaeol recycling by

sedimentary archaea (Takano et al., 2010; Lipsewers et al., 2018). IPL crenarchaeol consist of dominantly 1G- and 2G-crenarchaeol in our samples. These IPL crenarchaeol with glycosidic head groups may be well preserved in sediments for hundreds of thousands of years (Schouten et al., 2010; Xie et al., 2013). In situ SIP experiment of marine sediments showed that the glycerol unit of crenarchaeol is synthesized de novo, whereas the isoprenoid unit is synthesized from relic archaeal membranes and detritus (Takano et al., 2010).

Exogenous iGDGT input to sediments is common in shallow or marginal marine environments (Pearson et al., 2016). However, its effect on the isotopic compositions of archaeal lipids in marine sediments has not been well constrained. Based on the $\delta^{13}C$ values of biphytanes along the transect from the northern slope of the upper Cap de Creus Canyon the to proximal Rhône River delta we observed a strong negative change of CL carbon isotopic compositions from pelagic to shelf environments. $\delta^{13}C_{CL\text{-}BP0}$ and $\delta^{13}C_{CL\text{-}BPcren}$ shifted from -19.9‰ to -32.0‰ and from -19.6‰ to -28.6‰, respectively (Fig. 1). This pattern highlights a substantial terrigenous iGDGT component that is ^{13}C-depleted relative to common planktonic sources. To calculate the relative contribution of terrigenous iGDGTs to marine sediments, we compared the $\delta^{13}C$ values of the different iGDGT classes with the commonly used BIT index from our samples (Fig. 5, Table. S4). For the Rhône River affected samples, the BIT index does not correlate well with $\delta^{13}C_{TOC}$ (Fig. 5; $R^2 = 0.51$) as similarly identified before for samples from a Norwegian fjord (Huguet et al., 2007) but nicely with $\delta^{13}C_{CL\text{-}BPcren}$ ($R^2 = 0.88$) and $\delta^{13}C_{CL\text{-}BP0}$ ($R^2 = 0.89$). This might be due to similar transport and structural behavior during degradation of iGDGTs and soil-derived branched GDGTs compared to bulk $\delta^{13}C_{TOC}$ as a general recorder of terrestrial input that includes waxes, lignin, and other pre-aged organic matter. The correlation is equally strong for $\delta^{13}C_{IPL\text{-}BPcren}$ ($R^2 = 0.88$), but less so for $\delta^{13}C_{IPL\text{-}BP0}$ ($R^2 = 0.55$). The poorer correlation is based on the much lower $\delta^{13}C_{IPL\text{-}BP0}$ values compared to $\delta^{13}C_{TOC}$ and is likely influenced by a portion of caldarchaeol being derived from in-situ production in the sediment either through anaerobic methanotrophy or methanogenesis (see below). Likewise, the steeper slope in $\delta^{13}C_{CL\text{-}BP0}$ relative to $\delta^{13}C_{CL\text{-}BPcren}$ (Fig. 5) is consistent with the impact of sedimentary production of caldarchaeol on the isotopic composition of the CL pool, either by degradation of IPLs or *de novo* production of CL caldarchaeol, which was observed during

radioisotope labeling experiments with sediments from the Rhône River delta location (Evans et al., 2019).

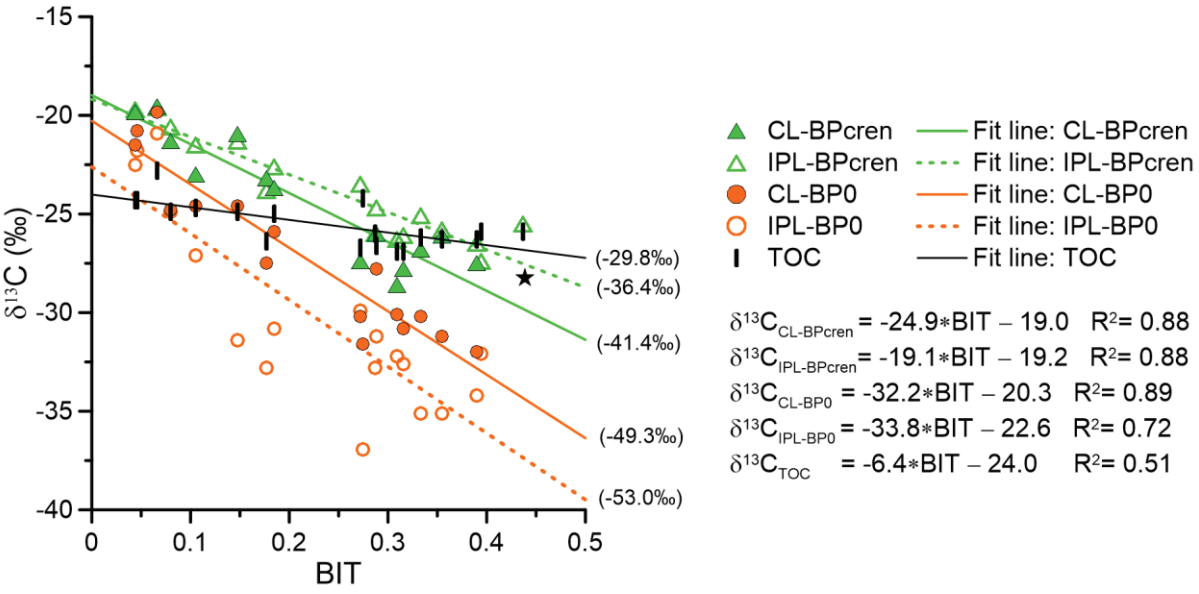

Fig. 5. Relationship of BIT to $\delta^{13}C_{TOC}$, $\delta^{13}C_{CL\text{-}BPcren}$, $\delta^{13}C_{IPL\text{-}BPcren}$, $\delta^{13}C_{CL\text{-}BP0}$, and $\delta^{13}C_{IPL\text{-}BP0}$ along the transect from the Rhône River Delta (more negative $\delta^{13}C$ values) to the Cap de Creus Canyon (less negative $\delta^{13}C$ values). The black star symbol represents $\delta^{13}C_{IPL\text{-}BP0}$ of one sample and was not included in the fitting line. The values in the brackets indicate the soil endmember values when BIT value is 0.9.

Based on the linear regression, the marine endmember (BIT = 0) of CL-crenarchaeol would have a $\delta^{13}C$ value of -19.0‰, which fits well with the expected fractionation by ammonia-oxidizing archaea assuming $\delta^{13}C_{DIC}$ = 0‰ (Könneke et al., 2012; Pearson et al., 2016). When a soil average BIT = 0.9 is applied (Schouten et al., 2013), the terrestrial end-member of CL-crenarchaeol would have a value of -41.4‰ (Fig. 5), which is lower than that of former reports of -30.4‰ in soils (Weijers et al., 2010; Lu et al., 2013) and -36.7‰ in a wetland (Segarra et al., 2015) but realistic given the variance of input data of the correlation and unknown $\delta^{13}C_{DIC}$ values in the upstream river soils. Calculating the relative contribution of soil-derived CL-crenarchaeol in Rhône River delta sediments via isotope mass balance (Eq. 2) we obtain an input between 2.5% and up to 42.9% (mean = 22.8%), which is decreasing as predicted from the most terrestrial-influenced proximal Rhône River site along the material transport pathway in the Gulf of Lions down to the Cap de Creus Canyon.

$$\delta^{13}C_{CL-BPcren} = X \times (-41.4) + (1 - X) \times (-19.0) \quad \text{Eq. 2}$$

Similar to crenarchaeol, the marine endmember of caldarchaeol would have a $\delta^{13}C$ value of -20.3‰. The respective extrapolation yields a corresponding soil endmember with a $\delta^{13}C$ value of -49.3‰ and is much lower than the corresponding value for crenarchaeol. If the archaeal sources of the caldarchaeol hypothetical caldarchaeol soil endmember would be identical to those of the corresponding crenarchaeol endmember, we would expect a nearly identical isotopic composition. Consequently the low caldarchaeol endmember value must reflect additional input of ^{13}C-depleted caldarchaeol by (i) terrestrial soil archaea and/or (ii) in-situ methanogenesis based on high inputs of terrestrial OM in the marine sediments (Zhuang et al., 2018; Evans et al., 2019). Nontheless, due to the undefined isotopic compositions of the low caldarchaeol endmember, the qutification of their contribution is not available.

In contrast to the Western Mediterranean Sea, the influence of terrestrial input on the $\delta^{13}C$ values of caldarchaeol and crenarchaeol in the Black Sea, the Marmara Sea and the sapropel samples in the Eastern Mediterranean Sea is negligible because $\delta^{13}C$ values are very close to the marine end member of -20‰. This result is contrasting to the $\delta^{13}C_{TOC}$ values indicating a substantial terrestrial input in the sediments of the Black Sea and the Marmara Sea (Fig.1). Presumably terrestrial archaeal lipid input is masked by high production of planktonic archaeal lipids in the overlying water column.

Multiple microbial sources contribute to the archaeol pool in sediments

Archaeols are ubiquitous archaeal lipids in the natural environment as well as in pure archaeal cultures (Hinrichs et al., 1999; Koga and Morii, 2005; Elling et al., 2017). The most striking result to emerge from our data is that both archaeol CL and IPLs are apparently depleted in ^{13}C relative to TOC, with $\delta^{13}C$ values being lowered by 0.2 to 32.7‰ (Fig. 2). $\delta^{13}C_{IPL\text{-}Phy}$ values are also lower than $^{13}C_{DIC}$ by up to 40.2‰. Compared to caldarchaeol and crenarchaeol, archaeol exhibited no regular isotopic patterns. The divergent range of isotopic relationships of archaeol relative to TOC and DIC is consistent with a mixture of multiple water column and post-depositional sources, which include chemolithoautotrophic (Pearson et al., 2016),

heterotrophic (Biddle et al., 2006), methanotrophic (Blumenberg et al., 2004), and hydrogenotrophic and acetoclastic methanogenic archaea (Summons et al., 1998). For example, the largest isotopic offset between archaeol and TOC (-32.7‰) occurred in SMTZs, where the ^{13}C-depleted signature was also imparted to the fossil pool (i.e., $\delta^{13}C_{CL\text{-}Phy}$; Fig. 2). $\delta^{13}C_{CL\text{-}Phy}$ values in Black Sea and Marmara Sea sediments were among the lowest (-41.5‰ and -37.8‰, respectively), and, in some horizons, were more negative by up to 9‰ than $\delta^{13}C_{IPL\text{-}Phy}$. This finding implies rapid turnover of labile, ^{13}C-depleted archaeol IPLs which were probably produced by methane-metabolizing archaea in Black Sea and Marmara Sea sediments. Thus, observed $\delta^{13}C_{CL\text{-}Phy}$ values here represent a signal of fossil IPLs that have been degraded over time. In conclusion, the stable carbon isotopic composition of archaeol CL and IPLs in sediments responds to inputs by benthic communities and due to its low input from the water column a more sensitive recorder of active microbial metabolism than caldarchaeol and crenarchaeol.

ACKNOWLEDGMENT. We are grateful to the crew and the scientific shipboard party of the FS Meteor cruise M84-1 (DARCSEAS) and FS Poseidon cruise POS450 (DARCSEAS II). Wendt Jenny, Prieto Xavier, and Taubner Heidi are thanked for supporting sampling and instrumental analyses. We further thank Weichao Wu and Felix J. Elling for providing constructive feedback to an earlier version of the manuscript. This study was funded by the European Research Council under the European Union's Seventh Framework Programme-Ideas Specific Programme; by ERC grant agreement No.247153 (Advanced Grant DARCLIFE; principal investigator, K.-U.H.); Deutsche Forschungsgemeinschaft (DFG) through the Gottfried Wilhelm Leibniz Prize, awarded to K.-U.H. (Hi 616-14-1); by DFG under Germany's Excellence Strategy, no. EXC-2077–390741603. Qing-Zeng Zhu was sponsored by the Chinese Scholarship Council (CSC) and the Bremen International Graduate School for Marine Sciences (GLOMAR).

Supplementary material

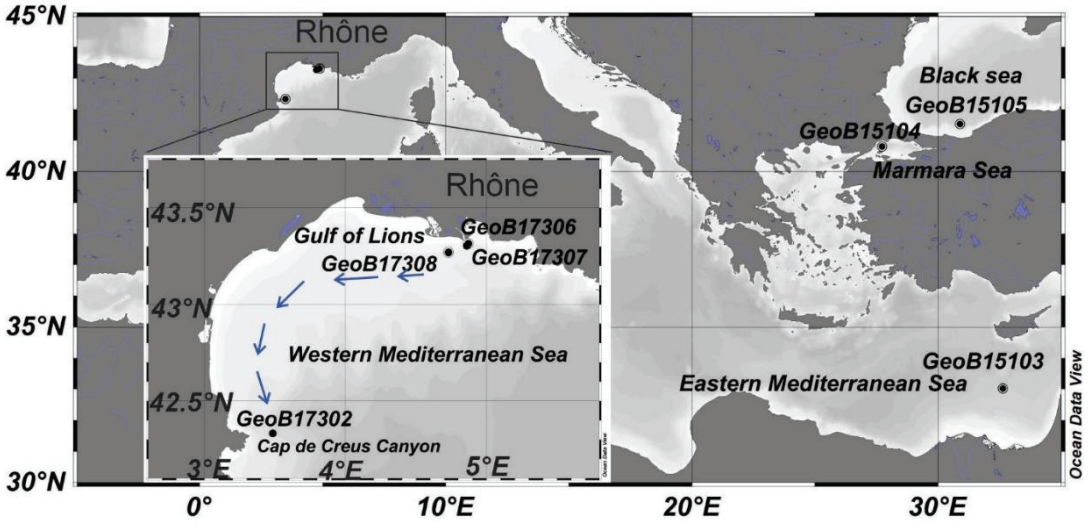

Fig. S1 Map of sampling locations in Mediterranean Sea, Marmara Sea and Black Sea. Arrow indicates preferential material transport pathways in the Gulf of Lions. Map was drawn with the help of Ocean data view software.

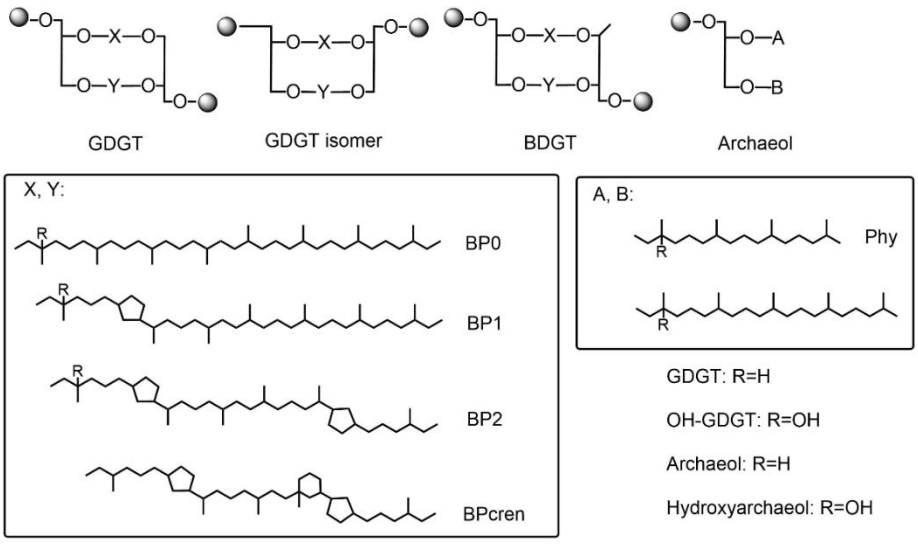

GDGTstructure	X	Y
GDGT-0/BDGT-0	BP0	BP0
GDGT-1/BDGT-1	BP0	BP1
GDGT-2	BP1	BP1
GDGT-3	BP1	BP2
GDGT-4	BP2	BP2
Crenarchaeol	BP2	BPcren

Fig. S2 Structures of the GDGT, BDGT and archaeol and their associated biphytanes (BPs) and phytane (Phy)

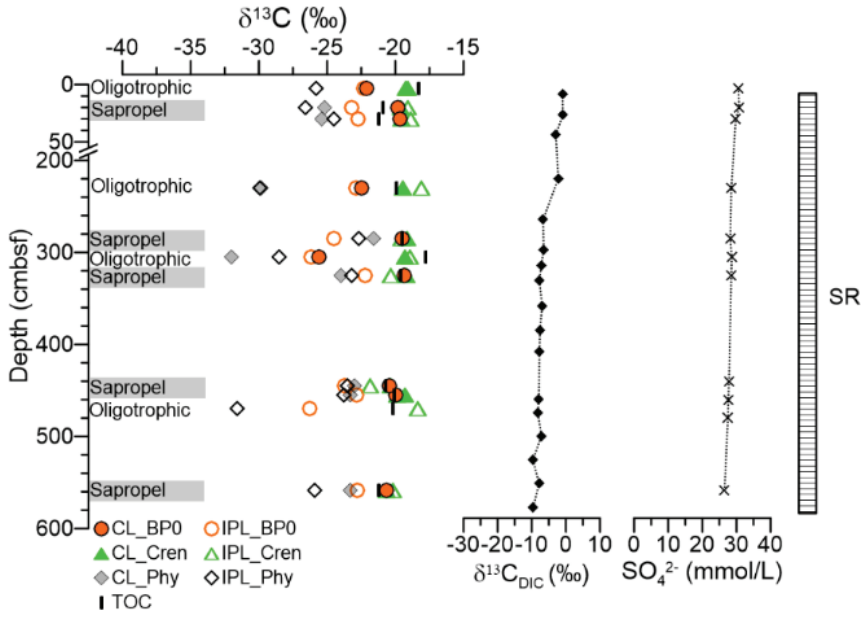

Fig. S3. Eastern Mediterranean Sea (GeoB15103): $\delta^{13}C$ values of phytanyl moieties released from CL and IPL archaeal diethers; $\delta^{13}C$ values of biphytanyl (BP0 and BPcren) moieties released from CL and IPL GDGTs. The depth profile of TOC and DIC isotopic compositions and sulfate concentrations. SR: sulfate reduction zone.

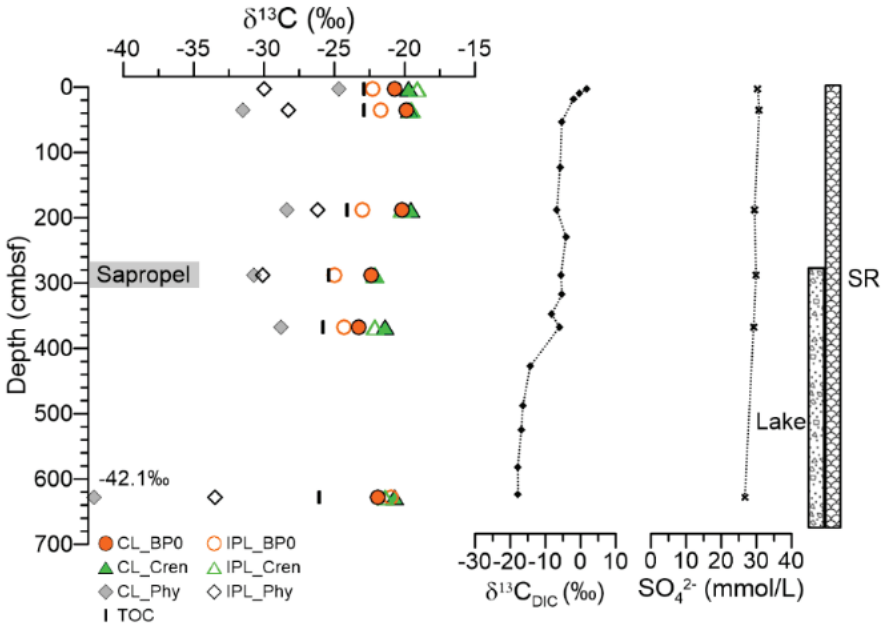

Fig. S4. Marmara Sea (GeoB15104): $\delta^{13}C$ values of phytanyl moieties released from CL and IPL archaeal diethers; $\delta^{13}C$ values of biphytanyl (BP0 and BPcren) moieties released from CL and IPL GDGTs. The depth profile of TOC and DIC isotopic compositions and sulfate concentrations. SR: sulfate reduction zone.

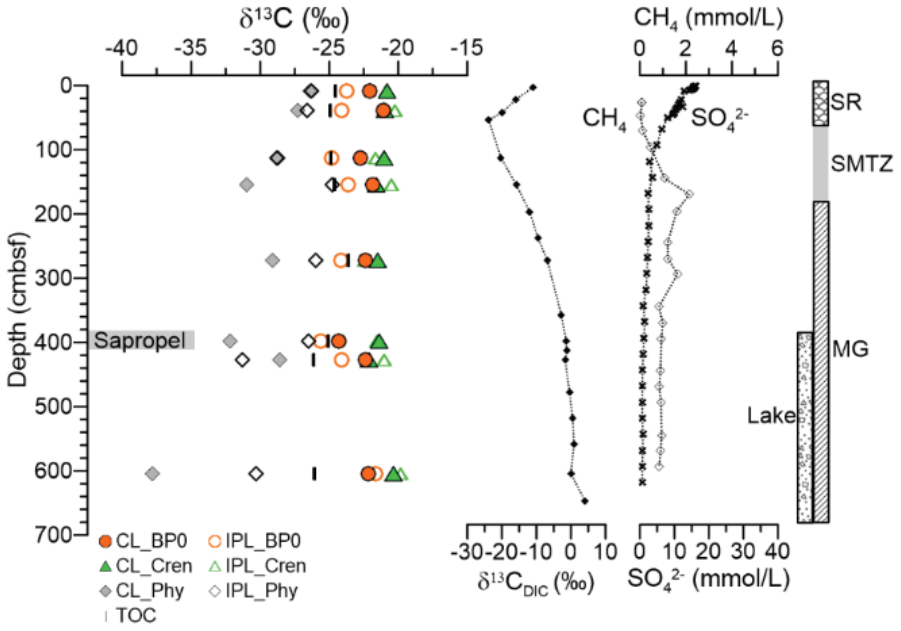

Fig. S5. Black Sea (GeoB15105): $\delta^{13}C$ values of phytanyl moieties released from CL and IPL archaeal diethers; $\delta^{13}C$ values of biphytanyl (BP0 and BPcren) moieties released from CL and IPL GDGTs. The depth profile of TOC and DIC isotopic compositions and sulfate and methane concentrations. SR: sulfate reduction zone; SMTZ: sulfate-methane transition zone; MG: methanogenic zone.

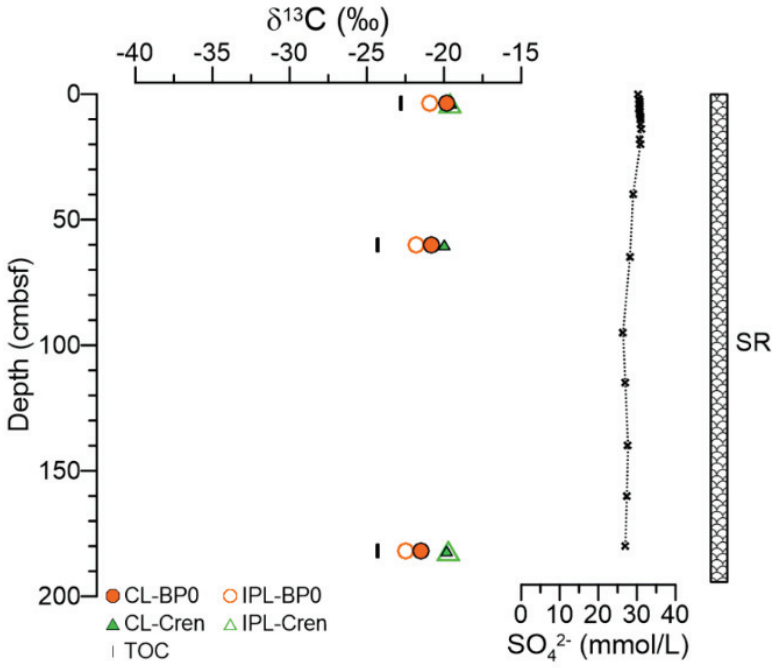

Fig. S6. Cap de Creus Canyon (GeoB17302): $\delta^{13}C$ values of biphytanyl (BP0 and BPcren) moieties released from CL and IPL GDGTs. The depth profile of TOC and sulfate concentrations. DIC isotopic data is not available at this site. SR: sulfate reduction zone.

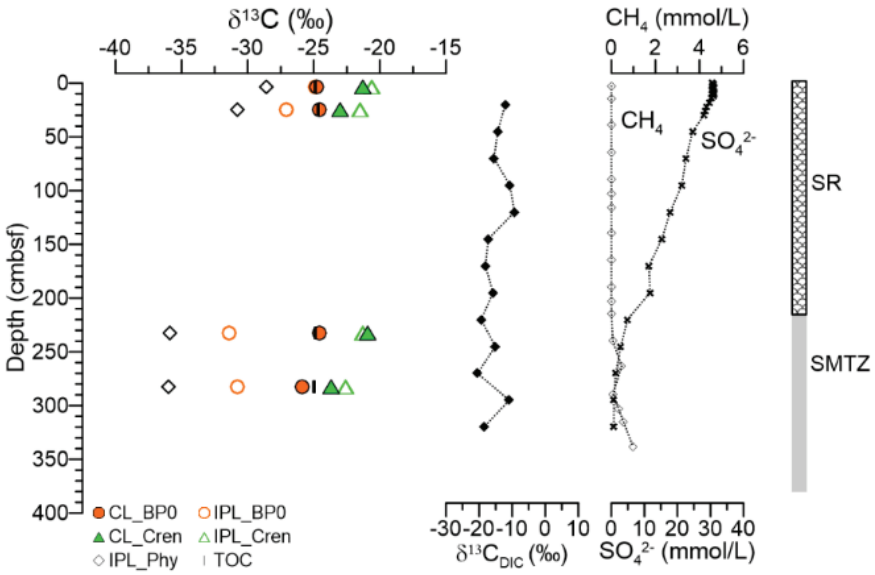

Fig. S7. Gulf of Lions shelf (GeoB17308): $\delta^{13}C$ values of phytanyl moieties released from CL and IPL archaeal diethers; $\delta^{13}C$ values of biphytanyl (BP0 and BPcren) moieties released from CL and IPL GDGTs. The depth profile of TOC and DIC isotopic compositions and sulfate and methane concentrations. SR: sulfate reduction zone; SMTZ: sulfate-methane transition zone; MG: methanogenic zone.

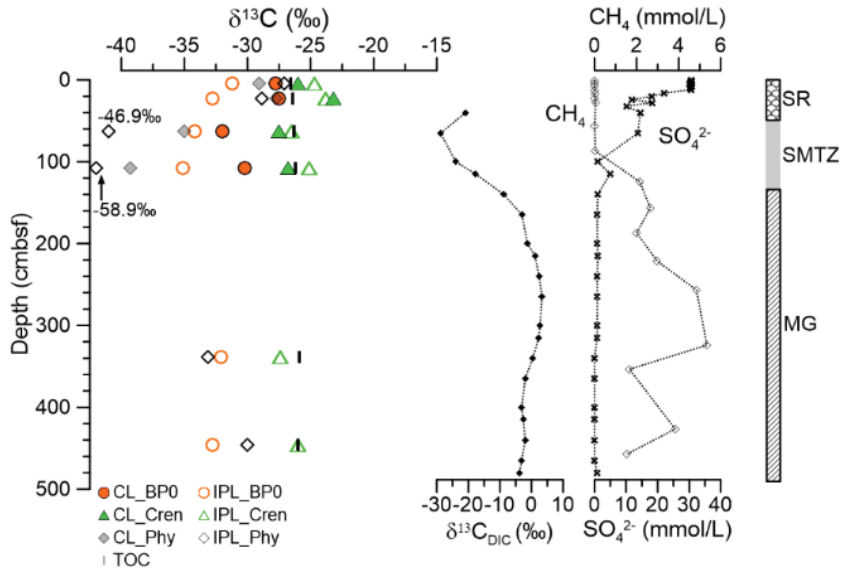

Fig. S8. Distal Rhone River delta (GeoB17307): $\delta^{13}C$ values of phytanyl moieties released from CL and IPL archaeal diethers; $\delta^{13}C$ values of biphytanyl (BP0 and BPcren) moieties released from CL and IPL GDGTs. The depth profile of TOC and DIC isotopic compositions and sulfate and methane concentrations. SR: sulfate reduction zone; SMTZ: sulfate-methane transition zone; MG: methanogenic zone.

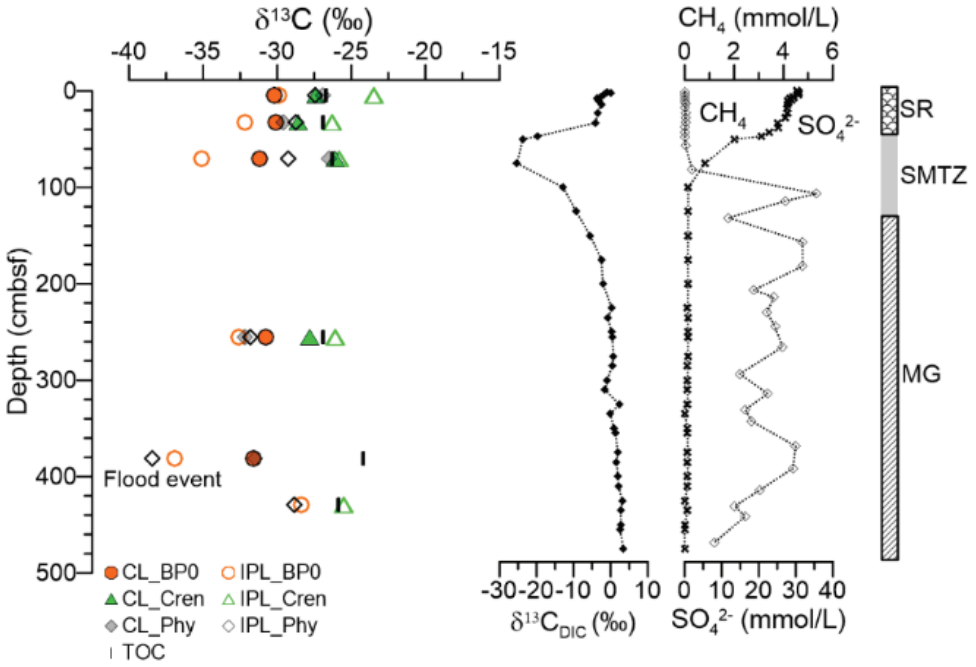

Fig. S9. Proximal Rhone River delta (GeoB17306): $\delta^{13}C$ values of phytanyl moieties released from CL and IPL archaeal diethers; $\delta^{13}C$ values of biphytanyl (BP0 and BPcren) moieties released from CL and IPL GDGTs. The depth profile of TOC and DIC isotopic compositions and sulfate and methane concentrations. SR: sulfate reduction zone; SMTZ: sulfate-methane transition zone; MG: methanogenic zone.

Table. S1 Variables used for PCA analysis; $\Delta\delta^{13}C_{BP0}$ (= $\delta^{13}C_{IPL\text{-}BP0}$ - $\delta^{13}C_{CL\text{-}BP0}$), TOC content (%), $\delta^{13}C_{TOC}$ (‰), $\delta^{13}C_{DIC}$ (‰), NH_4^+ concentration (µm/L), IPL content (%), and Age (ky).

Sample	$\Delta\delta^{13}C_{BP0}$	$\delta^{13}C_{TOC}$	$\delta^{13}C_{DIC}$	TOC(%)	IPL (%)	NH_4^+(µm/L)	Age (ky)
GeoB15103-3_2-4cm	-0.2	-18.3	-1.0	0.27	12.8	0	0.675
GeoB15103-1_19-34cm	-3.4	-20.9	-0.9	1.58	4.2	14	9.300
GeoB15103-1_291-303cm	-0.5	-17.8	-6.5	0.16	15.5	133	73.150
GeoB15103-1_308-320cm	-2.9	-19.6	-7.2	2.33	7.5	137	77.210
GeoB15103-1_453-466cm	-2.9	-20.1	-7.9	4.34	8.9	173	121.045
GeoB15103-2_21-34cm	-3.1	-21.2	-0.8	1.89	14.2	17	9.300
GeoB15103-2_220-240cm	-0.4	-19.9	-3.4	0.5	23.0	115.5	60.235
GeoB15103-2_287-298cm	-5.0	-19.5	-6.2	2.02	11.2	143.6	77.210
GeoB15103-2_435-455cm	-3.3	-20.7	-5.5	3.77	10.2	243.8	121.045
GeoB15103-2_465-480cm	n. a	-20.2	-5.5	0.1	24.9	259.6	131.900
GeoB15103-2_550-567cm	-2.2	-21.2	-2.5	1.31	8.3	307	173.300
GeoB15104-1_2-4cm	-1.6	-22.9	1.7	0.86	5.5	4.9	0.051
GeoB15104-1_34-36cm	-1.8	-22.9	-1.8	0.69	9.9	32.1	0.632
GeoB15104-2_180-196cm	-2.8	-24.1	-6.7	1.03	10.9	120.3	4.760
GeoB15104-2_280-296cm	-2.6	-25.4	-5.6	0.87	18.3	120.3	10.100
GeoB15104-2_360-375cm	-1.1	-25.8	-6.0	0.45	4.4	232.8	14.990
GeoB15104-2_620-635cm	0.9	-26.1	-17.8	0.58	18.0	489.7	19.870
GeoB15105-4_8-10cm	-1.7	-24.6	-13.5	1.26	11.4	267.3	0.230
GeoB15105-4_38-40cm	-3.0	-24.9	-19.8	1.2	12.4	534.7	0.920
GeoB15105-2_105-120cm	-2.1	-24.9	-20.3	1.32	11.7	1020.4	2.599
GeoB15105-2_147-162 cm	-1.8	-24.6	-15.8	1.43	12.7	1129.8	3.570
GeoB15105-2_265-280 cm	-1.8	-23.6	-6.9	1.88	11.4	1370.6	5.312
GeoB15105-2_390-405 cm	-1.3	-25.1	-1.4	4.37	7.7	1677	7.162
GeoB15105-2_420-435 cm	-1.7	-26.1	-1.7	1.23	5.3	1370.6	7.840
GeoB15105-2_596-613cm	0.5	-26.1	0.0	0.571	7.2	1338	15.132
GeoB17302-5_0-7cm	-1.1	-22.8	n. a	0.6	38.7	53	0.040
GeoB17302-5_50-70cm	-1.0	-24.3	n. a	0.3	6.0	191	0.600
GeoB17302-5_174-186cm	-1.0	-24.3	n. a	0.3	6.5	389	1.800
GeoB17306-1_3-6cm	0.3	-26.7	-2.2	1.3	45.3	115	0.0001
GeoB17306-1_30-35cm	-2.1	-26.9	-4.1	1.4	48.7	439	0.001
GeoB17306-2_67-73cm	-3.9	-26.3	-25.3	1.2	55.5	3850	0.002
GeoB17306-2_251-259cm	-1.8	-26.9	0.2	1.4	50.9	6860	0.007
GeoB17306-2_378-385cm	-5.4	-24.2	1.8	0.6	24.1	6730	0.011
GeoB17306-2_426-433cm	n. a	-25.9	2.9	1.2	61.5	7520	0.012
GeoB17307-5_3-6cm	-3.4	-26.6	-2.8	1.2	51.9	36	0.000
GeoB17307-5_20-25cm	-5.3	-26.4	-12.8	1.1	39.7	599	0.002
GeoB17307-8_60-65cm	-2.2	-26.3	-28.8	1.0	47.7	2160	0.004
GeoB17307-8_105-110cm	-4.9	-26.2	-20.8	0.7	52.3	4030	0.008
GeoB17307-8_332-345cm	n. a	-25.9	0.4	1.1	45.4	8250	0.023
GeoB17307-8_440-452cm	n. a	-26.0	-2.0	1.4	39.3	6290	0.030
GeoB17308-1_1-6cm	-0.1	-24.9	-10.0	0.9	19.2	10	0.006
GeoB17308-4_20-30cm	-2.5	-24.7	-12.1	0.6	30.9	392	0.039
GeoB17308-4_225-240cm	-6.8	-24.9	-17.5	0.5	23.0	2340	0.359
GeoB17308-4_275-290cm	-4.9	-25.0	-15.9	0.5	36.3	2930	0.435

Table. S2 concentrations of different lipid pools (ng/g sed dw)

Sample	CL archaeol	IPL archaeol	CL-GDGT	IPL-GDGT
	archaeol, OH-archaeol, methoxy (MeO) - archaeol	1G, 2G	majority: GDGT0, crenarchaeol minority: GDGT1-4, BDGT was added in GDGT but they account for less than 1%	1MH>2DH>>3TH>HPH
GeoB15103-3_2-4cm	0.4	1.0	78.8	10.7
GeoB15103-1_19-34cm	5.0	25.2	27651.7	1182.7
GeoB15103-1_291-303cm	n. d	n. d	36.4	6.7
GeoB15103-1_308-320cm	10.6	297.4	31966.7	2301.1
GeoB15103-1_453-466cm	21.0	449.9	57816.8	5212.9
GeoB15103-2_21-34cm	5.7	30.2	6852.3	1106.3
GeoB15103-2_220-240cm	n. d	0.5	33.6	9.6
GeoB15103-2_287-298cm	6.8	287.4	12743.7	1324.5
GeoB15103-2_435-455cm	26.3	398.5	25494.6	2489.6
GeoB15103-2_465-480cm	n. d	n. d	41.9	13.9
GeoB15103-2_550-567cm	1.6	61.9	4552.4	350.9
GeoB15104-1_1-3cm	39.3	n. d	1421.5	85.2
GeoB15104-1_34-36cm	10.9	n. d	1657.7	183.4
GeoB15104-2_180-196cm	12.2	n. d	1852.9	227.3
GeoB15104-2_280-296cm	56.7	n. d	3667.4	835.0
GeoB15104-2_360-375cm	8.6	n. d	967.7	44.9
GeoB15104-2_620-635cm	24.6	n. d	450.4	104.4
GeoB15105-4_9-10 cm	163.1	40.3	14699.0	1875.1
GeoB15105-4_39-40cm	131.5	30.8	10926.1	1529.2
GeoB15105-2_105-120cm	264.5	35.1	15002.1	1980.3
GeoB15105-2_147-162 cm	216.1	36.0	13213.5	1919.4
GeoB15105-2_265-280 cm	291.3	77.7	17579.0	2225.2
GeoB15105-2_390-405 cm	551.3	279.7	50261.7	3975.3
GeoB15105-2_420-435 cm	95.6	55.6	10343.9	527.9
GeoB15105-2_596-613cm	137.0	58.1	7162.2	506.5
GeoB17302-5_0-7cm	63.1	38.0	293.7	187.7
GeoB17302-5_50-70cm	20.4	16.5	754.6	33.4
GeoB17302-5_174-186cm	28.8	27.4	990.7	43.4
GeoB17306-1_1-5cm	206.8	270.8	398.4	230.0
GeoB17306-1_30-34cm	253.9	241.5	322.1	305.0
GeoB17306-2_75-90cm	227.5	224.0	199.2	307.7
GeoB17306-2_230-245cm	408.3	367.4	472.9	547.6
GeoB17306-2_379-395cm	122.9	91.4	263.5	30.9
GeoB17306-2_422-435cm	351.1	293.7	66.5	373.1
GeoB17307-5_3-6cm	266.5	400.9	497.1	424.6
GeoB17307-5_20-24cm	137.7	170.2	506.6	254.8
GeoB17307-8_55-68cm	261.1	205.9	169.7	186.9
GeoB17307-8_105-118cm	264.5	237.7	120.2	184.8
GeoB17307-8_332-345cm	409.0	244.2	177.0	243.4
GeoB17307-8_440-452cm	483.6	238.2	228.8	222.4
GeoB17308-1_1-6cm	202.0	181.9	2610.8	486.7
GeoB17308-4_20-30cm	167.1	102.4	444.3	171.5
GeoB17308-4_225-240cm	96.2	50.2	265.1	58.0
GeoB17308-4_275-290cm	52.3	44.4	125.1	56.5

Table. S3 Carbon isotopic compositions of BP1 and BP2 from CL and IPL lipids.

Sample	$^{13}C_{CL\text{-}BP1}$	$^{13}C_{IPL\text{-}BP1}$	$^{13}C_{CL\text{-}BP2}$	$^{13}C_{IPL\text{-}BP2}$
GeoB15103-3_2-4cm	-19.8	-20.1	-19.0	-18.0
GeoB15103-1_19-34cm	-19.5	-21.6	-18.5	-21.9
GeoB15103-1_291-303cm	n. a	n. a	n. a	n. a
GeoB15103-1_308-320cm	-19.5	-19.0	-18.8	-19.9
GeoB15103-1_453-466cm	-19.8	-19.8	-18.8	-19.8
GeoB15103-2_21-34cm	-19.4	-19.2	-18.8	-21.3
GeoB15103-2_220-240cm	-19.9	-19.0	-17.6	-17.4
GeoB15103-2_287-298cm	-18.7	-20.6	-17.5	-19.5
GeoB15103-2_435-455cm	-19.9	-21.4	-18.7	-23.0
GeoB15103-2_465-480cm	n. a	-20.6	n. a	-19.2
GeoB15103-2_550-567cm	-19.9	-19.9	-19.9	-20.8
GeoB15104-1_2-4cm	-19.9	-18.4	-19.1	-19.2
GeoB15104-1_34-36cm	-18.7	-18.4	-19.3	-18.5
GeoB15104-2_180-196cm	-18.5	-19.2	-19.5	-18.7
GeoB15104-2_280-296cm	-21.8	n. a	-22.0	n. a
GeoB15104-2_360-375cm	n. a	-20.5	-20.7	-21.5
GeoB15104-2_620-635cm	-19.1	-18.4	-19.4	-20.0
GeoB15105-4_8-10cm	-20.9	-21.2	-20.7	-18.8
GeoB15105-4_38-40cm	n. a	-18.9	-20.3	-18.6
GeoB15105-2_105-120cm	n. a	-20.2	-21.3	-18.5
GeoB15105-2_147-162 cm	n. a	n. a	-19.6	-19.6
GeoB15105-2_265-280 cm	n. a	n. a	-21.0	-20.6
GeoB15105-2_390-405 cm	n. a	-21.5	-21.4	-21.3
GeoB15105-2_420-435 cm	-20.3	-21.0	-20.9	-19.9
GeoB15105-2_596-613cm	-19.3	-19.2	-20.2	-19.5
GeoB17302-5_0-7cm	-19.0	-19.1	-20.1	-19.3
GeoB17302-5_50-70cm	n. a	n. a	-20.6	n. a
GeoB17302-5_174-186cm	n. a	n. a	-20.7	n. a
GeoB17306-1_3-6cm	n. a	n. a	n. a	n. a
GeoB17306-1_30-35cm	n. a	n. a	n. a	n. a
GeoB17306-2_67-73cm	n. a	n. a	n. a	n. a
GeoB17306-2_251-259cm	n. a	n. a	n. a	n. a
GeoB17306-2_378-385cm	n. a	n. a	n. a	n. a
GeoB17306-2_426-433cm	n. a	n. a	n. a	n. a
GeoB17307-5_3-6cm	n. a	n. a	n. a	n. a
GeoB17307-5_20-25cm	n. a	n. a	n. a	n. a
GeoB17307-8_60-65cm	n. a	n. a	n. a	n. a
GeoB17307-8_105-110cm	n. a	n. a	n. a	n. a
GeoB17307-8_332-345cm	n. a	n. a	n. a	n. a
GeoB17307-8_440-452cm	n. a	n. a	n. a	n. a
GeoB17308-1_1-6cm	n. a	n. a	-21.5	n. a
GeoB17308-4_20-30cm	n. a	n. a	-22.1	n. a
GeoB17308-4_225-240cm	n. a	n. a	n. a	n. a
GeoB17308-4_275-290cm	n. a	n. a	n. a	n. a

Table S4 BIT and the relevant lipid concentrations (ng/g sed dw)

Sample	BIT	B-GDGT-I	B-GDGT-II	B-GDGT-III	Crenarchaeol	Crenarchaeol'
GeoB15103-3_2-4cm	0.13	1.1	0.7	0.6	13.8	1.4
GeoB15103-1_19-34cm	0.07	34.3	18.9	10.8	764.8	63.7
GeoB15103-1_291-303cm	0.48	3.2	2.3	3.6	9.2	0.5
GeoB15103-1_308-320cm	0.10	30.0	19.7	13.5	527.1	35.2
GeoB15103-1_453-466cm	0.09	24.4	16.3	10.9	468.4	48.1
GeoB15103-2_21-34cm	0.09	9.1	4.8	2.8	167.0	13.0
GeoB15103-2_220-240cm	0.45	0.8	0.6	0.9	2.7	0.1
GeoB15103-2_287-298cm	0.11	15.6	10.3	7.9	247.0	13.6
GeoB15103-2_435-455cm	0.09	15.4	8.9	5.8	268.0	21.0
GeoB15103-2_465-480cm	0.28	1.7	2.0	2.9	16.5	1.0
GeoB15103-2_550-567cm	0.09	4.6	5.4	4.4	142.3	5.0
GeoB15104-1_1-3cm	0.04	1.2	1.1	0.4	61.4	5.4
GeoB15104-1_34-36cm	0.04	1.5	1.3	0.7	89.2	6.5
GeoB15104-2_180-196cm	0.05	1.4	1.5	0.5	62.7	5.1
GeoB15104-2_280-296cm	0.01	1.1	0.6	0.2	161.3	3.5
GeoB15104-2_360-375cm	0.03	0.4	0.8	1.1	87.2	1.0
GeoB15104-2_620-635cm	0.04	0.1	0.3	0.6	23.2	0.3
GeoB15105-4_9-10 cm	0.09	14.8	13.3	10.8	370.9	10.5
GeoB15105-4_39-40cm	0.11	15.5	15.8	11.3	327.6	9.7
GeoB15105-2_105-120cm	0.10	16.8	13.1	11.3	346.2	7.5
GeoB15105-2_147-162 cm	0.10	12.8	9.9	8.1	269.7	6.3
GeoB15105-2_265-280 cm	0.09	10.0	10.0	8.0	260.7	10.6
GeoB15105-2_390-405 cm	0.13	19.8	12.4	23.1	366.1	4.3
GeoB15105-2_420-435 cm	0.26	13.4	23.7	34.0	196.6	5.0
GeoB15105-2_596-613cm	0.22	9.4	14.2	26.1	171.3	3.6
GeoB17302-5_0-7cm	0.07	0.7	0.4	0.1	16.2	0.3
GeoB17302-5_50-70cm	0.05	2.1	1.3	0.2	73.6	1.0
GeoB17302-5_174-186cm	0.04	2.6	1.5	0.3	93.9	1.2
GeoB17306-1_1-5cm	0.27	1.4	0.8	0.3	6.5	0.1
GeoB17306-1_30-34cm	0.31	1.0	0.6	0.4	4.3	0.1
GeoB17306-2_75-90cm	0.35	0.9	0.5	0.3	3.0	0.1
GeoB17306-2_230-245cm	0.32	1.2	0.6	0.3	4.5	0.1
GeoB17306-2_379-395cm	0.27	1.9	1.3	0.6	9.8	0.2
GeoB17306-2_422-435cm	0.44	0.1	0.1	0.0	0.2	0.0
GeoB17307-5_3-6cm	0.29	1.5	0.9	0.6	7.3	0.1
GeoB17307-5_20-24cm	0.18	1.3	0.7	0.4	11.1	0.2
GeoB17307-8_55-68cm	0.39	0.8	0.5	0.3	2.3	0.1
GeoB17307-8_105-118cm	0.33	0.7	0.6	0.4	3.3	0.1
GeoB17307-8_332-345cm	0.39	0.5	0.3	0.2	1.4	0.1
GeoB17307-8_440-452cm	0.29	0.5	0.3	0.2	2.5	0.1
GeoB17308-1_1-6cm	0.08	5.4	2.6	0.6	96.3	1.7
GeoB17308-4_20-30cm	0.11	1.6	0.7	0.2	21.7	0.4
GeoB17308-4_225-240cm	0.15	2.0	0.8	0.3	17.4	0.7
GeoB17308-4_275-290cm	0.18	1.1	0.5	0.2	7.6	0.3

Chapter IV

Isotope geochemistry of archaeal lipids in the Black Sea and underlying sediments constrains their sources and turnover

Qing-Zeng Zhu, Marcus Elvert, Travis B. Meador, Kevin W. Becker, Jan M. Schröder, Verena B. Heuer, Matthias Zabel, Kai-Uwe Hinrichs

MARUM Center for Marine Environmental Sciences and Department of Geosciences, University of Bremen, Germany

Abstract

Archaeal lipids in sediments are typically a mixture derived from diverse planktonic and benthic archaea. The relative proportions contributed by these diverse sources are poorly constrained. Moreover, these proportions may differ between archaeal core lipids (CLs), which are commonly regarded as fossil remnants, and intact polar lipids (IPLs), which are regarded as pool enriched in signals from active archaea. In order to add constraints on sources and turnover of archaeal lipids, we determined the stable carbon isotopic compositions of archaeal IPLs and CLs by analyzing phytane (Phy) and biphytane (BP) moieties through the water column (N=5) and within an 8-m long sediment core (N=28) of the Black Sea. The sediment core encompasses the complete Holocene as well as underlying limnic sediments deposited during the last glacial. The $\delta^{13}C$ values of lipids range from -19.9 to -43.1‰; the most positive $\delta^{13}C$ values are observed in the lower suboxic zone of the water column and within analytical uncertainty are identical to those in the surface sediment. This suggests that archaea living in the lower suboxic zone are the primary contributor of lipids found in surface sediments, including a large fraction of IPLs. $\delta^{13}C$ values of IPL- and CL-crenarchaeol are indistinguishable within our analytical uncertainty, suggestive of a long turnover time of plankton-derived IPL-crenarchaeol and the lack of production by sedimentary archaea. This interpretation is supported by the concurrent positive isotope shift of CL and IPL-crenarchaeol during limnic deposition within the last glacial. Intriguingly, IPL derived BP0 in sediments is on average depleted in ^{13}C by 3‰ relative to its CL analogue. This offset is consistent with sedimentary archaea producing intact polar caldarchaeol by utilizing carbon pools that are isotopically distinct from those utilized by planktonic archaea, which are the presumed main source of CL GDGTs (Glycerol Dibiphytanyl Glycerol Tetraethers). By using the $\delta^{13}C$ value

of lactate as a reference value for organic substrates utilized by heterotrophic archaea, we estimate that on average 34% of IPL caldarchaeol is produced by sedimentary archaea. In addition, we observed more negative $\delta^{13}C_{CL\text{-}BP0}$ values in the interval between 100 and 600 cmbsf in comparison to the sediment surface; this negative deviation is consistent with the addition of hydrolytic products from the ^{13}C-depleted IPL caldarchaeol pool. More evidence for the degradation of caldarchaeol came from its decreasing IPL content with depth compared to IPL-crenarchaeol. We have used two independent approaches to estimate the contribution of CL caldarchaeol derived from degradation of IPL caldarchaeol. One approach is based on the assumption that IPL caldarchaeol from benthic and planktonic sources is degraded at identical rates. The other approach assumes that only the IPL caldarchaeol fraction contributed by the extant benthic archaea degrades because this fraction is not well protected by association with sediment particles and thus turned over more rapidly. Isotope mass balance calculations based on these approaches suggest that on average 35% and 18% of CL-caldarchaeol, respectively, is derived from IPL degradation. Isotopic analysis of archaeol indicates a source with a different carbon metabolism than the GDGT producing archaea. In the methanic zone, where isotope profiles of acetate and DIC are suggestive of active methanogenesis, archaeol became increasingly depleted in ^{13}C with depth, and this trend corresponded to increasing IPL archaeol content with depth. The high-resolution isotopic records of both CL and IPL in water column and sediments give insight into the sources and turnover of archaeal lipids in sediments.

Introduction

Archaeal lipids in marine sediments have two principal sources: marine planktonic archaea (Pearson et al., 2016) and sedimentary benthic archaea (Biddle et al., 2006). These lipids are present either as the comparatively labile intact polar lipids (IPLs) or as their more recalcitrant analogs, the core lipids (CLs), with the latter being frequently used for paleoenvironmental reconstruction (Schouten et al., 2002; Wörmer et al., 2014). Archaeal membrane lipids can be classified into two major types, archaeols and GDGTs. Archaeols can be synthesized almost by all archaea but are often used as biomarkers of methanogens or methanotrophs when associated with relatively negative $\delta^{13}C$ values (Summons et al., 1998; Hinrichs et al., 1999; Blumenberg et al., 2004). GDGT-0, known as caldarchaeol, is the most commonly occurring GDGT in both cultivated archaea and marine systems (Ingalls et al., 2006; Schouten et al., 2013). Due to the multiple microbial sources of caldarchaeol and its high contributions to the

GDGT pool, it qualifies as comprehensive biomarker that registers the gross archaeal activity in water and sedimentary environments. Different from archaeols and caldarchaeol, crenarchaeol appears to be exclusively produced by ammonia-oxidizing Thaumarchaeota (Elling et al., 2017) which use the 3-hydroxypropionate/4-hydroxybutyrate pathway for carbon fixation (Könneke et al., 2014). The direct utilization of bicarbonate by Thaumarchaeota enables crenarchaeol $\delta^{13}C$ as a tracer for $\delta^{13}C_{DIC}$ in the ocean (Elling et al., 2019). The carbon isotopic fractionation between crenarchaeol and DIC is -19.7±0.5‰ (Könneke et al., 2012).

Black Sea is the largest stratified anoxic basin on earth and the strong redox gradients of water column stimulate the growth of diverse archaeal groups. Complex archaeal communities have been found in Black Sea water columns, including Thaumarchaeota, Marine Group II, ANME, DPANN, and Bathyarchaeota, etc. (Sollai et al., 2019). Thaumarchaeota are dominant in the suboxic chemocline and play a crucial role nitrogen cycling (Coolen et al., 2007). Marine Group II resides mainly in the marine photic zone and genome analysis showed that they are motile photoheterotrophs (Rinke et al., 2019). ANMEs are actively performing AOM in the deep anoxic water (Wakeham et al., 2003; Schubert et al., 2006). As in the water column, marine sediments have been shown to host complex archaeal communities (Biddle et al., 2006). Bathyarchaeota and Marine Benthic Group-B and -D are the most abundant groups in the marine subsurface archaeal community and possibly live as mixotrophs or heterotrophs consuming buried recalcitrant organic matter (Biddle et al., 2006; Zhou et al., 2018). Environmental diversity of the sedimentary biosphere increases its complexity as different biogeochemical zones consist of different microbial communities and metabolic activities. Biogeochemical stratification in Black Sea sediments can be identified by dissolved constituents in the pore water such as sulfate and methane concentration etc. Sulfate-reducing bacteria (SRB) outcompete methanogens for a common substrate such as acetate or H_2 until the sulfate pool is depleted. Consequently, high rates of methanogenesis in marine sediments occur only after almost all sulfate has been reduced (Jørgensen and Kaster, 2006). This relationship results in the methanogenic zone (MGZ) underneath the sulfate-reducing zone (SRZ). Anaerobic oxidation of methane (AOM) is carried out by syntrophic associations between sulfate-reducing bacteria and methane-oxidizing archaea (Hinrichs et al., 1999; Boetius et al., 2000) at the diffusion-controlled interface, the so-called sulfate-methane transition zone (SMTZ).

Until now, the isotopic analysis of archaeal lipids at Black Sea has mainly been carried out on bulk lipids (Schouten et al., 2001; Wakeham et al., 2003; Blumenberg et al., 2004). Based on the comparison of lipid carbon isotope composition of suspended particulate matter (SPM) and sediments, Wakeham et al. (2003) found that the majority of GDGTs reaching to surface sediment are derived from suboxic waters in Black Sea. Meanwhile, the ^{13}C depleted lipids from deep anoxic waters failed to be transported to sediments along sinking particles, leaving no fingerprint in surface sediments (Schouten et al., 2001). Nonetheless, direct isotopic analysis on IPLs in water column and sediments of Black Sea have been so far not reported even though it can help to constrain the in situ productivity and metabolic details of their corresponding organisms (Biddle et al., 2006; Schubotz et al., 2011). Moreover, debate still exists on whether and how much the overlying water column contributes IPLs to sediments (Lipp and Hinrichs, 2009; Schouten et al., 2010). If this is the case, isotope patterns of archaeal CLs and IPLs may aid in distinguishing "live" (in-situ sedimentary production) from "fossil" (water column) IPLs. Here, we determined the isotopic compositions of IPLs and CLs in both water column and sediments of the Black Sea to constrain their sources and turnover in sediments, including the deposition of water-derived IPL and CL lipids into sediments, the in situ production of lipids as well as the degradation of IPLs and its influence on the CL pools.

Material and methods

Suspended particulate matter (SPM), sediment, and pore water sampling

Samples were retrieved in the southwestern Black Sea (43°31.70'N, 30°53.10'E) in February of 2011 during cruise No. 84, Leg1 of R/V meteor (Zabel et al., 2011). Seawater was filtered with in-situ pumps through two overlying 0.7 µm glass fiber filters. Recovered filters were wrapped sofort in combusted aluminum foil and stored at -20 °C. Pore water was extracted from sediment cores with Rhizon micro-suction samplers (0.1-µm filter width; Rhizosphere Research Products, Wageningen, the Netherlands) immediately after core recovery and split into subsamples for onshore and offshore analysis. Sediment samples were collected by using multi corer and stored at -20 °C in brown bottles. All samples are now stored in MARUM GeoB Core Repository with supporting data archived in PANGAEA Data Publisher for Earth & Environmental Science or related publications (Becker et al., 2018).

Bulk sediment and pore water analysis.

TOC content and $\delta^{13}C$ of TOC have been analyzed on a Thermo Scientific Flash 2000 elemental analyzer connected to a Thermo Delta V Plus IRMS (Thermo Fisher Scientific, Bremen, Germany). Briefly, sediments were decalcified with 10% HCl and then washed with Mili-Q water. After freeze-drying, sediments were homogenized and weighed into tin capsules for measurement. Concentrations of dissolved methane were determined on board (Zabel et al., 2011). 2-3 mL of wet sediment was enclosed in a gas-tight glass vial and heated for 20 min at 60 °C. After heating, an aliquot of headspace gas was measured by a gas chromatograph equipped with a flame ionization detector (GC-FID). The total amount of released methane was quantified and normalized to the pore-water volume of sediments based on the partial pressure and headspace volume. The same samples were used for $\delta^{13}C_{CH4}$ measurement with a Trace GC Ultra coupled to a Delta Plus XP isotope ratio mass spectrometer via a GC Combustion III interface (Ertefai et al., 2010). SO_4^{2-} was measured by ion chromatography (Metrohm Compact IC, ASupp5 column, conductivity detection after chemical suppression) following the protocols described by Lloyd et al. (Lloyd et al., 2011). PO_4^{3-} concentrations were determined by forming phosphomolybdenum blue complexes (1 ml sample, 50 µl ammonium molybdate solution, 50 µl ascorbic acid solution, and 10 min of incubation) and measuring extinction at 820 nm using a Hach Lange DR 5000 spectrophotometer. Ferrous iron was analyzed photometrically onboard directly after sample collection (Stookey, 1970). Dissolved ammonium was detected with a flow injection, Teflon tape gas separator technique after Hall and Aller (1992) using a temperature-compensated conductivity meter (no. 1056; Amber Scientific) equipped with a micro-flow-through cell (529; Amber Scientific) and a strip chart recorder. Dissolved hydrogen sulfide was determined in samples fixed with $ZnCl_2$ using the photometric methylene blue method (Cline, 1969). The carbon isotopic composition of dissolved inorganic carbon (DIC) in pore water was analyzed using a gas bench coupled to a Finnigan MAT 252 mass spectrometer (Thermo Fisher Scientific). Samples were prepared according to Heuer et al. (2009), such that 100 µl of phosphoric acid were transferred to glass tubes, which were subsequently sealed with butyl septa and plastic caps and purged with helium. The liquid sample was injected into the purged tubes by using a syringe. Samples were allowed to degas CO_2 from the acidified aqueous matrix for five hours before carbon isotopic composition of CO_2 was analyzed in subsamples of the gas phase. The precision of the analysis

was less than 0.1‰ (1σ). Concentration and carbon isotopic composition of acetate and lactate were analyzed by IRMS-LC/MS as previously described by Heuer et al. (2006).

Lipid extraction.

Freeze-dried samples were extracted using a modified Bligh and Dyer method (Sturt et al., 2004). In Brief, samples were extracted by ultra-sonication in a mixture of DCM: MeOH: buffer (1:2:0.8; v/v/v) for 10 min for four times. A phosphate buffer (K_2HPO_4, 50 mmol L^{-1} at pH 7.4) was used in the first two times, and a trichloroacetic acid buffer (TCA, 50 g L^{-1}, pH 2) for another two times. Combined extracts were washed with distilled water and after partitioning, the organic phase was gently evaporated to dryness under a stream of nitrogen and stored at -20 °C until analysis.

Lipid concentration analysis

Archaeal lipids were quantified by injecting an aliquot of the total lipid extract (TLE) on a Dionex Ultimate 3000 ultra-high performance liquid chromatography (UPLC) system. UPLC is connected to a Bruker maXis Ultra-High Resolution quadrupole time-of-flight tandem mass spectrometer (MS) with electrospray ionization (ESI) ion source operating in positive mode (Bruker Daltonik, Bremen, Germany). The MS was set to a resolving power of 27000 at m/z 1222. Each analysis was mass-calibrated by loop injections of a calibration standard and correction by lock mass, leading to a mass accuracy of typically less than 1 ppm (Wörmer et al., 2013; Zhu et al., 2013). Ion source and other MS parameters were optimized by infusion of standards (caldarchaeol, 1G-caldarchaeol, 2G-caldarchaeol) into the eluent flow from the UPLC system using a T-piece.

Separation of core and intact polar lipids.

Aliquots of total lipid extract (TLE) samples were separated into apolar (containing CLs) and polar (containing IPLs) fractions using preparative high-performance liquid chromatography (HPLC, Meador et al., 2014). In detail, an Inertsil Diol column (5 µm, 150×10 mm, GL Sciences Inc., Tokyo, Japan) was connected to an Agilent 1200 series HPLC equipped with an

Agilent 1200 series fraction collector. The eluent flow was split with a ratio of 100:1 and introduced to an Agilent 6130 Single Quadrupole mass spectrometer to monitor GDGT ions (Meador et al., 2015). The flow rate was set to 3 mL min^{-1} and the eluent gradient was: 100% A to 10% B in 5 min, to 85% in 1 min, hold at 85% B for 9 min, then column re-equilibration with 100% A for 6 min, where eluent A was composed of n-hexane/2-propanol (85:15, v: v) and eluent B was 2-propanol/MilliQ water (90:10, v: v). The fraction collection time windows are from 0.1 to 5 min for the apolar fraction and from 5 to 15 min for the polar fraction. Aliquots of sample fractions were reanalyzed on the analytical column on HPLC-qTOF-MS (Bruker, Bremen, Germany) to check the separation and purity (Wörmer et al., 2013). The carryover rate of core GDGT in IPL fraction should be less than 5% to minimize the interference of the fossil signal. This method diminishes the mixing of signals from living cells and fossil lipids and provides more comprehensive insights into the complexity of the microbial community structure.

Ether cleavage and $\delta^{13}C$ analysis.

Phytanes (Phy) and biphytanes (BP) were prepared from the CL and IPL fractions by using ether cleavage. Aliquots of all fractions were treated with 300 µl of Boron tribromide (BBr_3, Aldrich) for 2 h at 60 °C under a stream of Argon. The alkyl bromides were subsequently converted to the corresponding hydrocarbons by reaction with an excess of lithium triethyl borohydride ($LiET_3BH$) in tetrahydrofuran for 2 h at 60 °C under a stream of Argon. After quenching the reaction with 1 ml MilliQ water added drop-wise, the products were extracted 4 times with 1 ml *n*-hexane. The combined organic fractions were evaporated to 0.5 ml and purified through a silica gel column eluted with 4ml *n*-hexane. Stable carbon isotopic compositions of ether cleavage derivatives were determined by gas chromatography isotope ratio mass spectrometry (GC-IRMS). Briefly, the samples were injected into the Trace GC Ultra (ThermoFinnigan) equipped with a Restek Rxi-5ms column (30m×250µm×0.25µm, Restek, Bad Homburg, Germany) and coupled a Delta V Plus IRMS via GC IsoLink connected to a ConFlow IV interface (Thermo Fisher Scientific GmbH, Bremen, Germany). The initial oven temperature was held at 60 °C for 1 min, increased to 150 °C at a rate of 10 °C min^{-1}, then raised to 310 °C at a rate of 4 °C min^{-1} and held at 310 °C for 40 min. The carrier gas was helium with a constant flow rate of 1.0 ml min^{-1}. The injector temperature was set at 290 °C.

The precision of the replicate analysis (n = 2) was ≤0.5‰. All isotopic values are reported in the delta notation as $\delta^{13}C$ relative to the Vienna PeeDee Belemnite (VPDB) standard.

Results

Geochemical conditions in the water column and sediments

Water column chemistry of the studying site in Black Sea has been in detail reported by Becker (Schröder, 2015; Becker et al., 2018). Geochemical data revealed a strong vertical stratification of the Black Sea water column (Fig. 1). Briefly, the oxygen concentrations decreased from more than 250 to below 5 µmol kg^{-1} at 170 m below sea level (mbsl) as a result of aerobic respiration (Fig. 1). Salinity changed from 17.7 to 22.3 g L^{-1} with increasing depth and the obvious increase of salinity occurred from 80 to 150 mbsl. Ammonia and sulfide were first detectable at 120mbsl and 100mbsl, respectively. Consequently, oxic, suboxic chemocline and anoxic zone can be defined as 0 to 90 mbsl, 90 to 150 mbsl, and 150 mbsl down to the seafloor, respectively. The sediment core in this study is 8-m long and consists of two major lithologies; the upper part is marine sedimentation characterized by coccolith ooze lamination and the lower part is lacustrine deposits. TOC concentration showed a general increasing trend with depth until 400 cmbsf, a sapropel horizon with a TOC concentration of 3.67% (Fig. 2). From 400 cmbsf to the core bottom, the TOC decreased gradually from 1.3 to 0.39%. Compared to TOC concentration, $\delta^{13}C_{TOC}$ values stayed relatively stable with depth and ranged from -24.6 to -27.4‰. A negative shift in $\delta^{13}C_{TOC}$ of 2.3‰ occurred at the boundary of marine and lacustrine sedimentation. DIC isotopes decreased from -11.0‰ in surface sediments to -23.8‰, a minimum value at 53.5 cmbsf and then increased gradually to +7.2‰ at 810 cmbsf (Fig. 3). SO_4^{2-} concentration was high at the surface sediments and decreased rapidly with increasing depth but remained detectable until 400 cmbsf. Below the sapropel at 400 cmbsf, both SO_4^{2-} and HS^- were below detection. CH_4 increased steeply below 60 cm. Based on DIC isotope, the peak of the sulfide profile and the steep decrease of methane concentrations, we place the sulfate methane transition zone (SMTZ) between 50 and 150 cmbsf. The methanogenic zone underlies the SMTZ and is characterized by low to undetectable SO_4^{2-} and an accumulation of CH_4. Acetate concentrations were highly variable and ranged from 2 to 250 µmol L^{-1} with the highest concentration observed in sapropel layer. $\delta^{13}C$ of acetate ranged from -7.8 to -33.8‰ (Fig. 3).

Lactate concentrations were less variable than acetate, ranging from 29 to 54 µmol L^{-1}. $\delta^{13}C$ of lactate ranged from -29.0 to -34.2‰.

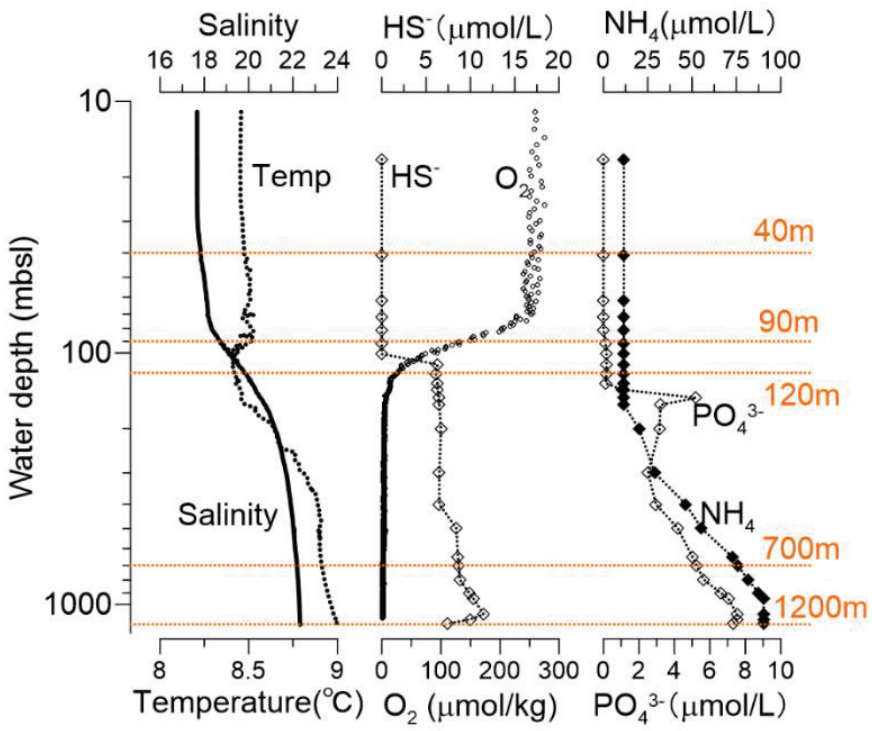

Fig. 1 Black Sea water column geochemistry, from left to right: salinity and temperature; hydrogen sulfide and dissolved oxygen; phosphate and ammonium concentrations. Sampling depths for lipid analyses are indicated by orange dashed lines. Water depth is shown by logarithmic scale from 10 to 1,200 mbsl

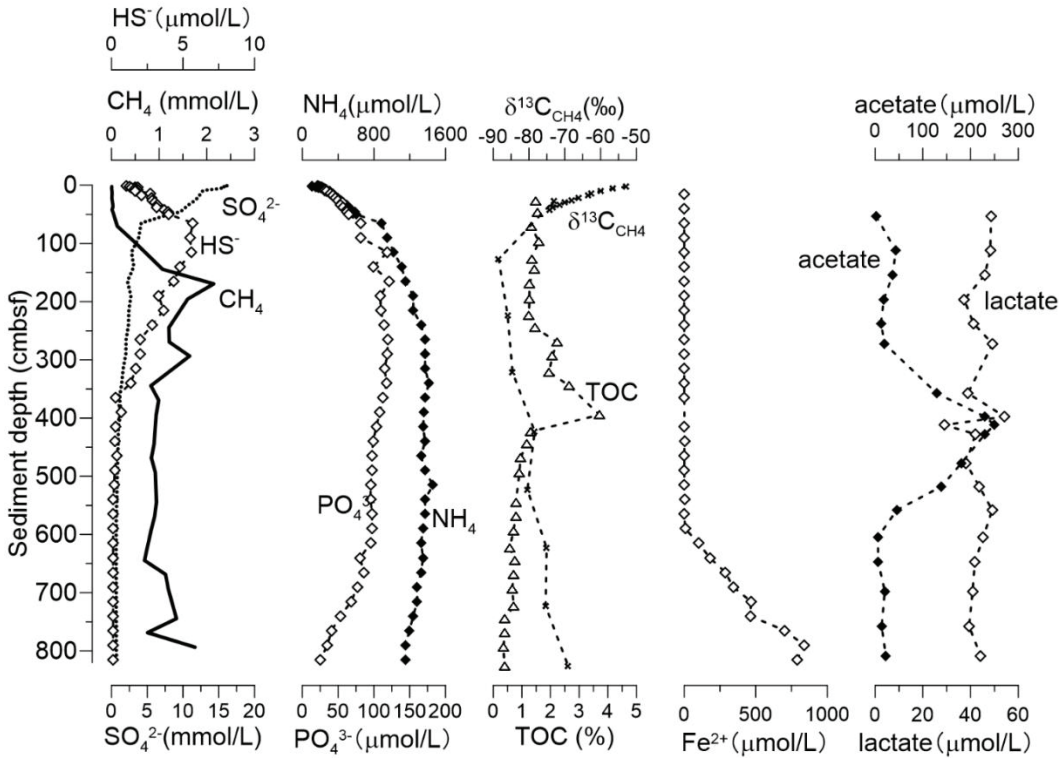

Fig. 2 Black Sea sedimentary pore water geochemistry, from left to right: sulfate, methane, and sulfide to identify different geochemical zones; phosphate and ammonium concentrations; $\delta^{13}C$ of methane and Total organic carbon (TOC) content; Fe^{2+} concentration; acetate and lactate concentration.

Compositions of intact and core archaeal lipids in the water columns and sediments.

Both core and intact archaeal lipids have been measured by (Schröder, 2015) in our study. CL-caldarchaeol includes mainly caldarchaeol, OH (monohydroxylated)-caldarchaeol, and 2OH (dihydroxylated)-caldarchaeol. IPL-caldarchaeol mainly consists of 1G- and 2G-caldarchaeol and their hydroxyl forms as well as a small amount of HPH-caldarchaeol. CL-crenarchaeol contains only crenarchaeol and its isomer. IPL-crenarchaeol contains mainly 1G- and 2G-crenarchaeol as well as a tiny fraction of HPH crenarchaeol. CL-archaeol contains archaeol, OH-archaeol, and methoxy-archaeol. IPL-archaeol comprised mainly 1G- and 2G-archaeol; archaeol with head groups of phosphatidylethanolamine (PE), phosphatidylglycerol (PG), and phosphatidylinositol (PI) were also detected in the samples but the concentrations were very low. In our study, we also calculated the proportion of IPL in total lipids (Fig. 4; cf. (Schröder, 2015)). The IPL proportion is highly variable in different archaeal lipids. IPL-caldarchaeol proportion ranged from 21 to 65% in the water column and from 10 to 56% in sediments, respectively. IPL-crenarchaeol proportion ranged from 11 to 37% in the water column and from

13 to 47% in sediments, respectively. IPL-archaeol proportion ranged from 1 to 86% in the water column and from 10 to 61% in sediments, respectively.

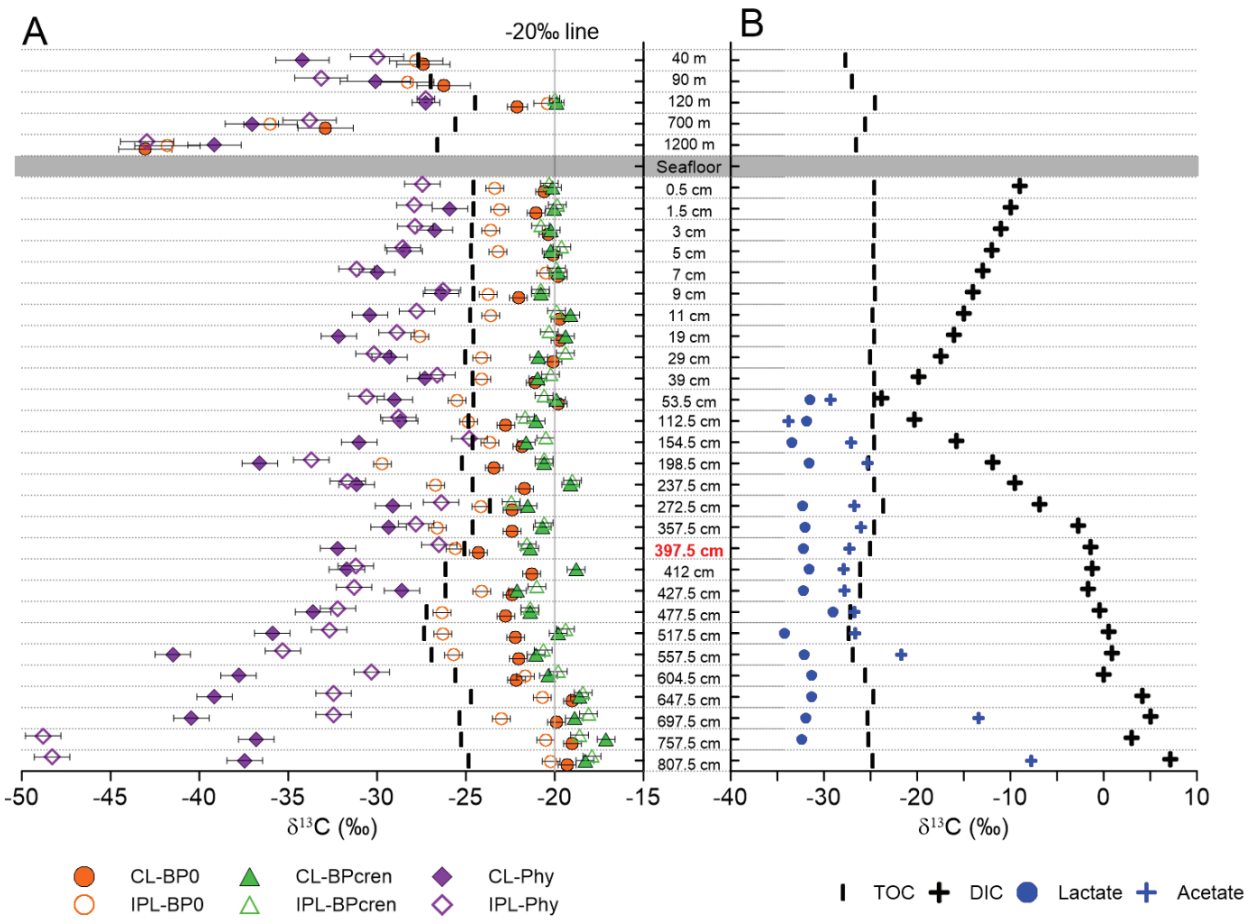

Fig. 3 Stable carbon isotopic compositions of (A) CL and IPL-GDGTs, CL and IPL-archaeol, and TOC and (B) DIC, TOC, acetate, and lactate in both water and sediments. $\delta^{13}C$ values of biphytanes (BP0 and BPcren) were released from archaeal CL and IPL GDGTs; $\delta^{13}C$ values of phytanes (Phy) were released from archaeal CL and IPL archaeol. Stable carbon isotopic compositions of TOC were drawn on both A and B as a reference. The depth marked with red color indicates the sapropel horizon which is the boundary between marine and lake sedimentation.

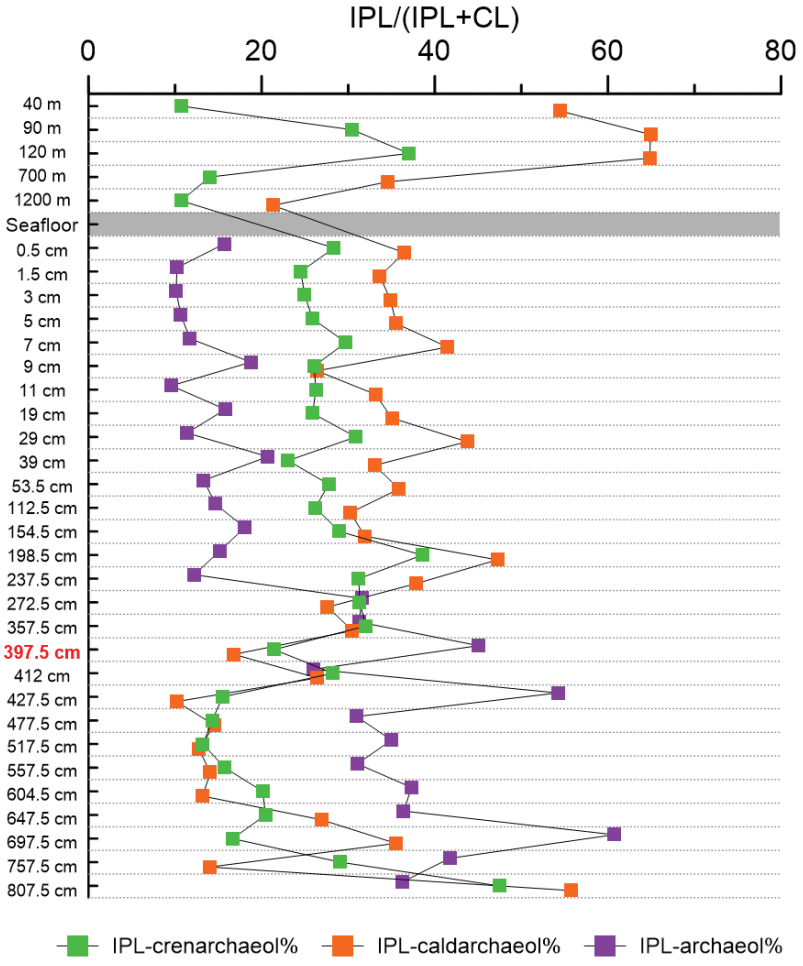

Fig. 4; IPL proportion in its corresponding total lipids (Schröder, 2015); IPL-archaeol proportion data in the water column is not available.

Carbon isotopic compositions of both intact and core archaeal lipids in the water columns

In this study, we measured both IPL and CL carbon isotopes from suspended particulate matter and determined their carbon isotopic pattern in the different chemical zones of the water column; comparison with sedimentary lipids will inform us on export and preservation of lipids from the water column in sediments. $\delta^{13}C_{CL\text{-}Phy}$ varied from -27.3 to -39.2‰ and $\delta^{13}C_{IPL\text{-}Phy}$ varied from -27.3 to -43.0‰ (Fig. 3). $\delta^{13}C_{CL\text{-}BP0}$ ranged from -23.1 to -43.1‰ and the corresponding $\delta^{13}C_{IPL\text{-}BP0}$ ranged from -21.4 to -41.8‰. The most ^{13}C-enriched lipids were produced in the suboxic zones while the most ^{13}C-depleted lipids are produced in the anoxic zone. As for crenarchaeol, we only obtained one data point from the suboxic zone due to its low concentration in other zones. $\delta^{13}C_{CL\text{-}BPcren}$ and $\delta^{13}C_{IPL\text{-}BPcren}$ are identical within measurement error.

Carbon isotopic compositions of both intact and core archaeal lipids in sediments

$\delta^{13}C_{CL\text{-}Phy}$ ranged from -25.9‰ in the surface sediments to -41.5‰ at 810 cmbsf. $\delta^{13}C_{IPL\text{-}Phy}$ values ranged from -24.8‰ in the surface sediments to -48.8‰ at 810 cmbsf. Both $\delta^{13}C_{CL\text{-}Phy}$ and $\delta^{13}C_{IPL\text{-}Phy}$ decreased in the top 20 cm of sediment from -25 to -30‰, and then remained relatively constant at around -30‰ until 450 cmbsf. From 450 down to 700 cmbsf where lacustrine sedimentation occurred, $\delta^{13}C_{CL\text{-}Phy}$ became more and more depleted with depth from -32 to -40‰ while the $\delta^{13}C_{IPL\text{-}Phy}$ remained around -32.5‰. Intriguingly, $\delta^{13}C_{IPL\text{-}Phy}$ values became more negative than $\delta^{13}C_{CL\text{-}Phy}$ below 700 cmbsf, with an average value of -48.5 and -37‰, respectively. $\delta^{13}C_{CL\text{-}BP0}$ ranged from -19 to -24.3‰, with an average value of -21.2‰. In sediments between 112 and 604 cm, $\delta^{13}C_{CL\text{-}BP0}$ was on average 2.3% more negative than in sediments above and below. $\delta^{13}C_{IPL\text{-}BP0}$ ranged from -20.2 to -29.7‰, with an average value of -24.2‰. An offset between $\delta^{13}C_{CL\text{-}BP0}$ and $\delta^{13}C_{IPL\text{-}BP0}$ was observed, with an average value of 3‰ ±1.8. $\delta^{13}C_{CL\text{-}BPcren}$ ranged from -17.1 to -22.1‰, with an average value of -20.1‰. $\delta^{13}C_{IPL\text{-}BPcren}$ ranged from -17.9 to -22.5‰, with an average value of -20.1‰. No difference was observed between $\delta^{13}C_{CL\text{-}BPcren}$ and $\delta^{13}C_{IPL\text{-}BPcren}$ in all samples. Both $\delta^{13}C_{CL\text{-}BPcren}$ and $\delta^{13}C_{IPL\text{-}BPcren}$ are 1.5‰ more positive in samples between 647.5 and 807.5 cmbsf than in shallower samples.

Discussion

Lower suboxic zone contributes the most lipids to the surface sediment.

A characterization of archaeal lipids in the water column is required for evaluating how planktonic archaeal lipids exported into and preserved within sediments. Previous studies about archaeal lipids in marine suspended particulate matter have focused on carbon isotopic compositions of bulk lipids (Hoefs et al., 1997; Schouten et al., 2001; Wakeham et al., 2003), while IPL-specific data have not been investigated. In order to obtain more insights into the fate of water-column derived IPLs and evaluate to what degree they represent “live” cells, we measured the isotopic compositions of archaeal lipids from oxic, suboxic, and anoxic zones of the water column as well as the sediment. The carbon isotopic compositions of IPLs and CLs in both water column and surface sediments suggest that archaea inhabiting in the lower suboxic zone are the main sources of archaeal lipids in the top centimeters of sediment (Fig. 3). The ^{13}C-depleted archaeal lipids from oxic and anoxic zones leave no characteristic

fingerprint in the sedimentary record. Recent data has shown that thaumarchaeal sequences are the dominant archaeal sequences detected in the oxic and suboxic waters of Black Sea (Sollai et al., 2019). Our lipid isotopic data indicate that there must be additional sources contributing to the lipid pool in the oxic and upper suboxic zones (40 and 90 m depth) because $\delta^{13}C$ values of caldarchaeol differ from those in the lower suboxic zone. The possible sources are photoheterotrophic or mixotrophic Euryarchaeota, which also produce GDGTs (Lincoln et al., 2014; Tully, 2019). Interestingly, in the lower suboxic zone $\delta^{13}C$ of BP-0 from CL pool is 2‰ more negative than its counterpart from the IPL pool. This may be caused by settling of particles with relatively ^{13}C-depleted CL from the oxic or upper suboxic zones, e.g. photoheterotrophic Marine Group II (Lincoln et al., 2014). Notably, the ^{13}C-depleted archaeal lipids from the anoxic zone, which reflect the contribution of planktonic anaerobic methane-oxidizing archaea (Schouten et al., 2001; Wakeham et al., 2003), do not significantly contribute to the sedimentary lipid pool. This likely reflects the combination of relatively low lipid production rates compared to shallower waters and the absence of grazers that package microbial cells into rapidly sinking fecal pellets (Schouten et al., 2001). Nearly identical isotopic compositions of crenarchaeol in water column and in surface sediments suggested that the majority of crenarchaeol in sediments is derived from the lower suboxic zone.

IPL crenarchaeol is deposited from the water column and has a long turnover time in sediments

Crenarchaeol is presumed to be exclusively synthesized by chemolithoautotrophic Thaumarchaeota (Pitcher et al., 2011; Sinninghe Damsté et al., 2012; Elling et al., 2017). In this study, we examined the isotopic compositions of both CL and IPL crenarchaeol in contrasting depositional regimes to constrain potentially differing sources (water column or sedimentary production). No differences were observed between $\delta^{13}C_{CL\text{-}BPcren}$ and $\delta^{13}C_{IPL\text{-}BPcren}$ in both water column and the 8-m sediment core. Moreover, $\delta^{13}C_{IPL\text{-}BPcren}$ did not respond to the large change of pore water $\delta^{13}C_{DIC}$. This suggests that the production of crenarchaeol by autotrophic Thaumarchaeota within the sediment is negligible. In addition, we observed a positive shift of 1.5‰ in $\delta^{13}C_{CL\text{-}BPcren}$ and $\delta^{13}C_{IPL\text{-}BPcen}$ in samples below 647 cmbsf deposited during the last glacial (Fig. 3). The nearly identical $\delta^{13}C_{CL\text{-}BPcren}$ and $\delta^{13}C_{IPL\text{-}BPcren}$, including their simultaneous shift at 647 cmbsf, suggests that IPL crenarchaeol is predominantly derived from thaumarchaeal activity in the water column and thus largely represents a fossil signal. All

cultivated Thaumarchaeota to date oxidize ammonia to nitrite aerobically (Könneke et al., 2014; Stieglmeier et al., 2014). Despite abundant ammonium in anoxic sediments, thaumarchaeal growth appears to be restricted to oxic sedimentary environments (Ren et al., 2019; Vuillemin et al., 2019). An in-situ experiment of ^{13}C-labelled glucose suggests that benthic archaea could synthesize crenarchaeol by recycling biphytane diols from decayed archaeal cells and synthesizing glycerol de novo (Takano et al., 2010). If this is the case, closely matching $\delta^{13}C_{CL\text{-}BPcren}$ and $\delta^{13}C_{IPL\text{-}BPcren}$ and their synchronous response to climatic event (last glacial) is not an unambiguous proof that IPL crenarchaeol is fossil. However, the similarity between $\delta^{13}C_{CL\text{-}BPcren}$ and $\delta^{13}C_{IPL\text{-}BPcren}$ indicates that there was no isotopic fractionation during lipid recycling even if it happened. Our results suggest that post-sedimentary microbial processes have a negligible impact on δ^{13}C values of crenarchaeol, which has been suggested to serve as proxy for paleo $\delta^{13}C_{DIC}$ in the ocean (Schoon et al., 2013; Polik et al., 2018; Elling et al., 2019).

In-situ activities of archaea in Black Sea sediments.

Caldarchaeol has multiple sources while crenarchaeol is mainly derived from Thaumarchaeota in marine environments. Studies have shown that caldarchaeol in marine surface sediment is 0.6‰ on average ^{13}C-depleted relative to crenarchaeol (Pearson et al., 2016). The difference was attributed to the heterogeneous contribution of various archaeal sources to the sedimentary pool (Pearson et al., 2016; Polik et al., 2018), such as component of terrigenous or in-situ sedimentary influence (Biddle et al., 2006), or contribution from photoheterotrophic Euryarchaeota (Lincoln et al., 2014). Additionally, contributions from sedimentary sources related to in-situ archaeal activity may increase in importance with increasing depth. Although IPL GDGTs are likely to contain fossil contributions, this pool is due to its higher reactivity and lower size presumably more sensitive to sedimentary contributions (Biddle et al., 2006; Schubotz et al., 2011). Our data showed that the difference between $\delta^{13}C_{CL\text{-}BP0}$ and $\delta^{13}C_{CL\text{-}BPcren}$ in the top 50 cm of sediment is on average 0.3‰, within the instrumental precision. This suggests Thaumarchaeota are the main predominant producer of core caldarchaeol and crenarchaeol in these sediments. Interestingly, BP-0 in the sedimentary IPL pool is on average depleted in ^{13}C by 3‰ relative to the CL pool. This offset is strong evidence for contributions of benthic archaea to intact polar caldarchaeol. Supporting evidence comes from the higher proportion of IPL-caldarchaeol in total caldarchaeol over IPL-crenarchaeol (Fig. 4). This extra proportion of IPL-caldarchaeol is good evidence of the contribution of benthic archaea.

$\delta^{13}C_{IPL\text{-}BP0}$ signal is contributed by mixed sources, such as water column derived caldarchaeol (endmember-1, Em1 in Eq. 1), as well as its sedimentary in-situ production (autotrophic, heterotrophic and possibly methanotrophic archaea; endmember-2, Em2). The IPL caldarchaeol derived from the water column has nearly identical isotopic compositions as crenarchaeol. Crenarchaeol can, therefore, represent Em1 isotopically. In order to investigate sedimentary in-situ production (Em2), we measured the carbon isotopic compositions of TOC, DIC, methane, acetate, and lactate as potential carbon pools utilized by sedimentary archaea. We observed that $\delta^{13}C_{IPL\text{-}BP0}$ did not covary with $\delta^{13}C_{DIC}$ but instead had roughly similar trends with $\delta^{13}C_{TOC}$. Moreover, $\delta^{13}C_{IPL\text{-}BP0}$ did not change in the SMTZ, suggesting that the contribution of methanotrophic archaea to the IPl-caldarchaeol pool was at most minimal. The cumulative evidence thus suggests that the benthic archaea responsible for caldarchaeol production assimilate mainly organic carbon but only limited inorganic carbon and carbon derived from methane. Our results are consistent with former studies that suggested the predominance of heterotrophic archaea in organic-rich sediments (Biddle et al., 2006; Lloyd et al., 2013). Microbes in sediments mainly use the small organic molecules enzymatically released from particulate organic matter such as acetate, lactate, and amino acids. Lactate has been shown to resemble isotopic compositions of dissolved organic carbon (DOC) (Heuer et al., 2009) and can serve as the isotopic endmember of the carbon pool utilized by heterotrophic archaea (Em2); the isotopic compositions of acetate on the other hand is more strongly influenced by biological sources and sinks associated with strong isotopic fractionation (cf. Heuer et al., 2009). We estimated the heterotrophic contribution to the caldarchaeol pool by using isotopic mass balance (Eq. 1). $\delta^{13}C_{IPL\text{-}BP0}$ is the measured value of IPL-BP0, f is the fraction of sedimentary in-situ production. The contribution ranges from 6 to 83%, with an average value of 34% (Table 1, contribution of sedimentary heterotrophic production to the IPL pool).

$$\delta^{13}C_{IPL-BP0} = (1-f)\delta^{13}C_{Em1} + f\delta^{13}C_{Em2} \qquad \text{Eq. 1}$$

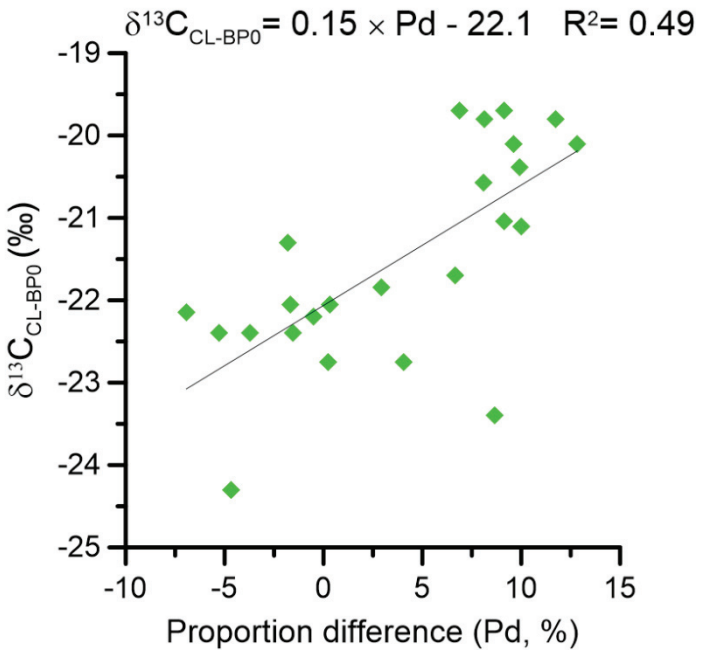

Fig. 5 Relationship between $\delta^{13}C_{CL\text{-}BP0}$ and proportion difference (Pd = proportion of IPL-caldarchaeol – proportion of IPL-crenarchaeol, %)

Evaluating IPL degradation in sediments by isotope mass balance

Degradation of IPL in sediments and its impact on the fossil pool has rarely been evaluated (Liu et al., 2011; Weijers et al., 2011). Liu et al. (2011) studied the relative distributions of IPL and CL GDGTs along with a core at a methane-rich site in the Black Sea. The result provided compelling evidence of in situ production of glycosidic IPL GDGTs and their subsequent degradation to corresponding CL GDGTs on timescales that are short in geological terms. In our study, we observed a more negative signal in $\delta^{13}C$ of BP-0 in the CL pool in subsurface sediments between 100 and 600 cmbsf relative to the surface; this negative deviation is consistent with the addition of hydrolytic products in the form of core caldarchaeol from the more strongly ^{13}C-depleted IPL pool. Supporting evidence comes from the comparison of IPL-caldarchaeol and -crenarchaeol proportion with depth. IPL-caldarchaeol proportion was observed to be higher than IPL-crenarchaeol in surface sediments from 0 to 240 cmbsl (average is 36% vs 28%) but became lower in deeper sediments from 290 to 615 cmbsl (average is 18% vs 21%). If we assume that the crenarchaeol pool exclusively originates from planktonic sources and that IPL crenarchaeol and caldarchaeol behave chemically highly similar in terms of their reactivity, the differences in the relative proportion of IPLs between these two pools

should provide information on the turnover of the IPL caldarchaeol fraction contributed by sedimentary archaea. A correlation between $\delta^{13}C_{CL\text{-}BP0}$ and the difference between the proportions of IPL-caldarchaeol and IPL-crenarchaeol was observed in our study (Fig. 5). Accordingly, in sediments in which the IPL proportion of caldarchaeol is lower than that of crenarchaeol, preferential degradation of ^{13}C-depleted IPL-caldarchaeol from benthic sources contributed to the corresponding CL pool and decreased its $\delta^{13}C$ values. For the quantitative evaluation of IPL degradation, we examined the isotopic data of both intact and core BP0 and applied an isotope mass balance (Eq. 2). The sedimentary core lipids ($\delta^{13}C_{CL\text{-}BP0}$) are assumed to be a two-component mixture, one component is the fossil input of IPL caldarchaeol from the water column ($\delta^{13}C_W$) and the other is from the degradation of IPL caldarchaeol formed by sedimentary archaea ($\delta^{13}C_S$). *F* is defined as the fraction of carbon incorporated from IPL degradation. We obtain an isotopic relationship between the sedimentary core lipid pool, the fossil lipid from the water column, and the degradation of IPL formed by sedimentary archaea.

$$\delta^{13}C_{CL-BP0} = (1-F)\delta^{13}C_W + F\delta^{13}C_S \qquad \text{Eq. 2}$$

In this study, $\delta^{13}C_W$ equals the measured $\delta^{13}C_{CL\text{-}BPcren}$ assuming that both sources of water column derived caldarchaeol and crenarchaeol are identical. This assumption is reasonable because the data from surface sediment samples showed that the difference between $\delta^{13}C_{CL\text{-}BP0}$ and $\delta^{13}C_{CL\text{-}BPcren}$ are indistinguishable within our analytical error. We distinguish two scenarios, using two different endmembers $\delta^{13}C_S$ values, dependent on two different assumptions. Assumption 1 (A1) is that IPL caldarchaeol has a uniform degradation rate, no matter whether it originates from the water column activity or from sedimentary activity. In A1, $\delta^{13}C_S$ equals the $\delta^{13}C_{IPL\text{-}BP0,}$ which is the measured isotopic value of BP0 in the IPL fraction. Assumption 2 (A2) is that IPL degradation predominantly affects the pool contributed by benthic heterotrophic archaea. The rationale for A2 is the presumed relatively high recalcitrance of planktonic material, presumably due to tight association with sedimentary minerals, whereas the biomass of sedimentary microbes resides in interstitial spaces with little protection against enzymatic attack. In A2, $\delta^{13}C_S$ thus equals the lactate isotopic composition which we use as a proxy for the organic matter pool utilized by sedimentary archaea. Isotope mass balance calculations based on the two different approaches suggest that on average 35% of

CL-caldarchaeol based on A1 and 18% based on A2 is derived from IPL degradation (Table 1).

Table 1. Estimate of the in-situ production (based on Eq. 1) and degradation (based on Eq. 2, using two different scenarios) of IPL-caldarchaeol in Black Sea sediment; the numbers in bold type mean the average value of $\delta^{13}C_{lactate}$ of the whole sample set because the data in these depths is not available. n.a (not available) refers to samples in which endmember values are absent. Blank areas refer to samples where $\delta^{13}C_{CL\text{-}BPcren}$ and $\delta^{13}C_{CL\text{-}BPcren}$ do not differ by more than ±0.7‰ (within the precision of instrumental analysis).

Depth cmbsf	$\delta^{13}C_{CL\text{-}BPcren}$ Em1	$\delta^{13}C_{CL\text{-}BP0}$	$\delta^{13}C_{IPL\text{-}BP0}$	$\delta^{13}C_{lactate}$ Em2	Contribution of sedimentary heterotrophic production to the IPL pool (%)	Contribution of IPL degradation to the CL pool based on A1 (%)	Contribution of IPL degradation to the CL pool based on A2 (%)
0.5	-20.1	-20.6	-23.4	**-31.9**	28%		
1.5	-20.0	-21.0	-23.1	**-31.9**	26%	33%	9%
3.0	-20.2	-20.4	-23.6	**-31.9**	29%		
5.0	-20.2	-20.1	-23.2	**-31.9**	26%		
7.0	-19.8	-19.8	-20.5	**-31.9**	6%		
9.0	-20.8	-22.1	-23.8	**-31.9**	27%	42%	11%
11.0	-19.1	-19.7	-23.6	**-31.9**	35%		
19.0	-19.4	-19.7	-27.6	**-31.9**	66%		
29.0	-20.9	-20.1	-24.1	**-31.9**	29%		
39	-20.95	-21.1	-24.1	**-31.9**	29%		
53.5	-19.9	-19.8	-25.5	-31.5	48%		
112.5	-21.05	-22.8	-24.9	-31.8	35%	45%	16%
154.5	-21.6	-21.8	-23.6	-33.4	17%		
198.5	-20.6	-23.4	-29.7	-31.6	83%	31%	26%
237.5	-19.1	-21.7	-26.7	**-31.9**	59%	34%	20%
272.5	-21.5	-22.4	-24.2	-32.3	24%	34%	8%
357.5	-20.7	-22.4	-26.6	-32.0	52%	29%	15%
397.5	-21.4	-24.3	-25.6	-32.2	39%	69%	27%
412	-18.8	-21.3	n.a.	-31.6	n.a.	n.a.	20%
427.5	-22.1	-22.4	-24.1	-32.2	20%		
477.5	-21.4	-22.8	-26.4	-29.0	65%	27%	18%
517.5	-19.8	-22.2	-26.3	-34.2	45%	37%	17%

557.5	-21.05	-22.1	-25.7	-32.1	42%	22%	9%
604.5	-20.35	-22.2	-21.7	-31.3	12%		
647.5	-18.6	-19.0	-20.7	-31.3	17%		
697.5	-18.9	-19.9	-23.0	-32.0	31%	24%	8%
760.5	-17.1	-19.0	-20.5	-32.3	22%	56%	12%
807.5	-18.3	-19.3	-20.2	**-31.9**	14%	53%	7%

$\delta^{13}C_{Phy}$ values indicating in-situ methanogenic activities in the Black Sea

Our study showed that $\delta^{13}C_{Phy}$ value is less variable in the marine-phase sedimentation zone compared to the lacustrine sediment. However, $\delta^{13}C_{Phy}$ values were systematically more negative than $\delta^{13}C_{BPcren}$ and $\delta^{13}C_{BP0}$. This indicates that archaeol is derived from different archaeal communities that utilize different carbon sources than the producers of caldarchaeol and crenarchaeol. Besides, we observed no particular pattern between $\delta^{13}C_{CL\text{-}Phy}$ and $\delta^{13}C_{IPL\text{-}Phy}$. This is probably due to the higher turnover of archaeol in sediment. The archaeol concentration in sediments is substantially lower than caldarchaeol and crenarchaeol, both of which have relatively large fossil pools from planktonic thaumarchaeal activity; accordingly, sedimentary contributions will have a stronger impact on the isotopic compositions of the archaeol pool. In the lacustrine-phase methanogenic zones from 450 down to 700 cmbsf, the IPL-archaeol proportion generally increased with depth, consistent with its formation by active sedimentary archaeal communities (Fig. 4). The acetate and DIC carbon isotopic compositions became more enriched with depth. This suggests that both are potential carbon sources utilized during the growth of archaeol-producing archaea, with the consequence that the residual substrate pools become enriched in ^{13}C. ^{13}C enrichments of the acetate and DIC pools are expected to be particularly expressed during acetoclastic and CO_2 reducing methanogenesis and are therefore feasible sources of archaeol. Moreover, recent radiotracer experiments suggested the active sedimentary production of core archaeol by methanogens (Evans et al., 2019). The apparent increase in the isotopic fractionation between archaeol and substrate (DIC or acetate) with depth (Fig. 3) can be explained by observations by Nguyen et al. (2019) who found that low energy flow could lead to larger fractionation between substrate and lipid biomarkers of methanogens. The decreasing availability of energy with depth in Black Sea sediments will probably result in the larger fractionation as observed in our samples. From 700 cmbsf downwards, $\delta^{13}C_{IPL\text{-}Phy}$ values became more depleted than $\delta^{13}C_{CL\text{-}Phy}$, with an average value of -48.5‰ and -37‰, respectively. The isotopic fractionation between archaeol and DIC reached up to 55‰. Such a large fractionation suggests methane-metabolic activities by methanogens or methanotrophs at low substrate concentration (Nguyen et al., 2019).

ACKNOWLEDGMENT.

We are grateful to the crew and the scientific shipboard party of the FS Meteor cruise M84-1 (DARCSEAS). Wendt Jenny, Prieto Xavier, and Tauber Heidi are thanked for supporting sampling and instrumental analyses. This study was funded by the European Research Council under the European Union's Seventh Framework Programme-Ideas Specific Programme, ERC grant agreement No.247153 (Advanced Grant DARCLIFE; principal investigator, K.-U.H.) and by the Deutsche Forschungsgemeinschaft through the Gottfried Wilhelm Leibniz Prize, awarded to K.-U.H. (Hi 616-14-1). Zhu was sponsored by the Chinese Scholarship Council (CSC) and the Bremen International Graduate School for Marine Sciences (GLOMAR).

Chapter V

Microbial heterotrophy in enrichment cultures dominated by anaerobic methane-oxidizing consortia

Qing-Zeng Zhu[1], Gunter Wegener[1,2], Kai-Uwe Hinrichs[1], Marcus Elvert[1]

[1]MARUM - Center for Marine Environmental Sciences, University Bremen, 28359 Bremen, Germany

[2]Max-Planck Institute for Marine Microbiology, 28359 Bremen, Germany.

Abstract

Consortia of anaerobic methanotrophic archaea (ANME) and sulfate-reducing bacteria (SRB) are responsible for the anaerobic oxidation of methane (AOM) in marine sediments. Enrichment cultures dominated by such consortia have been frequently obtained but still contain additional community members unrelated to AOM, even after years of repeated dilution and inoculation. To study the potential heterotrophic activity of these ancillary microorganisms, we amended enrichments of AOM cultures dominated by ANME-1 archaea and different partner bacteria (Seep-SRB-2 and *Candidatus* Desulfofervidus auxilii-HotSeep-1 clade) with L-leucine-3-^{13}C (^{13}C-leu) and quantified the uptake in individual lipids. Most ^{13}C-leu incorporation was observed in bacterial fatty acids, especially iso and anteiso-branched $C_{15:0}$ and $C_{17:0}$, according to predictions based on biosynthetic utilization via heterotrophy. Compared to bacterial fatty acids, archaeal ether lipids were substantially less ^{13}C-labeled, indicating a dominant utilization of dissolved inorganic carbon produced from the respiration of ^{13}C-leu, but also providing some evidence of organic substrate use by ancillary archaea other than ANME. Uptake patterns of both bacterial and archaeal lipids were independent of the addition of methane to the enrichments. Pure cultures of the partner bacterium *Ca.* Desulfofervidus auxilii (*Ca.* D. auxilii) did not show ^{13}C-leu incorporation. Our results (1) provide evidence that ^{13}C-depleted branched bacterial fatty acids in environmental samples hosting AOM communities are diagnostic of heterotrophic microbes that utilize amino acids derived from AOM consortia necromass and 2) confirm that ANME-1 and their partner

bacteria are strict autotrophs. Bacterial candidate organisms are members of the Chloroflexi (i.e. Anaerolineae) and Spirochaetes, which both have been frequently observed in AOM cultures and marine environments. Ancillary heterotrophic archaea (i.e. Thermoplasmatales and Bathyarchaeota) also coexist under these conditions but activities are much more sluggish compared to heterotrophic bacteria.

Introduction

Methane is the most abundant hydrocarbon in marine sediments. The emission of methane from sediments to the water column and eventually the atmosphere is attenuated by the anaerobic oxidation of methane (AOM). Two decades of studies have shown that consortia of anaerobic methanotrophic archaea (ANME) and sulfate reducing bacteria (SRB) are responsible for AOM in marine sediments (Hinrichs et al., 1999; Boetius et al., 2000; Reeburgh, 2007; Wegener et al., 2016b). Three different clades of ANME archaea are known, ANME-1, ANME-2, and ANME-3 (Orphan et al., 2002; Niemann et al., 2006; Knittel et al., 2018) with syntrophic partner bacteria consisting of SRB of the *Desulfosarcina/Desulfococcus* (DSS) cluster (ANME-1 and -2; Boetius et al., 2000; Michaelis et al., 2002) or *Desulfobulbus* species (ANME-3; Niemann et al., 2006). The different consortia types can be identified by diagnostic lipid patterns. ANME-1 dominantly synthesizes glycerol dialkyl glycerol tetraethers (GDGTs) with phosphoglycerol and glycosidic head groups, while ANME-2 and ANME-3 clusters are characterized by archaeol-based diethers (Blumenberg et al., 2004; Rossel et al., 2008; 2011). Compared to ANMEs, their bacterial partners have been shown to possess more complex lipid patterns, which are taxonomically only partly distinctive (Blumenberg et al., 2004; Elvert et al., 2005; Niemann and Elvert, 2008). However, it has been shown that ANME-2a/DSS aggregates are found to be associated with a high abundance of $C_{16:1w5c}$ and $cyC_{17:0w5,6}$ fatty acids (Blumenberg et al., 2004; Elvert et al., 2005) while branched-chain fatty acids such as $aiC_{15:0}$ are prevailing in bacteria associated with ANME-1 (Niemann and Elvert, 2008).

Based on stable isotope probing (SIP) experiments of lipids in AOM consortia, Wegener et al. (2008) provided evidence that ANME types assimilate both methane and inorganic carbon into biomass and that SRB partners are exclusively autotrophic. Expanding this approach by dual SIP on a mesophilic AOM enrichment from hot vents of the Guaymas Basin, Gulf of California,

ANME-1 had even been shown to use methane solely as energy source and predominantly assimilate inorganic carbon and thus should be classified as methane-oxidizing chemoorganoautotrophs (Kellermann et al., 2012). These sediment-free and long-term AOM enrichments are successfully cultivated at 37 °C (named G37) dominated by a consortium of ANME-1 and Seep-SRB2 and at 50 °C (named G50) dominated by ANME-1 and *Ca.* D. auxilii – HotSeep-1 (Wegener et al., 2015; 2016b). The latter has been found to express direct electron transfer via nanowires and might explain a principal mechanism of AOM under thermophilic conditions (Wegener et al., 2015). The partner bacterium in this consortium, *Ca.* D. auxilii, is purely autotrophic and was isolated with hydrogen as sole electron donor and sulfate as electron acceptor (Krukenberg et al., 2016).

Even though sediment-free AOM enrichments have been obtained by long-term cultivation, microbial community members with no obvious relationship to AOM remain in substantial quantities (Wegener et al., 2016b). Most studies to date have been focusing on the AOM consortia members, but the functions of ancillary microbes remain largely unknown. Only Kellermann et al. (2012) identified the ancillary bacteria in the previous AOM enrichment of G37 to have a heterotrophic character. However, the medium used for maintaining the AOM enrichment for years is very oligotrophic (Widdel and Bak, 1992), which makes the strategy of survival of the ancillary community members very enigmatic.

Here we explore the functions of ancillary community members in the G37 and G50 AOM enrichment cultures using position-specifically labeled L-leucine-3-^{13}C (^{13}C-leu). Leucine is one of the most abundant amino acids in the microbial protein and represents an important source of carbon, nitrogen, and energy for metabolism maintenance (Kirchman et al., 1985). Leucine catabolism is inhibited when sugar or other preferential substrates are available but becomes extremely important under oligotrophic conditions (Harwood and Canale-Parola, 1981; Mårdén et al., 1987). For example, anaerobic marine spirochaetes can prolong their survival under starvation conditions by obtaining energy derived from leucine fermentation (Harwood and Canale-Parola, 1981). Studies also found high expression of L-leucine transporters as a response to starvation (Fonseca et al., 2011). Moreover, leucine catabolism supplies isovaleryl-CoA as a primer for the synthesis of odd iso-branched fatty acids which are

used as biomarkers for heterotrophic bacteria (Kaneda, 1991; Middelburg et al., 2000; Veuger et al., 2012). Moreover, leucine has been shown to be directly used in archaeal lipid biosynthesis by the extremely halophilic heterotrophic *Halobacterium salinarum* (Yamauchi, 2010) but never before in any other archaeon.

Based on the above-mentioned studies, leucine as a precursor molecule for lipid biosynthesis is ideal to track heterotrophic activity under starvation conditions or in slow-growing enrichment cultures such as AOM enrichments. Using the position-specific ^{13}C-leu labeling approach outperforms uniform isotope labeling, as produced labeling patterns allow a careful inspection of microbial biosynthetic pathways (Scandellari et al., 2009; Fischer and Kuzyakov, 2010). This approach also largely circumvents the ^{13}C flow into the pool of dissolved inorganic carbon (DIC), which may cause indirect labeling via autotrophy and thus would interfere with the interpretation of carbon source use. Results will show that ancillary microbes in AOM enrichment cultures are dominantly heterotrophic bacteria, which can be identified via diagnostic fatty acids, and that coexisting heterotrophic archaea are present but are much more sluggish.

Materials and methods

The production and maintenance of the sediment-free AOM cultures from the Guaymas Basin were described in detail before (Wegener et al., 2016b; Laso-Perez et al., 2018). In brief, both G37 and G50 were incubated with marine sulfate reducer medium (Widdel and Bak, 1992), and a methane atmosphere was supplied. Generally, G37 and G50 have an activity optimum at 37 °C and 50 °C and doubling times of 69 d and 55 d, respectively. Cultures were stored at their designated temperatures and sulfide concentrations were measured as described before (Cord-Ruwisch, 1985). When sulfide concentrations exceeded 15 mM, microbial cells were inoculated into a new medium. Pure sulfate reducer *Ca.* D. auxilii was isolated from G50 with hydrogen as the sole electron donor and sulfate as electron acceptor (Krukenberg et al., 2016). It is chemolithoautotrophic and grows at temperatures between 50 °C and 70 °C with an activity optimum at 60 °C and doubling time of 4–6 d.

Culture experiments

For all experiments with the AOM cultures, the culture medium was exchanged and cultures were equally distributed in 156 ml cultivation bottles. In the case of the culture of *Ca.* D. auxilii new dilutions were prepared (5 ml active culture for inoculation). L-leucine-3-^{13}C (Sigma-Aldrich, Germany; the rest of the manuscript will use ^{13}C-leu as a simplified form) was dissolved in MilliQ water and sterilized by filtration with a 0.1 µm filter. G37 and G50 were amended with 100 µM of sterilized ^{13}C-leu and incubated under three different conditions for 28 d (Table.1): experiment 1) with methane and without L-leucine-3-^{13}C as a negative control; experiment 2) with methane and ^{13}C-leu; experiment 3) with ^{13}C-leu and without methane as a positive control; experiment 4) with methane and ^{13}C-leu but treated with 1M $ZnCl_2$ as dead control. In comparison to these concerted experiments, the autotrophic *Ca.* D. auxilii culture, growing anaerobically with a H_2 headspace, was amended with 100 µM of sterilized ^{13}C-leu in experiment 5 that lasted for 40 d.

Table 1. Overview of conditions in incubation experiments; CH_4 is provided as energy source in G37 and G50 while Ca. D. auxilii uses H_2 as energy source; N.A: not available

Name	$\delta^{13}C_{DIC}$ at T_0	Incubation Time	experiment1 w CH_4 w/o ^{13}C-leu	experiment2 w CH_4 w ^{13}C-leu	experiment3 w/o CH_4 w ^{13}C-leu	experiment4 Dead control	experiment5 w H_2 w ^{13}C-leu
G37	-14.9	12 h-28 d*	2	2	2	2	
G50	-25.8	28 d	2	2	2	N.A	
Ca. D. auxilii	-17.5	40 d				N.A	2

** G37 was incubated for 12h, 3d, 7d, 14d, 28d to track continuous labeling in this study*

Determination of sulfide concentration and isotopic composition of dissolved inorganic carbon

Sulfide concentrations were used for monitoring the growth of AOM consortia and *Ca.* D. auxilii. The subsampling of G37 for sulfide concentrations analysis was at 0 h, 12 h, 3 d, 7 d, 14 d, 21 d, and 28 d. The subsampling of G50 for sulfide concentrations analysis was at 7 d, 21 d, and 28 d. The subsampling of *Ca.* D. auxilii for sulfide concentrations analysis was only at 0 h and 40 d. At the same time, the DIC isotopic composition ($\delta^{13}C_{DIC}$) was measured to

constrain the leucine mineralization according to (Aepfler et al., 2019). The subsampling of G37 for $\delta^{13}C_{DIC}$ analysis was at 0 h, 12 h, 3 d, 7 d, 14 d, 21 d, and 28 d. The subsampling of G50 for $\delta^{13}C_{DIC}$ analysis was at 7 d, 21 d, and 28 d. The subsampling of *Ca.* D. auxilii for $\delta^{13}C_{DIC}$ analysis was only at 0 h and 40 d. 1 ml of the sample was taken by syringe from the incubation serum bottles and filtered with a 0.2-µm filter to remove cells and other particles. Finally, the samples were acidified with 100 µl phosphoric acid for overnight in an Exetainer® vial pre-purged with CO_2 free air before isotopic analysis. All samples were measured with a Thermo Scientific Delta Ray isotope ratio infrared spectrometer with an analytical error of ±1‰. All isotopic values are reported in the delta notation as $\delta^{13}C$ relative to the Vienna PeeDee Belemnite (VPDB) standard.

Lipid extraction, identification, quantification, and isotopic analysis

In our experiments, subsampling for lipid extraction from the same bottle at each time point was avoided due to potential contamination. Instead, each time point is corresponding to a different bottle. Cell pellets from the AOM enrichment cultures were extracted using a modified Bligh and Dyer protocol (Sturt et al., 2004). Bacterial fatty acids were retrieved by saponification of the total lipid extract and analyzed as fatty acid methyl esters (FAMES) after derivatization with BF_3 in methanol (Elvert et al., 2003). Archaeal lipids were separated into intact polar lipids (IPLs) and apolar core lipids (CLs) fractions. The separation was performed using an Inertsil Diol column (5 µm, 150*10 mm, GL Sciences Inc., Tokyo, Japan), which was connected to an Agilent 1200 series HPLC equipped with an Agilent 1200 series fraction collector (Meador et al., 2015). In brief, solution A and B were prepared with n-hexane/2-propanol (85:15, v:v) and 2-propanol/MilliQ water (90:10, v:v), respectively. The flow rate was set to 3 ml min^{-1} and the eluent gradient was: 100% A to 10% B in 5 min, to 85% in 1 min, hold at 85% B for 9 min, then column re-equilibration with 100% A for 6 min The fraction collection time windows are from 0.1 to 5 min for the apolar fraction and from 5 to 15 min for the polar fraction. Aliquots of sample fractions were reanalyzed on the analytical column on HPLC-qTOF-MS (Bruker, Bremen, Germany) to check the separation quality (Wörmer et al., 2013). After successful separation, both IPL and CL fractions were treated with boron tribromide (BBr_3) treatment to cleave ethers (Jahn et al., 2004), followed by reduction of the resulting alkyl bromides with superhydride (Aldrich). The products were purified by silica gel column chromatography using 4 ml hexane as eluent. Both FAMEs and isoprenoidal

hydrocarbons were measured by gas chromatography coupled to a flame ionization detector (GC-FID, ThermoFinnigan) for quantification and GC–mass spectrometry (GC-MS, ThermoFinnigan Trace GC coupled to TraceMS) for structural identification using protocols described before (Aepfler et al., 2019). Lipid carbon isotope compositions were determined using GC-isotope ratio-MS (ThermoFinnigan Trace GC coupled to ThermoFinnigan Delta V Plus) connected via a GC Isolink interface and using the same GC conditions as for GC-FID and GC-MS measurements. The precision of replicate analysis (n = 2) was ⩽1‰. All isotopic values are reported in the delta notation as $\delta^{13}C$ relative to the Vienna PeeDee Belemnite (VPDB) standard. Uptake of ^{13}C-leu into bacterial lipids, expressed as percentage ^{13}C incorporation, was calculated as the product of excess ^{13}C and the amount of fatty acid carbon based on quantification via GC-FID. Excess ^{13}C is derived from the difference between the fractional abundance (F) of ^{13}C in fatty acids after 28 d relative to T_0 with $F = {}^{13}C/({}^{13}C+{}^{12}C) = R/(R+1)$ and R being derived from the measured $\delta^{13}C$ values as $R = (\delta^{13}C /1000 + 1) \times R_{VPDB}$.

Results

Sulfide production during incubation

Sulfide concentrations were measured to monitor the metabolic activity of the organisms involved in AOM and of *Ca.* D. auxilii (Fig. 1). In G37 and G50 cultures without methane, sulfide concentrations did not change over time, indicating a lack of activity of sulfate reducing bacteria. When CH_4 was provided, the sulfide concentration increased gradually from 2.8 to 15.5 mM for G37 and from 2.2 to 24.7 mM for G50 after 28 d of incubation. There was no substantial difference between incubations with ^{13}C-leu and without ^{13}C-leu addition, indicating that leucine did not affect the sulfate reduction rate. Sulfide did not change in the dead control of G37. For *Ca.* D. auxilii, the sulfide concentration increased from 2.7 to 26.1 mM after 40 d incubation.

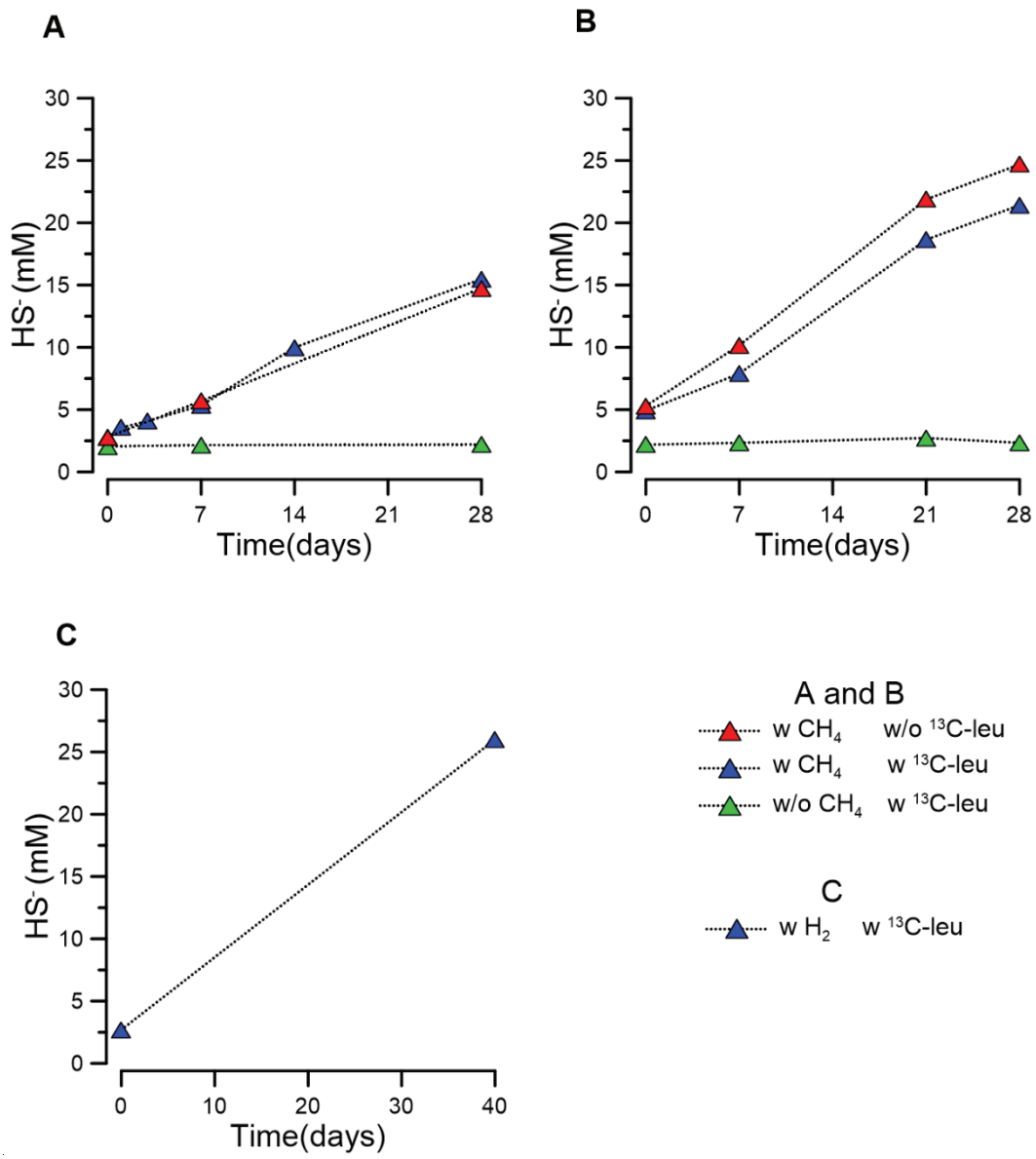

Fig.1. Development of sulfide concentrations in the different experiments. (A) G37 and (B) G50 enrichment cultures amended with (w) and without (w/o) ^{13}C-leu, (C) Ca. D. auxilii incubated with ^{13}C-leu under H_2 headspace for 40 d.

Temporal development of carbon isotopic compositions in ^{13}C-leu experiments

In all samples, we measured the development of $\delta^{13}C_{DIC}$ values as an indicator of microbial oxidation of position-3 carbon of ^{13}C-leu (Fig. 2). In the G37 incubation (experiment 2), $\delta^{13}C_{DIC}$ changed from -14.9‰ to +50.7‰ after 28 d under the condition of supplying both CH_4 and ^{13}C-leu. When incubation was only provided with ^{13}C-leu but no CH_4 (experiment 3), $\delta^{13}C_{DIC}$ changed from -14.9‰ to +68.1‰ in G37. In contrast, in experiment 1 of G37 supplied

with methane but no ^{13}C-leu, $\delta^{13}C_{DIC}$ decreased from -14.9‰ to -19.7‰ caused by ongoing AOM. Moreover, our dead control (experiment 4) showed that $\delta^{13}C_{DIC}$ stayed at -20 ± 0.3‰ after 28 d of incubation in G37. In G50 incubation, $\delta^{13}C_{DIC}$ changed from -26.2‰ to +117.7‰ after 28 d under the condition of supplying both CH_4 and ^{13}C-leu (experiment 2). When we only provided ^{13}C-leu but no CH_4, $\delta^{13}C_{DIC}$ changed from -26.2‰ to +124.8‰ in G50 (experiment 3). In contrast, in experiment 1 of G50 the $\delta^{13}C_{DIC}$ decreased from -26.2‰ to -34‰ which was caused by ongoing AOM. In experiment 5 using *Ca.* D. auxilii with the addition of ^{13}C-leu, the $\delta^{13}C_{DIC}$ value was steady at -17.5‰ and did not change during incubation.

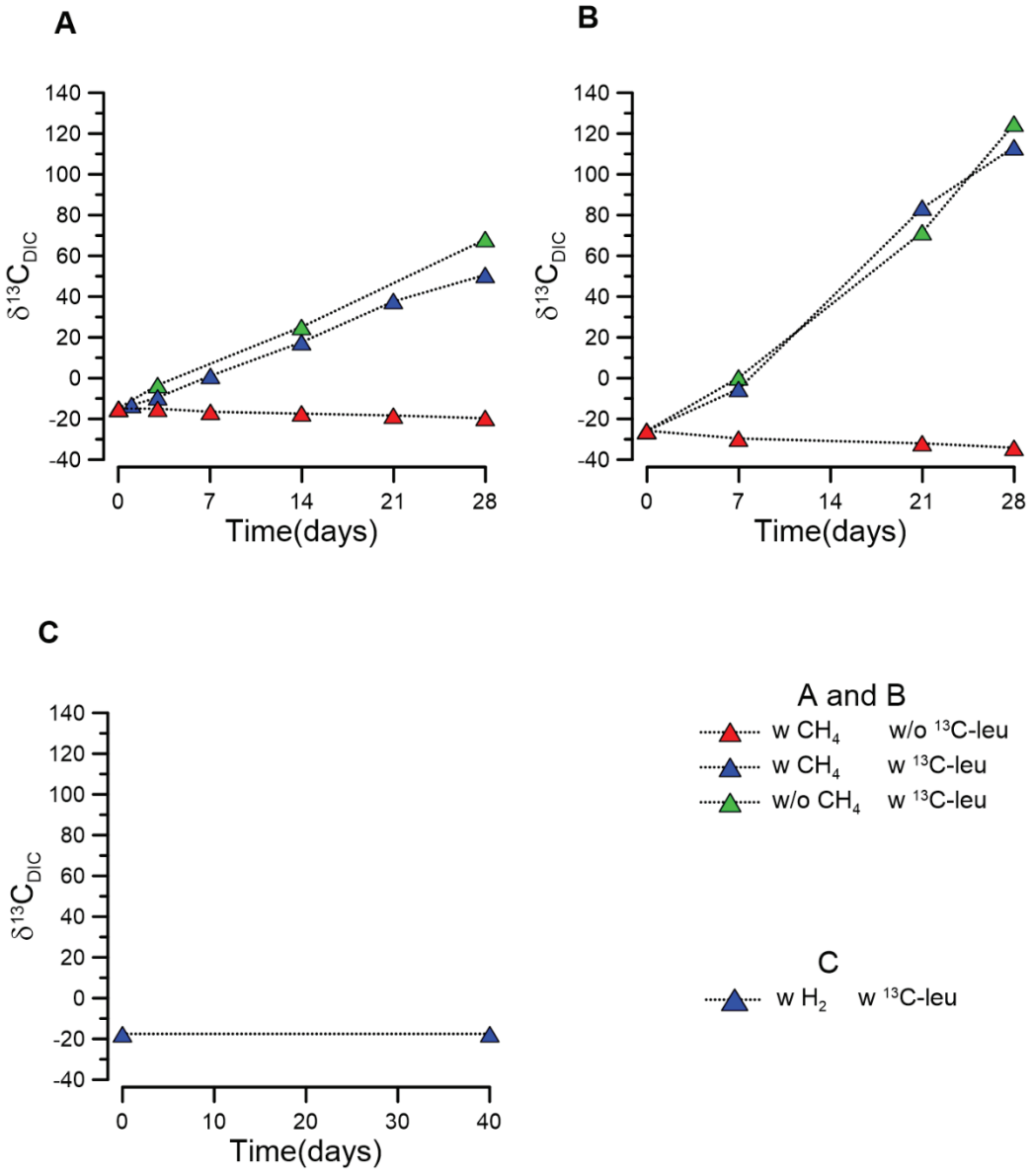

Fig. 2. Development of $\delta^{13}C_{DIC}$ in different experiments of G37 (A), G50 (B), and Ca. D. auxilii (C) cultures; G37 and G50 were amended with and without ^{13}C-leu. Ca. D. auxilii was incubated with ^{13}C-leu under H_2 headspace for 40 d.

Original bacterial lipid patterns and isotopic compositions of AOM enrichments and *Ca*. D. auxilii

Sulfate reducing bacteria in G37 are dominated by Seep SRB2 (Wegener et al., 2016b). The most dominant fatty acids in G37 are $C_{18:1w7}$ (37%), $C_{16:0}$ (24%), and $C_{18:0}$ (21%) (Fig. 3). The total of all branched-chain fatty acids in G37 accounted for 7%. In G50, where *Ca.* D. auxilii is dominant, $C_{16:0}$ and $C_{18.0}$ are the main fatty acids with a content of 46% and 28%, respectively. The total of all branched-chain fatty acids in G50 accounted for 12%. In both enrichments, the remaining fatty acids amount to less than 6% of the total bacterial fatty acid pools. The fatty acid composition of *Ca.* D. auxilii is similar to G50, but the content of $C_{16:0}$ (39%) and $C_{18.0}$ (52%) occupied 91%. The total of all branched-chain fatty acids in *Ca.* D. auxilii accounted for less than 0.7%. Our GC-FID analysis did not show discernible changes in fatty acid patterns and compositions in all samples before and after incubation. All branched and most monounsaturated fatty acids in G37 were relatively ^{13}C-depleted with δ^{13}C values of branched-chain fatty acids ranging from -46‰ to -61‰ and $C_{17:1w8}$ and $C_{17:0}$ being even more negative down to -81‰ (Fig. 3). Monounsaturated fatty acids ranged from -55‰ to -68‰ except $C_{18:1w9}$ with a rather positive value of -17‰, while saturated $C_{14:0}$, $C_{16:0,}$ and $C_{18:0}$ fatty acids had less negative δ^{13}C values between -25‰ and -38‰. The fatty acids in G50 are generally more enriched in ^{13}C compared to G37 ranging between -25‰ and -45‰ (Fig. 3), showing the most negative δ^{13}C values for the branched-chain fatty acids *i*$C_{16:0}$ and *ai*$C_{17:0}$. By contrast, δ^{13}C values of all fatty acids in *Ca.* D. auxilii were in a relatively narrow range between -21‰ and -30‰.

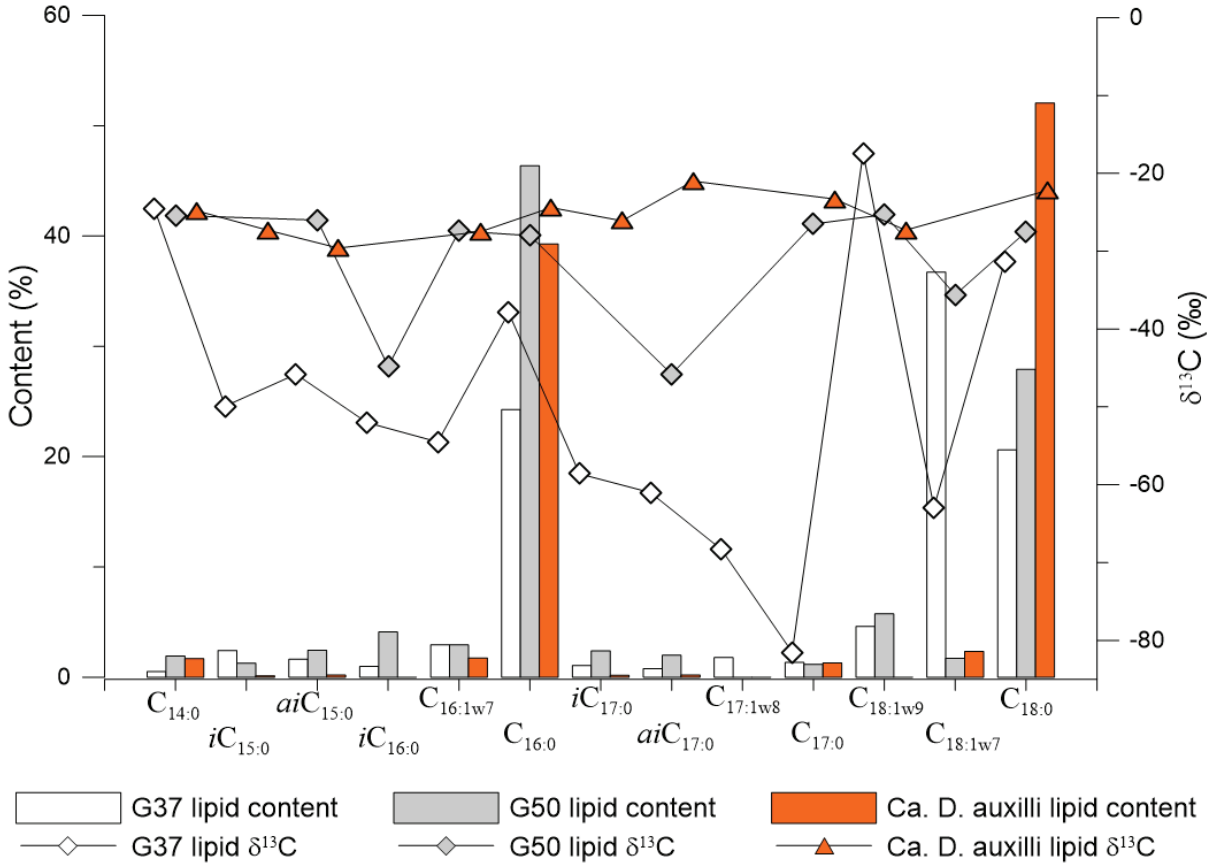

Fig.3. Bacterial fatty acid pattern (in %) and stable carbon isotopic compositions (in ‰) in G37, G50, and Ca. D. auxilii.

Temporal development of isotopic composition of bacterial and archaeal lipids in SIP with position-specific labeled leucine

The changes in $\delta^{13}C$ values of some representative fatty acids treated with ^{13}C-leu are shown in Fig. 4 (Table S1 showed all fatty acids detected in the experiment). ^{13}C-labeling was immediately seen after 12 h in the G37 experiment and continuously increasing over time showing strong ^{13}C-enrichment with $\delta^{13}C$ values of up to 260‰ for the branched-chain fatty acids $iC_{15:0}$ and $iC_{17:0}$. After 14 d, however, even stronger ^{13}C-labeling was detected in $aiC_{15:0}$, which was enriched in ^{13}C by 2100‰ relative to the iso-branched fatty acids. Even higher ^{13}C uptake with $\delta^{13}C$ values of up to 6400‰ was detected in the G50 experiment after 28 d for $iC_{15:0}$ and $iC_{17:0}$. Besides, the monounsaturated fatty acid $C_{18:1w9}$ was also highly labeled in the G37 experiment with a $\delta^{13}C$ value of 2200‰, which was not the case in the G50 enrichment culture. Even-carbon-number saturated fatty acids were the least labeled in both enrichment

cultures. Their isotopic compositions were lower than the accumulation of ^{13}C in DIC. The changes in $\delta^{13}C$ values of fatty acids with no methane supplied are shown in Fig. 4. Their ^{13}C-labeling patterns in both G37 and G50 after 28d were generally similar to the corresponding ones treated with methane. In particular, some lipids were less labeled when no methane was supplied. *Ca.* D. auxilii as a pure autotrophic culture showed a different ^{13}C labeling uptake compared to G50, from which it had been originally isolated from. After 40 d of incubation $iC_{17:0}$ and $iC_{15:0}$ were only slightly labeled in *Ca.* D. auxilii with $\delta^{13}C$ values reaching 40‰ and 250‰, respectively. This is rather low compared to G50. All other fatty acids did not show ^{13}C label uptake.

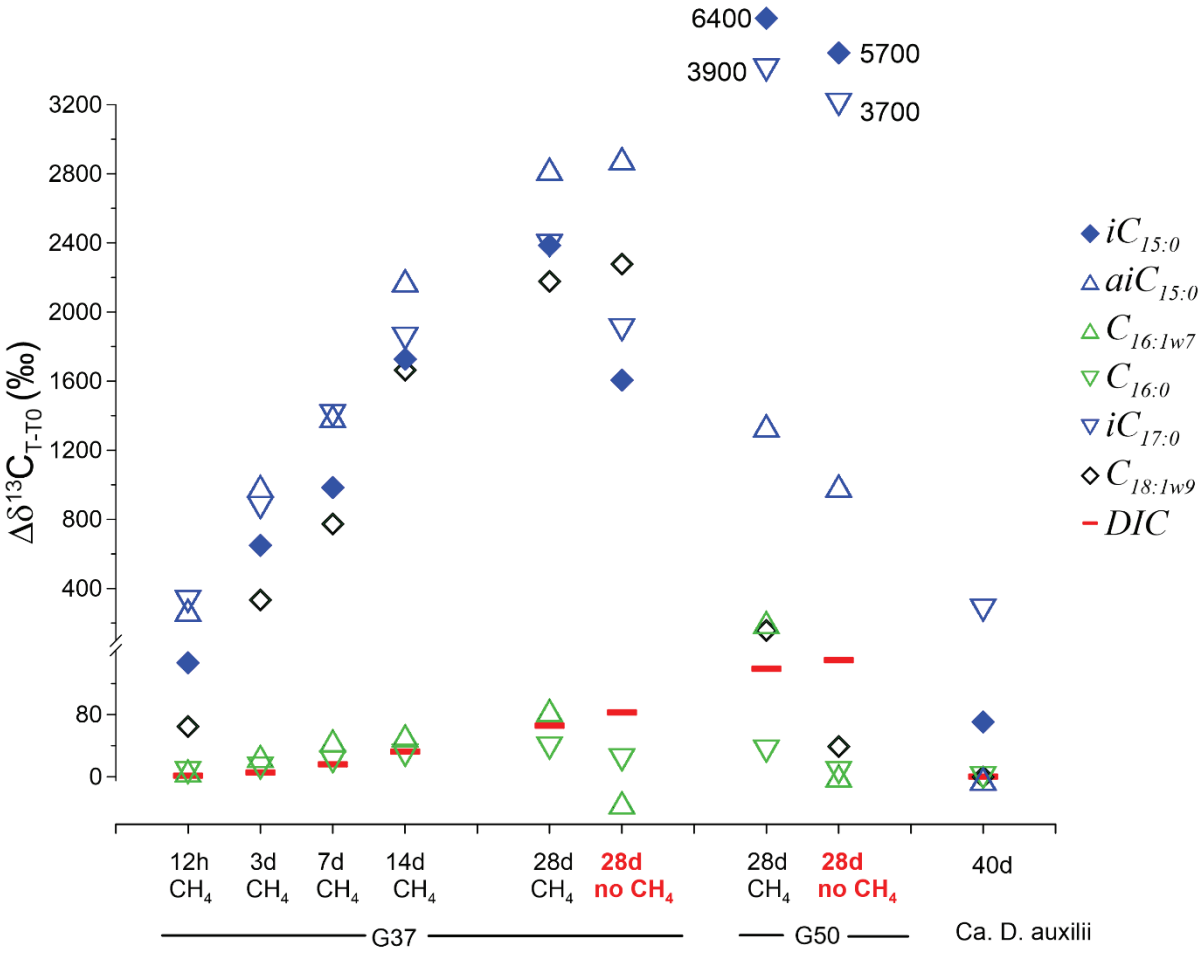

Fig. 4. Development of carbon isotopic compositions of bacterial fatty acids during incubation of G37, G50, and Ca. D. auxilii cultures; all data are shown as $\Delta = \delta^{13}C_T - \delta^{13}C_{T0}$; numbers marked in the figure are the $\delta^{13}C$ values out of axis limits.

In this study, all the lipid was extracted from the wet biomass, so the dry weight was not available. The absolute ^{13}C incorporation is not available due to the absence of dry weight. Instead, we calculated the relative ^{13}C-incorporation pattern of bacterial fatty acids. The total fatty acids in an enrichment contribute 100% of ^{13}C incorporation. The contribution of one single fatty acid compared to total lipids is the relative ^{13}C incorporation. Relative ^{13}C incorporation is decided by two factors, initial lipid abundance and the change of lipid isotopic composition. Thus the relative ^{13}C incorporation can directly compare the amount of ^{13}C incorporation among different lipids. Most ^{13}C-incorporation is observed for monounsaturated $C_{18:1w7}$ and $C_{18:1w9}$, as well as branched fatty acids in the G37 enrichment culture while the incorporation pattern of the G50 enrichment culture is dominated by *iso*$C_{15:0}$ and *iso*$C_{17:0}$ having highest ^{13}C incorporation. The iso branched fatty acids are higher incorporated by ^{13}C than anteiso branched ones. The even-number saturated fatty acids have the least incorporation even though they are the main fatty acids in all enrichments (See Fig. 3 for their relative concentration and Fig. 5 for their relative ^{13}C incorporation).

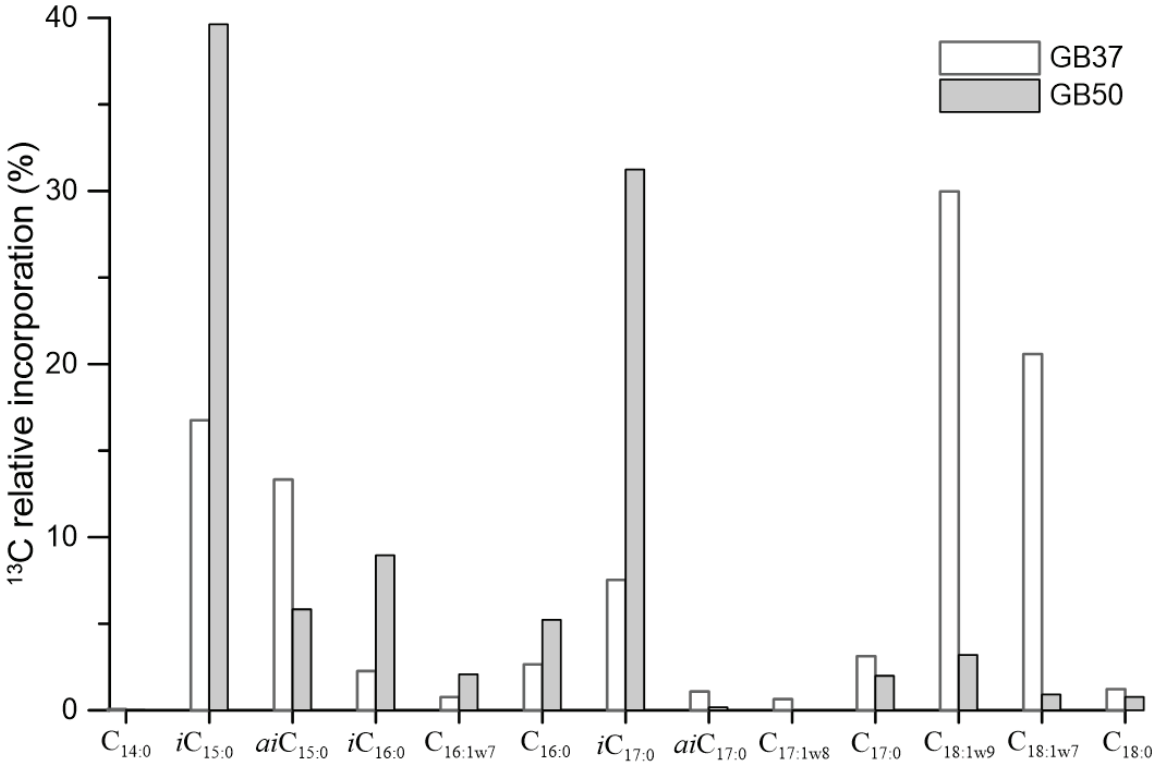

Fig. 5. Relative incorporation of ^{13}C into different fatty acids extracted from the ^{13}C-leu incubation of G37 and G50 cultures after 28 d.

Changes in carbon isotopic compositions of archaeal lipids treated with ^{13}C-leu are partly shown in Fig. 6 (See Table S2 for all the archaeal lipids). The ^{13}C-labeling intensity of phytane (Phy) and biphytanes (Bp) derived from ether-cleavage of IPL and core lipid fractions were extremely low in both ^{13}C-leu experiments and remained below the isotopic enrichment of the DIC pool after 28 d. There was only a slight difference between experiments with and without CH_4 supply. After 28 d, $\delta^{13}C$ values of IPL-derived Phy increased by 113‰ with CH_4 and 118‰ without CH_4 in the G37 while the corresponding CL-derived Phy increased by 71‰ with CH_4 and 50‰ without CH_4. Throughout the experiments, Bps had much lower $\delta^{13}C$ values than Phy, regardless of being analyzed in the CL or IPL fractions. IPL-Bp0 revealed only marginal ^{13}C-enrichment of 2.8‰ with CH_4 and 5.7‰ without CH_4 relative to a T_0 of -70.2‰, so was also its corresponding CL-Bp0 (increase by 2.5‰ with CH_4 and 4.4‰ without CH_4). No ^{13}C uptake was observed for Bp1 and Bp2, both in CLs and IPLs after 28 d. In the G50 enrichment culture, only CL-derived Phy and Bps could be successfully measured. CL-derived Phy increased from -74.3‰ to -7.3‰ with CH_4 and -23.4‰ without CH_4. CL-derived Bp0 showed a ^{13}C-enrichment of 16‰ with CH_4 and 5.6‰ without CH_4 relative to a T_0 of -70.6‰. No ^{13}C label uptake was observed in Bp1 and Bp2 after 28 d.

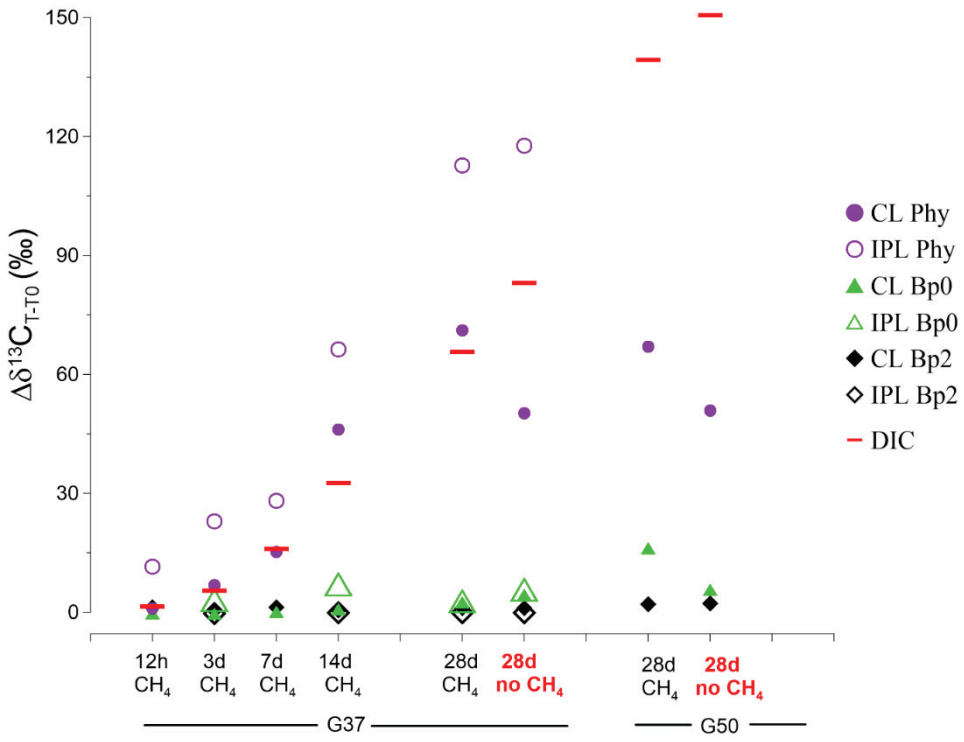

Fig. 6. Development of carbon isotopic composition of archaeal lipids during incubation of G37 and G50 enrichment cultures; all the data are shown as $\Delta\delta^{13}C = \delta^{13}C_T - \delta^{13}C_{T0}$. *Some IPL Bp0 and Bp2 values are not shown in the figure due to low concentration.*

Discussion

Leucine catabolism and assimilation are performed by ancillary microorganisms but not AOM consortia

In the studied AOM enrichment cultures, sulfide production almost quantitatively depends on methane as energy source. The turnover of leucine as observed by changes in $\delta^{13}C_{DIC}$ values had only a minor effect on sulfide production (Fig. 1). Interestingly, leucine turnover occurred no matter whether CH_4 was provided to the cultures or not, indicating that leucine was metabolized by ancillary microbes, which are not involved in AOM. Direct ^{13}C-leu incubation of *Ca.* D. auxilii cultures showed no change in $\delta^{13}C_{DIC}$ after 40 d incubation and confirmed that this AOM partner bacterium is not involved in leucine catabolism.

The catabolism of leucine is comprised of diverse reactions, generating initially isovaleryl-CoA and finally acetoacetate and acetyl-CoA (Yamauchi, 2010; Diaz-Perez et al., 2016). These products undergo further metabolic processes, including complete oxidation and generation of bacterial odd iso-branched fatty acids or, in case of halophilic archaea, isoprenoid lipids (Harwood and Canale-Parola, 1981; Yamada et al., 2006; Aepfler et al., 2019). In our experiments, high ^{13}C incorporation into selected fatty acids such as $iC_{15:0}$ and $iC_{17:0}$ was independent of CH_4 supply. This shows that some bacteria, which are not involved in sulfate-dependent AOM, are assimilating amino acids and potentially other organic compounds available for lipid biosynthesis. This is consistent with the previous study performed by Kellermann et al. (2012) who found that in the absence of methane the residual fraction of metabolically active bacteria are heterotrophs. In comparison to experiments with AOM consortia, direct test on *Ca.* D. auxilii showed only very limited ^{13}C-incorporation into $iC_{15:0}$ and $iC_{17:0}$ fatty acids after 40 d of incubation (Fig. 4 and Table S1), probably caused by a minor abundance of heterotrophic bacteria still present in this enrichment culture. This confirms that SRB in AOM consortia do not participate in leucine assimilation and mineralization. In comparison to bacterial fatty acids, the addition of ^{13}C-leu did not yield archaeal lipids with a strong change in $\delta^{13}C$ values (Fig. 6), highly suggesting that archaea are less competitive in amino acid turnover than bacteria. Moreover, the observed ^{13}C incorporation specifically into archaeol-based lipids was also independent of CH_4 supply, which indicates that there are archaea other than ANME present in the enrichments.

The lipid ^{13}C-labeling pattern indicates heterotrophy of ancillary bacteria

^{13}C-leu was intensively incorporated into $iC_{15:0}$ and $iC_{17:0}$ in both G37 and G50 (Fig. 5). This is metabolically expected because the primer isovaleryl-CoA produced after deamination and decarboxylation can be channeled into the fatty acid biosynthetic pathway leading to the formation of odd carbon-numbered, iso-branched fatty acids (Kaneda, 1963). Next to these, we observed high labeling of aiC_{15} and aiC_{17} and even-numbered iC_{16}. This could be explained by the inter-conversion of the catabolic pathways of leucine to isoleucine, leading to the formation of 2Me-Butyryl-CoA which serves as a primer molecule for the synthesis of anteiso-branched fatty acids, and inter-conversion of leucine to valine, giving rise to isobutyryl-CoA as a primer of even-numbered iso-branched fatty acids (Diaz-Perez et al., 2016; Aepfler et al., 2019). When compared to G37, G50 tends to channel more leucine into iso-branched fatty

acids than anteiso derivatives (G50, iso: anteiso = 92:8; G37, iso: anteiso = 63:37). Moreover, large incorporation of ^{13}C into straight-chain fatty acids $C_{18:1w9}$ and $C_{18:1w7}$ was observed in G37 but not in G50. Such straight-chain fatty acids may be synthesized by the continuous release of ^{13}C-enriched metabolites other than isovalerate such as acetate. The relative incorporation pattern suggests that two different heterotrophic communities exist in G37 and G50.

Utilization of leucine in archaeal lipid synthesis by ancillary archaea and ANME-1

^{13}C label uptake into both archaeal di- or tetraethers was substantially lower than for bacterial fatty acids (Fig. 6). No matter whether CH_4 was added or not, phytane derived from archaeol-based lipids had a similar ^{13}C labeling. This suggests that newly produced archaeol during the course of incubation is mostly synthesized by archaea unrelated to AOM. Rather more, indirect incorporation from DIC must be taken into consideration because ^{13}C-leu turnover will contribute ^{13}C to the DIC pool. This is extremely important when constraining the carbon sources of the archaeal lipids. In the G37 enrichment, the highest $\delta^{13}C$ value obtained for phytane derived from archaeol-based lipids was lower than $\delta^{13}C_{DIC}$ after 28 d (Table S2). However, the absolute change of phytane ($\Delta\delta^{13}C = \delta^{13}C_T - \delta^{13}C_{T0}$) relative to T_0 was higher by 47‰ than for the accompanying DIC (Fig. 6). This indicates that DIC is not the only carbon source for archaeol biosynthesis during incubation, but eventually leucine or, more likely, secondary metabolites derived from leucine catabolism of the bacteria such as acetate mentioned earlier.

ANME-1 archaea mainly comprise GDGTs which are characterized by ^{13}C-depleted carbon isotopic compositions in natural samples (Michaelis et al., 2002; Blumenberg et al., 2004). In the ^{13}C-leu incubation of this study, no strong ^{13}C-enrichment of biphytanes was observed during the course of the experiments. The largest change of $\delta^{13}C$ values occurred in Bp0 of G50, with a $\Delta\delta^{13}C$ value of 16‰. $\Delta\delta^{13}C$ of all biphytanes is much lower than that of DIC (Fig. 6). Formerly, Kellermann et al. (2012) obtained a $\Delta\delta^{13}C$ of DIC up to 940‰ (see Table S2 in Kellermann 2012) based on $^{13}CH_4$ oxidation but this value is much higher than in our experiment ($\Delta\delta^{13}C$ = 151‰). However, the $\Delta\delta^{13}C$ of Bp0 is only 3‰ in the same experiment of Kellermann et al. (2012) which is much lower than that (16‰) in our experiment, which

may point to some additional organic carbon derived directly or indirectly from leucine metabolism.

Minor bacterial and archaeal communities may thrive on AOM biomass

Analysis of the microbial composition of Guaymas Basin AOM cultures (G37 and G50) based on 16S rRNA showed a large diversity of side bacteria unrelated to AOM (i.e. Anaerolinaceae, Caldithrix, Spirochaetes or relatives of the Candidate divisions JS1, OD1, and OP11) (Kellermann et al., 2012; Wegener et al., 2016b) of which many are heterotrophs. Anaerolineae, for example, members of the phylum *Chloroflexi,* are characterized by a chemoorganotrophic lifestyle on the basis of carbohydrates and amino acid degradation under strictly anaerobic conditions (Rosenkranz et al., 2013; Liang et al., 2016; Swiatczak et al., 2017). So far, several pure cultures belonging to this bacterial family have been isolated and iso and anteiso C_{15} and C_{17} are their major cellular fatty acids (Yamada et al., 2006). This is consistent with our incubation results, which indicated the highest ^{13}C-label uptake into these lipids (Fig. 4). Spirochaetes, another heterotrophic candidate group, were also detected even though not in very high abundance. Genome sequencing and proteome analysis indicated that the Spirochaetes are obligate fermenters that metabolize proteins and carbohydrates (Paster, 2010; Dong et al., 2018) and are specifically consuming detrital biomass in anoxic hydrocarbon-rich habitats (Dong et al., 2018). The presence of this phylum in our enrichments strongly suggests that bacterial heterotrophs recycle AOM necromass. This further indicates that starving AOM biomass components such as amino acids and carbohydrates may be quickly utilized by heterotrophic scavengers in natural environments. For example, different fatty acid patterns have been associated with the two main ANME types -1 and -2 at cold seeps or microbial mats (Blumenberg et al., 2004; Niemann and Elvert, 2008). ANME-1 dominated environments are related to lower methane flux and limited energy availability and characterized by *ai*$C_{15:0}$ as well as other branched-chain fatty acids (Stadnitskaia et al., 2008). Looking at the results of our study, although focusing on leucine metabolism in AOM enrichments only, such fatty acid patterns obviously originate from heterotrophic bacteria instead of SRB. These heterotrophic bacteria effectively live on ^{13}C-depleted AOM necromass such as protein-derived materials (i.e., valine, leucine, and isoleucine) which results in the production of branched-chain fatty acids. Such utilization of AOM biomass by heterotrophs sometimes creates fatty acids being

even more negative in $\delta^{13}C$ values than fatty acids derived from autotrophic SRBs associated with ANMEs (Elvert et al., 2005).

Low lipid labeling indicates only minor activities of heterotrophic archaea AOM enrichment. The archaeal 16S rRNA analysis showed that Thermoplasmatales, Bathyarchaeota, and Lokiarchaeota coexist with ANMEs in Guaymas Basin enrichments even after years of dilution and inoculation (Wegener et al., 2016b). Of these, the order of Thermoplasmatales includes potential heterotrophs (Huber and Stetter, 2006). Bathyarchaeota (formerly known as Miscellaneous Crenarchaeotal Group, MCG), on the other hand, are extraordinarily widespread in anoxic sediments but have not been obtained in culture yet. However, based on their genomes they contain acetyl-coenzyme A-centralized heterotrophic pathways for energy conservation (Zhou et al., 2018) and are potentially able to anaerobically utilize detrital proteins (Lloyd et al., 2013). Of the class of Lokiarchaeota, finally, there was only recently a related isolate obtained in a stable culture that was degrading amino acids via syntrophy (Imachi et al., 2019). Long-term cultivation or a transcriptomic assessment of leucine-treated cultures is required to assess which microorganisms thrive in the AOM cultures on proteins.

Conclusion

The incubations of meso- and thermophilic AOM cultures from the Guaymas Basin with position-specifically labeled ^{13}C-leu as organic carbon source was used to investigate lipid formation via heterotrophy of consortia members and ancillary communities. Most of the ^{13}C from leucine is incorporated into branched-chain fatty acids, especially iso and anteiso $C_{15:0}$ and $C_{17:0}$, by heterotrophic bacteria such as Anaerolineae or Spirochaetes, with the latter being less abundant in our enrichment cultures but a specialist for necromass recycling in anoxic hydrocarbon-rich habitats. No assimilation of ^{13}C-leu into fatty acids was observed for the cultured *Ca. D. auxilii* SRB representative, isolated from a thermophilic AOM enrichment of the Guaymas Basin. A combination with former environmental information of fatty acid patterns of different AOM consortia indicates that bacterial heterotrophs thrive on ^{13}C-depleted AOM-derived necromass in the marine environment, thus explaining the common absence of AOM lipid signals in sedimentary records. In contrast, the activities of ancillary heterotrophic archaea such as Thermoplasmatales and Bathyarchaeota are much more sluggish than that of

heterotrophic bacteria. The assimilation of ^{13}C-leu into archaeal di- or tetraethers of ANMEs is not evident from our data. Targeted cultivation approaches are required to identify more specific heterotrophs in cultures and the environment.

ACKNOWLEDGMENT.

We are grateful to Susanne Menger for assisting in the cultivation; Heidi Taubner for helping to measure the DIC. Xavier Prieto and Jenny Wendt are thanked for supporting instrumental maintenance. This study was funded by the European Research Council under the European Union's Seventh Framework Programme-Ideas Specific Programme, ERC grant agreement No.247153 (Advanced Grant DARCLIFE; principal investigator, K.-U.H.); by the Deutsche Forschungsgemeinschaft through the Gottfried Wilhelm Leibniz Prize, awarded to K.-U.H. (Hi 616-14-1); by DFG under Germany's Excellence Strategy, no. EXC-2077–390741603. Zhu was sponsored by the Chinese Scholarship Council (CSC) and the Bremen International Graduate School for Marine Sciences (GLOMAR).

Supplementary material

Table S1. Temporal development of carbon isotopic compositions of DIC and bacterial lipids during incubation of G37, G50, and Ca. D. auxilii

Name	Condition	Time	DIC	C_{14}	*i*C_{15}	*ai*C_{15}	*i*C_{16}	$C_{16:1w7}$	C_{16}	*i*C_{17}	*ai*C_{17}	$C_{17:1}$	C_{17}	$C_{18:1w9}$	$C_{18:1w7}$	C_{18}
G37	w CH_4 w ^{13}C-leu	0 h	-14.9													
	w CH_4 w ^{13}C-leu	12 h	-13.5	-27	97	230	58	-46	-33	264	47	-53	-51	48	-52	-30
	w CH_4 w ^{13}C-leu	3 d	-9.5	-18	601	946	231	-28	-27	807	162	-16	61	317	-10	-28
	w CH_4 w ^{13}C-leu	7 d	1.1	-10	933	1353	301	-8	-19	1338	246	4	246	756	50	-22
	w CH_4 w ^{13}C-leu	14 d	17.7	3	1678	2136	529	-2	-11	1788	342	18	431	1645	98	-15
	w CH_4 w ^{13}C-leu	28 d	50.7	22	2335	2782	730	31	-1	2323	404	51	698	2160	120	-12
	w CH_4 w/o ^{13}C-leu	28 d	-19.7	-25	-50	-46	-52	-55	-38	-59	-61	-68	-82	-17	-63	-31
	w/o CH_4 w ^{13}C-leu	28 d	68.1	24	1556	2842	843	-88	-17	1836	332		405	2261	82	-13
G50	w CH_4 w ^{13}C-leu	0 h	-25.8													
	w CH_4 w ^{13}C-leu	28 d	113.4	21	6439	1316	589	176	5	3881	-21	51	467	132	114	-20
	w CH_4 w/o ^{13}C-leu	28 d	-34.0	-25		-26	-45	-27	-28		-46		-27	-25	-36	-28
	w/o CH_4 w ^{13}C-leu	28 d	124.7	-19	5669	968		-26	-23	3689	169		234	14		-29
Ca. D. auxilii	w H_2 w/o ^{13}C-leu	0h	-17.5	-25	-27	-30		-28	-24	-26	-21		-23	-27		-22
	w H_2 w/o ^{13}C-leu	40 d	-17.5	-26	43	-32			-26	246	-26		-24	-28		-24

Table S2. Temporal development of carbon isotopic compositions of DIC and archaeal lipids during incubation of G37and G50

Name	Condition	Time	DIC	CL-Phy	CL-Bp0	CL-Bp1	CL-Bp2	IPL-Phy	IPL-Bp0	IPL-Bp1	IPL-Bp2
G37	w CH_4 w ^{13}C-leu	0 h									
	w CH_4 w ^{13}C-leu	12 h	-13.5	-71.4	-71.1	-71.9	-70.6	-59.5	n.a	n.a	n.a
	w CH_4 w ^{13}C-leu	3 d	-9.5	-65.5	-71.2	-72.4	-71.3	-48.1	-67.1	-67.8	-67.8
	w CH_4 w ^{13}C-leu	7 d	1.1	-57.1	-70.7	-73.1	-70.6	-42.9	n.a	n.a	n.a
	w CH_4 w ^{13}C-leu	14 d	17.7	-26.2	-70	-73.8	-71.3	-4.7	-63.1	-66.2	-67.6
	w CH_4 w ^{13}C-leu	28 d	50.7	-1.2	-68.3	-72.9	-70.8	41.7	-67.4	-69.6	-67.6
	w CH_4 w/o ^{13}C-leu	28 d	-19.7	-72.3	-70.8	-73.3	-71.8	-71	-70.2	-71.5	-67.5
	w/o CH_4 w ^{13}C-leu	28 d	68.1	-22.1	-66.4	-72.8	-70.8	46.7	-64.5	-70	-67.6
G50	w CH_4 w ^{13}C-leu	0 h									
	w CH_4 w ^{13}C-leu	28 d	113.4	-7.3	-54.5	-70.4	-68.4	n.a	n.a	n.a	n.a
	w CH_4 w/o ^{13}C-leu	28 d	-34.0	-74.3	-70.6	-70.5	-70.4	n.a	n.a	n.a	n.a
	w/o CH_4 w ^{13}C-leu	28 d	124.8	-23.4	-65	-69	-68.2	n.a	n.a	n.a	n.a

Chapter VI

Conclusion and Outlook

This Ph.D. project investigated the fate of microbial lipids and characterized the microbial life in diverse marine environments. Microbial membrane lipids in environments leave signatures that reflect either paleo (fossil lipids) or modern (newly synthesized lipids, some labile IPLs) physicochemical and physiological conditions (Brocks and Pearson, 2005; Biddle et al., 2006; Brocks and Banfield, 2009). However, the application of lipids as life and chemotaxonomic biomarkers has restrictions since most lipids are not taxonomically specific and their distribution patterns are a response to multiple environmental factors. The separate carbon isotope analysis of CL and IPL provides a powerful complementary approach. In my Ph.D. project, I combined environmental stable carbon isotopic analysis and SIP incubations in the lab. Environmental sample analysis provided fundamental constraints on archaeal activity and sedimentary lipid input and preservation signatures in different marine environments. Terrestrial input of archaeal lipids to marine sediments in the Western Mediterranean Sea is substantial (up to 43%) which suggests caution when applying some existing molecular proxies such as BIT. Similar $\delta^{13}C$ values of core and intact crenarchaeol in all studied sites suggest intact crenarchaeol is not newly synthesized. $\delta^{13}C$ offset (on average 2.6‰) of core and intact caldarchaeol indicates in-situ activity of sedimentary archaea, similar to the observations in a high-resolution sediment core in the Black Sea. Based on a two endmember mixing model, an average of 34% IPLs in sediments are produced by benthic archaea. In addition, the negative shift of core caldarchaeol $\delta^{13}C$ values in deeper sediments compared to surface is consistent with the addition of hydrolytic products from the ^{13}C-depleted IPL pool. Two independent approaches of isotope mass balance calculations demonstrated that on average 18% and 35% of CL-caldarchaeol is derived from IPL degradation, respectively. Compared to caldarchaeol and crenarchaeol, the highly variable isotopic compositions of archaeol indicate a different carbon source or metabolism in archaea. In order to find out which organisms utilize the AOM biomass, we performed an L-leucine-3-^{13}C labeling study in a mesophilic AOM culture dominated by ANME-1 archaea and its partner bacteria. Our results showed that members of Anaerolineae and Spirochaetes thrive on AOM biomass in the oligotrophic medium. These heterotrophs explain the absence of AOM lipid signals in the sedimentary records below the SMTZ. This thesis highlights the presence of various archaeal lipid inputs from terrestrial,

planktonic and sedimentary sources in marine sediments. Meanwhile, the subseafloor is an active biosphere where new lipids are continuously produced and overturned. Heterotrophic bacteria and archaea may play an important role in lipid turnover in marine sediments.

Perspectives that have emerged during the course of this Ph.D. project are presented in the following paragraphs:

1. In the DARCLIFE project, genetic sequencing data and intact polar lipids distribution patterns are available. Combining the genetic sequencing data, lipid distribution and lipid isotopic data is necessary to achieve a profound understanding of benthic archaeal activities. To achieve this, big data analysis and mathematic statistics will be helpful in the future study.

2. Bulk IPL was separated from CL in our study. However, a large fraction of IPL has shown to be deposited from the water column and represents fossil components. It is important to further separate the living IPL from fossil IPL. One possible solution is to further separate the IPL into different fractions according to head group types (Schubotz et al., 2011). IPLs with different head groups contain more specific taxonomic information and could be better used for constraining the benthic archaeal activities.

3. From the perspective of analytical methods, we could use the non-pyrolytic method for the isotopic analysis, Spooling Wire Microcombustion (SWiM)-isotope ratio mass spectrometry (IRMS) (Pearson et al., 2016). This method overcomes the shortage of conventional ether cleavage which erases information revealed by the isotopic heterogeneity of GDGTs.

4. Heterotrophic activities are successfully detected in AOM enrichment, and possibly affect the degradation of AOM biomass in the enrichment. It is necessary to perform the direct investigation on the necromass degradation in sediments. One possible

approach is to use ^{13}C labeled biomass in the incubation of sediment slurry and try to observe the ^{13}C flow in different carbon pools.

Chapter VII

Contribution as Co-author

Iron-Coupled Anaerobic Oxidation of Methane Performed by a Mixed Bacterial-Archaeal Community Based on Poorly Reactive Minerals

Published in *Environmental Science and Technology*

Itay Bar-Or,† Marcus Elvert,*,‡ Werner Eckert,§ Ariel Kushmaro,‖ Hanni Vigderovich,† **Qing-Zeng Zhu**,‡ Eitan Ben-Dov,‖,⊥ and Orit Sivan*,†

†Department of Geological and Environmental Sciences, Ben Gurion University of the Negev, Beer-Sheva 84105, Israel; ‡MARUM - Center for Marine Environmental Sciences and Department of Geosciences, University of Bremen, Leobener Strasse 8, 28359 Bremen, Germany; §Israel Oceanographic and Limnological Research, The Yigal Allon Kinneret Limnological Laboratory, P.O. Box 447, 14950 Migdal, Israel; ‖Avram and Stella Goldstein-Goren Department of Biotechnology Engineering, Faculty of Engineering Sciences and The Ilse Katz Center for Meso and Nanoscale Science and Technology, Ben-Gurion University of the Negev, P.O. Box 653, Beer-Sheva 84105, Israel ⊥Department of Life Sciences, Achva Academic College, Achva, M.P. Shikmim 79800, Israel

ABSTRACT:

Anaerobic oxidation of methane (AOM) was shown to reduce methane emissions by over 50% in freshwater systems, its main natural contributor to the atmosphere. In these environments iron oxides can become main agents for AOM, but the underlying mechanism for this process has remained enigmatic. By conducting anoxic slurry incubations with lake sediments amended with ^{13}C-labeled methane and naturally abundant iron oxides the process was evidenced by significant ^{13}C-enrichment of the dissolved inorganic carbon pool and most pronounced when poorly reactive iron minerals such as magnetite and hematite were applied. Methane incorporation into biomass was apparent by strong uptake of ^{13}C into fatty acids indicative of methanotrophic bacteria, associated with increasing copy numbers of the functional methane monooxygenase pmoA gene. Archaea were not directly involved in full methane oxidation, but

their crucial participation, likely being mediators in electron transfer, was indicated by specific inhibition of their activity that fully stopped iron coupled AOM. By contrast, inhibition of sulfur cycling increased ^{13}C-methane turnover, pointing to sulfur species involvement in a competing process. Our findings suggest that the mechanism of iron-coupled AOM is accomplished by a complex microbe-mineral reaction network, being likely representative of many similar but hidden interactions sustaining life under highly reducing low energy conditions.

Lipidomic analysis shows that carbon fixation sustains deep aquifer-associated microbial communities

Resubmitted to *ISME*

Alexander J. Probst[1,#,$,*], Felix J. Elling[2,#,§,*], Cindy Castelle[1,2], **Qing-Zeng Zhu**[2], Marcus Elvert[2], Giovanni Birarda[3,4], Hoi-Ying Holman[4], Katherine R. Lane[1], Bethany Ladd[5], M. Cathryn Ryan[5], Tanja Woyke[6], Kai-Uwe Hinrichs[2,*], Jillian F. Banfield[1,*]

[1]Department of Earth and Planetary Science, University of California, Berkeley, CA 94720, USA; [2]MARUM Center for Marine Environmental Sciences, University of Bremen, Bremen, Germany; [3]Elettra-Sincrotrone Trieste, Strada Statale 14 - km 163,5, 34149 Basovizza, Trieste, Italy; [4]Molecular Biophysics & Integrated Bioimaging, Lawrence Berkeley National Laboratory, USA; [5]Department of Geoscience, University of Calgary, Calgary, AB, T2N 1N4, Canada; [6]DOE Joint Genome Institute, Walnut Creek, USA

[#]authors contributed equally *corresponding authors

$present address: University of Duisburg-Essen, GAME - Group for Aquatic Microbial Ecology, Biofilm Center, Department for Chemistry, Essen, 45141, Germany

§present address: Department of Earth and Planetary Sciences, Harvard University, Cambridge, MA 02138, USA

ABSTRACT:

Sediment-hosted CO_2-rich aquifers deep below the Colorado Plateau (USA) contain a remarkable diversity of uncultivated microorganisms, including Candidate Phyla Radiation (CPR) bacteria that are putative symbionts unable to synthesize membrane lipids. The origin of organic carbon in these ecosystems is unknown and the source of CPR membrane lipids remains elusive. We collected cells from deep groundwater brought to the surface by eruptions of Crystal Geyser, sequenced the community, and analyzed the whole community lipidome over time. Characteristic stable carbon isotopic compositions of microbial lipids suggest that bacterial and archaeal CO_2 fixation ongoing in the deep subsurface provides organic carbon for the complex communities that reside there. Coupled lipidomic-metagenomic analysis indicates that CPR bacteria lack complete lipid biosynthesis pathways but still possess regular lipid

membranes. These lipids may, therefore, originate from other community members, which also adapt to high in situ pressure by increasing fatty acid unsaturation. An unusually high abundance of lysolipids attributed to CPR bacteria may represent an adaptation to membrane curvature stress induced by their small cell sizes. Our findings provide new insights into the carbon cycle in the deep subsurface and suggest the redistribution of lipids into putative symbionts within this community.

Structural elucidation and environmental distributions of butanetriol and pentanetriol dialkyl glycerol tetraethers (BDGTs and PDGTs)

Accepted by *Biogeosciences*

Sarah Coffinet[1#]; Travis B. Meador[1*]; Lukas Mühlena[1]; Kevin W. Becker[1**]; Jan Schröder[1]; **Qing-Zeng Zhu**[1]; Julius S. Lipp[1]; Verena B. Heuer[1]; Matthew P. Crump[2]; Kai-Uwe Hinrichs[1]

[1]MARUM – Center for Marine Environmental Sciences, University of Bremen, Germany
[2]School of Chemistry, University of Bristol, United Kingdom

Correspondence to: Sarah Coffinet (scoffinet@marum.de)

Present addresses:

* Biology Centre CAS, SoWa-RI, České Budějovice, Czechia

** GEOMAR Helmholtz Centre for Ocean Research Kiel, Germany

ABSTRACT:

Butanetriol and pentanetriol dialkyl glycerol tetraethers (BDGTs and PDGTs) are membrane lipids recently discovered in sedimentary environments and in the methanogenic archaeon Methanomassiliicoccus luminyensis. They possess an unusual structure, which challenges fundamental assumptions in lipid biochemistry. Indeed, they bear a butanetriol or a pentanetriol backbone instead of a glycerol at one end of their core structure. In this study, we unambiguously located the additional methyl group of the BDGT compound on the C3 carbon of the lipid backbone via high-field two-dimensional NMR experiments. We further systematically explored the abundance, distribution and isotopic composition of BDGTs and PDGTs as both intact polar and core lipid forms in marine sediments collected in contrasting environments of the Mediterranean Sea and Black Sea. In addition, relatively ^{13}C-depleted BDGTs from the Rhone delta and from the Black Sea are in agreement with a probable methanogenic source for these lipids. In line with this interpretation, high proportions of intact polar BDGTs and PDGTs were detected in the deeper methane-laden sedimentary layers.

However, relatively ^{13}C enriched BDGTs and contrasting headgroup distribution patterns of BDGTs and PDGTs in sediments of the Eastern Mediterranean Sea imply that additional archaeal groups also produce these unique lipids.

Rates and Microbial Players of Iron-Driven Anaerobic Oxidation of Methane in Methanic Marine Sediments

Accepted by *Frontiers in Microbiology*

David A. Aromokeye[1,2,3‡], Ajinkya C. Kulkarni[1,2,3‡], Marcus Elvert[2,4], Gunter Wegener[2,5], Susann Henkel[2,6], Sarah Coffinet[2], Thilo Eickhorst[7], Oluwatobi E. Oni[1], Tim Richter-Heitmann[1], Annika Schnakenberg[1,2,3], Heidi Taubner[2,4], Lea Wunder[1], Xiuran Yin[1,2,3], **Qing-Zeng Zhu**[2], Kai-Uwe Hinrichs[2,4], Sabine Kasten[2,4,6], Michael W. Friedrich[1,2]*

[1]Microbial Ecophysiology Group, Faculty of Biology/Chemistry, University of Bremen, Bremen, Germany; [2]MARUM – Center for Marine Environmental Sciences, University of Bremen, Bremen, Germany; [3]International Max Planck Research School for Marine Microbiology, Max Planck Institute for Marine Microbiology, Bremen, Germany; [4]University of Bremen, Faculty of Geosciences, Bremen, Germany; [5]Max Planck Institute for Marine Microbiology, Bremen, Germany; [6]Alfred Wegener Institute Helmholtz Centre for Polar and Marine Research, Bremerhaven, Germany; [7]Faculty of Biology/Chemistry, University of Bremen, Bremen, Germany

‡ These authors contributed equally to this work

*Correspondence: Email: michael.friedrich@uni-bremen.de

ABSTRACT:

The flux of methane, a potent greenhouse gas, from the seabed is largely controlled by anaerobic oxidation of methane (AOM) coupled to sulfate reduction (S-AOM) in the sulfate methane transition (SMT). S-AOM is estimated to oxidize 90% of the methane produced in marine sediments and is governed by a consortium of anaerobic methanotrophic archaea (ANME) and sulfate reducing bacteria. An additional methane sink, i.e., iron oxide coupled AOM (Fe-AOM), has been suggested to be active in the methanic zone of marine sediments. Geochemical signatures below the SMT such as high dissolved iron, low to undetectable sulfate and high methane concentrations, together with the presence of iron oxides are taken as prerequisites for this process. So far, neither has Fe-AOM been proven in marine sediments nor have the governing key microorganisms been identified. Here, using a multidisciplinary approach, we show that Fe-AOM occurs in iron oxide-rich methanic sediments of the Helgoland Mud Area (North Sea). When sulfate reduction was inhibited, different iron oxides

facilitated Fe-AOM in long-term sediment slurry incubations but manganese oxide did not. Especially magnetite triggered substantial Fe-AOM activity and caused an enrichment of ANME-2a archaea. Methane oxidation rates of 0.095 ± 0.03 nmol cm^{-3} d^{-1} attributable to Fe-AOM were obtained in short-term radiotracer experiments. The decoupling of AOM from sulfate reduction in the methanic zone further corroborated that AOM was iron oxide-driven below the SMT. Thus, our findings prove that Fe-AOM occurs in methanic marine sediments containing mineral-bound ferric iron and is a previously overlooked but likely important component in the global methane budget. This process has the potential to sustain microbial life in the deep biosphere.

Differential archaeal carbon metabolism in surface sediment of Pearl River Estuary

In preparation for *Chemical Geology*

Simin Gao[a,b], **Qing-Zeng Zhu[c]**, Marcus Elvert[c], Peng Wang[b], Xin Zhao[a], Wenpeng Li[a], Yufei Chen[a,b], Kai-Uwe Hinrichs[c], Chuanlun Zhang[a], Xinxin Li[a,*]

[a] Shenzhen Key Laboratory of Marine Archaea Geo-Omics, Department of Ocean Science and Engineering, Southern University of Science and Technology, Shenzhen 518055, China; [b] State Key Laboratory of Marine Geology, Tongji University, Shanghai, 200092, China; [c] MARUM & Department of Geosciences, University of Bremen, Bremen, D-28334, Germany

* Corresponding author: lixinxin@sustech.edu.cn

ABSTRACT:

Estuaries play a critical role in global carbon budget because they link the land and ocean, which is characterized by dynamic biogeochemical processes. Yet, the linkage between complex carbon sources and microbial populations mediating carbon metabolism in these complex settings is poorly delineated. Here we presented an integrated study of organic geochemistry and geomicrobiology on surface sediment at four sites along a salinity gradient in the Pearl River Estuary. The sources of organic carbon, major archaeal glycerol dialkyl glycerol tetraether (GDGT) membrane lipids, archaeal community structure, as well as their potential carbon synthetic pathways were evaluated. Relative abundance of core GDGTs, and 16S rRNA pyrosequencing of archaea suggested that planktonic Thaumarchaeota were predominant sources of both GDGT 0 and crenarchaeol at saline sites; whereas, methanogens derived from terrestrial input mainly produced GDGT 0 at the freshwater site, compounding the GDGT 0 signature from freshwater Thaumarchaeota. Thus, significantly different isotope compositions between GDGT 0 and crenarchaeol were observed at sites with lower salinities, while similar isotope values (-21.2‰ to -19.7‰) were observed at marine sites. Different from previously reported $\varepsilon_{BP\text{-}0\text{-}DIC}$ of -19.7‰ for autotrophic Thaumarchaeota, our modeling results and significant correlation (R^2 = 0.73) between $\delta^{13}C_{TOC}$ and $\delta^{13}C_{BPcren}$, suggested

Thaumarchaeota being mixotrophic or heterotrophic, through metabolizing sedimentary organic carbon. Variations in freshwater discharge and salt wedges likely made estuaries a dynamic transition zone with complex sources and metabolisms of organic carbon by archaeal communities.

Chapter VIII

References

Aepfler, R.F., Bühring, S.I., Elvert, M., 2019. Substrate characteristic bacterial fatty acid production based on amino acid assimilation and transformation in marine sediments. FEMS Microbiology Ecology 95.

Apostel, C., Dippold, M., Glaser, B., Kuzyakov, Y., 2013. Biochemical pathways of amino acids in soil: assessment by position-specific labeling and ^{13}C-PLFA analysis. Soil Biology & Biochemistry 67, 31-40.

Apostel, C., Dippold, M., Kuzyakov, Y., 2015. Biochemistry of hexose and pentose transformations in soil analyzed by position-specific labeling and ^{13}C-PLFA. Soil Biology & Biochemistry 80, 199-208.

Aristegui, J., Gasol, J.M., Duarte, C.M., Herndl, G.J., 2009. Microbial oceanography of the dark ocean's pelagic realm. Limnology and Oceanography 54, 1501-1529.

Azam, F., Malfatti, F., 2007. Microbial structuring of marine ecosystems. Nature Reviews Microbiology 5, 782.

Bassham, J.A., Benson, A.A., Kay, L.D., Harris, A.Z., Wilson, A.T., Calvin, M., 1954. The path of carbon in photosynthesis. XXI. The cyclic regeneration of carbon dioxide acceptor1. Journal of the American Chemical Society 76, 1760-1770.

Becker, K.W., Elling, F.J., Schröder, J.M., Lipp, J.S., Goldhammer, T., Zabel, M., Elvert, M., Overmann, J., Hinrichs, K.U., 2018. Isoprenoid quinones resolve the stratification of redox processes in a biogeochemical continuum from the photic zone to deep anoxic sediments of the Black Sea. Applied and Environmental Microbiology 84.

Berg, I.A., Kockelkorn, D., Buckel, W., Fuchs, G., 2007. A 3-hydroxypropionate/4-hydroxybutyrate autotrophic carbon dioxide assimilation pathway in Archaea. Science 318, 1782-1786.

Berg, I.A., Kockelkorn, D., Ramos-Vera, W.H., Say, R.F., Zarzycki, J., Hugler, M., Alber, B.E., Fuchs, G., 2010a. Autotrophic carbon fixation in archaea. Nature Reviews Microbiology 8, 447-460.

Berg, I.A., Ramos-Vera, W.H., Petri, A., Huber, H., Fuchs, G., 2010b. Study of the distribution of autotrophic CO_2 fixation cycles in Crenarchaeota. Microbiology 156, 256-269.

Biddle, J.F., Lipp, J.S., Lever, M.A., Lloyd, K.G., Sorensen, K.B., Anderson, R., Fredricks, H.F., Elvert, M., Kelly, T.J., Schrag, D.P., Sogin, M.L., Brenchley, J.E., Teske, A., House, C.H., Hinrichs, K.U., 2006. Heterotrophic Archaea dominate sedimentary subsurface ecosystems off Peru. Proceedings of the National Academy of Sciences of the United States of America 103, 3846-3851.

Blumenberg, M., Seifert, R., Reitner, J., Pape, T., Michaelis, W., 2004. Membrane lipid patterns typify distinct anaerobic methanotrophic consortia. Proceedings of the National Academy of Sciences of the United States of America 101, 11111-11116.

Boetius, A., Ravenschlag, K., Schubert, C.J., Rickert, D., Widdel, F., Gieseke, A., Amann, R., Jorgensen, B.B., Witte, U., Pfannkuche, O., 2000. A marine microbial consortium apparently mediating anaerobic oxidation of methane. Nature 407, 623-626.

Boschker, H., Nold, S., Wellsbury, P., Bos, D., De Graaf, W., Pel, R., Parkes, R.J., Cappenberg, T., 1998. Direct linking of microbial populations to specific biogeochemical processes by ^{13}C-labelling of biomarkers. Nature 392, 801.

Bradley, A.S., Hayes, J.M., Summons, R.E., 2009. Extraordinary ^{13}C enrichment of diether lipids at the Lost City Hydrothermal Field indicates a carbon-limited ecosystem. Geochimica et Cosmochimica Acta 73, 102-118.

Brassell, S., Wardroper, A., Thomson, I., Maxwell, J., Eglinton, G., 1981. Specific acyclic isoprenoids as biological markers of methanogenic bacteria in marine sediments. Nature 290, 693.

Breitburg, D., Levin, L.A., Oschlies, A., Grégoire, M., Chavez, F.P., Conley, D.J., Garçon, V., Gilbert, D., Gutiérrez, D., Isensee, K., 2018. Declining oxygen in the global ocean and coastal waters. Science 359, eaam7240.

Brocks, J.J., Banfield, J., 2009. Unravelling ancient microbial history with community proteogenomics and lipid geochemistry. Nature Reviews Microbiology 7, 601-609.

Brocks, J.J., Pearson, A., 2005. Building the Biomarker Tree of Life. Reviews in Mineralogy and Geochemistry 59, 233-258.

Bryant, D.A., Frigaard, N.-U., 2006. Prokaryotic photosynthesis and phototrophy illuminated. Trends in Microbiology 14, 488-496.

Buchanan, B.B., Arnon, D.I., 1990. A reverse KREBS cycle in photosynthesis: consensus at last. Photosynthesis Research 24, 47-53.

Campbell, D., Hurry, V., Clarke, A.K., Gustafsson, P., Öquist, G., 1998. Chlorophyll fluorescence analysis of cyanobacterial photosynthesis and acclimation. Microbiology and Molecular Biology Reviews 62, 667-683.

Canfield, D.E., Thamdrup, B., 2009. Towards a consistent classification scheme for geochemical environments, or, why we wish the term 'suboxic' would go away. Geobiology 7, 385-392.

Castelle, C.J., Brown, C.T., Anantharaman, K., Probst, A.J., Huang, R.H., Banfield, J.F., 2018. Biosynthetic capacity, metabolic variety and unusual biology in the CPR and DPANN radiations. Nature Reviews Microbiology 16, 629-645.

Chong, P.L., 2010. Archaebacterial bipolar tetraether lipids: Physico-chemical and membrane properties. Chemistry and Physics of Lipids 163, 253-265.

Cline, J.D., 1969. Spectrophotometric determination of hydrogen sulfide in natural waters. Limnology and Oceanography 14, 454-458.

Coffinet, S., Meador, T.B., Mühlena, L., Becker, K.W., Schröder, J., Zhu, Q.Z., Lipp, J.S., Heuer, V.B., Crump, M.P., Hinrichs, K.U., 2019. Structural elucidation and environmental distributions of butanetriol and pentanetriol dialkyl glycerol tetraethers (BDGTs and PDGTs). Biogeosciences (Online) 2019, 1-17.

Coolen, M.J., Abbas, B., Van Bleijswijk, J., Hopmans, E.C., Kuypers, M.M., Wakeham, S.G., Sinninghe Damsté, J.S., 2007. Putative ammonia-oxidizing Crenarchaeota in suboxic waters of the Black Sea: a basin-wide ecological study using 16S ribosomal and functional genes and membrane lipids. Environmental Microbiology 9, 1001-1016.

Cord-Ruwisch, R., 1985. A quick method for the determination of dissolved and precipitated sulfides in cultures of sulfate-reducing bacteria. Journal of Microbiological Methods 4, 33-36.

Dalsgaard, T., Thamdrup, B., Canfield, D.E., 2005. Anaerobic ammonium oxidation (anammox) in the marine environment. Research in Microbiology 156, 457-464.

Del Giorgio, P.A., Duarte, C.M., 2002. Respiration in the open ocean. Nature 420, 379.

Diaz-Perez, A.L., Diaz-Perez, C., Campos-Garcia, J., 2016. Bacterial L-leucine catabolism as a source of secondary metabolites. Reviews in Environmental Science and Bio-Technology 15, 1-29.

Dippold, M.A., Kuzyakov, Y., 2016. Direct incorporation of fatty acids into microbial phospholipids in soils: Position-specific labeling tells the story. Geochimica et Cosmochimica Acta 174, 211-221.

Doney, S.C., Ruckelshaus, M., Duffy, J.E., Barry, J.P., Chan, F., English, C.A., Galindo, H.M., Grebmeier, J.M., Hollowed, A.B., Knowlton, N., 2011. Climate change impacts on marine ecosystems.

Dong, X., Greening, C., Bruls, T., Conrad, R., Guo, K., Blaskowski, S., Kaschani, F., Kaiser, M., Laban, N.A., Meckenstock, R.U., 2018. Fermentative Spirochaetes mediate necromass recycling in anoxic hydrocarbon-contaminated habitats. The ISME Journal 12, 2039-2050.

Dowhan, W., 1997. Molecular basis for membrane phospholipid diversity: why are there so many lipids? Annual Review of Biochemistry 66, 199-232.

Ducklow, H.W., Steinberg, D.K., Buesseler, K.O., 2001. Upper ocean carbon export and the biological pump. OCEANOGRAPHY-WASHINGTON DC-OCEANOGRAPHY SOCIETY- 14, 50-58.

Eiler, A., 2006. Evidence for the ubiquity of mixotrophic bacteria in the upper ocean: implications and consequences. Applied and Environmental Microbiology 72, 7431-7437.

Elling, F.J., Gottschalk, J., Doeana, K.D., Kusch, S., Hurley, S.J., Pearson, A., 2019. Archaeal lipid biomarker constraints on the Paleocene-Eocene carbon isotope excursion. Nature Communications 10, 4519.

Elling, F.J., Könneke, M., Nicol, G.W., Stieglmeier, M., Bayer, B., Spieck, E., de la Torre, J.R., Becker, K.W., Thomm, M., Prosser, J.I., Herndl, G.J., Schleper, C., Hinrichs, K.U., 2017. Chemotaxonomic characterisation of the thaumarchaeal lipidome. Environmental Microbiology 19, 2681-2700.

Elvert, M., Boetius, A., Knittel, K., Jorgensen, B.B., 2003. Characterization of specific membrane fatty acids as chemotaxonomic markers for sulfate-reducing bacteria involved in anaerobic oxidation of methane. Geomicrobiology Journal 20, 403-419.

Elvert, M., Hopmans, E., Treude, T., Boetius, A., Suess, E., 2005. Spatial variations of methanotrophic consortia at cold methane seeps: implications from a high-resolution molecular and isotopic approach. Geobiology 3, 195-209.

Elvert, M., Suess, E., Greinert, J., Whiticar, M.J., 2000. Archaea mediating anaerobic methane oxidation in deep-sea sediments at cold seeps of the eastern Aleutian subduction zone. Organic Geochemistry 31, 1175-1187.

Elvert, M., Suess, E., Whiticar, M.J., 1999. Anaerobic methane oxidation associated with marine gas hydrates: superlight C-isotopes from saturated and unsaturated C20 and C25 irregular isoprenoids. Naturwissenschaften 86, 295-300.

Eme, L., Spang, A., Lombard, J., Stairs, C.W., Ettema, T.J.G., 2017. Archaea and the origin of eukaryotes. Nature Reviews Microbiology 15, 711.

Ertefai, T.F., Heuer, V.B., Prieto-Mollar, X., Vogt, C., Sylva, S.P., Seewald, J., Hinrichs, K.-U., 2010. The biogeochemistry of sorbed methane in marine sediments. Geochimica et Cosmochimica Acta 74, 6033-6048.

Evans, T.W., Coffinet, S., Könneke, M., Lipp, J.S., Becker, K.W., Elvert, M., Heuer, V., Hinrichs, K.-U., 2019. Assessing the carbon assimilation and production of benthic archaeal lipid biomarkers using lipid-RIP. Geochimica et Cosmochimica Acta 265, 431-442.

Falkowski, P.G., Barber, R.T., Smetacek, V., 1998. Biogeochemical controls and feedbacks on ocean primary production. Science 281, 200-206.

Fischer, H., Kuzyakov, Y., 2010. Sorption, microbial uptake and decomposition of acetate in soil: Transformations revealed by position-specific C-14 labeling. Soil Biology & Biochemistry 42, 186-192.

Fonseca, P., Moreno, R., Rojo, F., 2011. Growth of Pseudomonas putida at low temperature: global transcriptomic and proteomic analyses. Environmental Microbiology Reports 3, 329-339.

Froelich, P.N., Klinkhammer, G.P., Bender, M.L., Luedtke, N.A., Heath, G.R., Cullen, D., Dauphin, P., Hammond, D., Hartman, B., Maynard, V., 1979. Early Oxidation of Organic-Matter in Pelagic Sediments of the Eastern Equatorial Atlantic - Suboxic Diagenesis. Geochimica et Cosmochimica Acta 43, 1075-1090.

Galloway, J.N., Dentener, F.J., Capone, D.G., Boyer, E.W., Howarth, R.W., Seitzinger, S.P., Asner, G.P., Cleveland, C.C., Green, P., Holland, E.A., 2004. Nitrogen cycles: past, present, and future. Biogeochemistry 70, 153-226.

Hall, P.J., Aller, R.C., 1992. Rapid, small-volume, flow injection analysis for CO_2, and NH_4^+ in marine and freshwaters. Limnology and Oceanography 37, 1113-1119.

Hansell, D.A., Carlson, C.A., Repeta, D.J., Schlitzer, R., 2009. Dissolved organic matter in the ocean: A controversy stimulates new insights. Oceanography 22, 202-211.

Harsha, H.C., Molina, H., Pandey, A., 2008. Quantitative proteomics using stable isotope labeling with amino acids in cell culture. Nature Protocols 3, 505-516.

Harvey, H.R., Fallon, R.D., Patton, J.S., 1986. The Effect of Organic-Matter and Oxygen on the Degradation of Bacterial-Membrane Lipids in Marine-Sediments. Geochimica et Cosmochimica Acta 50, 795-804.

Harwood, C., Canale-Parola, E., 1981. Branched-chain amino acid fermentation by a marine spirochete: strategy for starvation survival. Journal of Bacteriology 148, 109-116.

Hayes, J.M., 2001. Fractionation of carbon and hydrogen isotopes in biosynthetic processes. Stable Isotope Geochemistry 43, 225-277.

Hayes, J.M., 2004. An introduction to isotopic calculations. Woods Hole Oceanographic Institution, Woods Hole, MA 2543.

Hayes, J.M., Freeman, K.H., Popp, B.N., Hoham, C.H., 1990. Compound-specific isotopic analyses: a novel tool for reconstruction of ancient biogeochemical processes. Organic Geochemistry 16, 1115-1128.

Hazel, J.R., Williams, E.E., 1990. The role of alterations in membrane lipid composition in enabling physiological adaptation of organisms to their physical environment. Progress in Lipid Research 29, 167-227.

Hedges, J.I., Keil, R.G., 1995. Sedimentary organic matter preservation: an assessment and speculative synthesis. Marine Chemistry 49, 81-115.

Herndl, G.J., Reinthaler, T., Teira, E., van Aken, H., Veth, C., Pernthaler, A., Pernthaler, J., 2005. Contribution of Archaea to total prokaryotic production in the deep Atlantic Ocean. Appl. Environ. Microbiol. 71, 2303-2309.

Heuer, V., Aiello, I., Elvert, M., Goldenstein, N., Goldhammer, T., Könneke, M., Liu, X., Pape, S., Schmidt, F., Wendt, J., 2014. Report and preliminary results of R/VPoseidon cruise POS450, DARCSEAS II–Deep subseafloor Archaea in the Western Mediterranean Sea: Carbon Cycle, Life Strategies, and Role in Sedimentary Ecosystems, Barcelona (Spain)–Malaga (Spain), April 2–13, 2013. Berichte, MARUM–Zentrum für Marine Umweltwissenschaften, Fachbereich Geowissenschaften, Universität Bremen, 42.

Heuer, V., Elvert, M., Tille, S., Krummen, M., Mollar, X.P., Hmelo, L.R., Hinrichs, K.-U., 2006. Online $\delta^{13}C$ analysis of volatile fatty acids in sediment/porewater systems by liquid chromatography–isotope ratio mass spectrometry. Limnology and Oceanography-Methods 4, 346-357.

Heuer, V.B., Pohlman, J.W., Torres, M.E., Elvert, M., Hinrichs, K.U., 2009. The stable carbon isotope biogeochemistry of acetate and other dissolved carbon species in deep subseafloor sediments at the northern Cascadia Margin. Geochimica et Cosmochimica Acta 73, 3323-3336.

Hinrichs, K.-U., Boetius, A., 2002. The anaerobic oxidation of methane: new insights in microbial ecology and biogeochemistry, Ocean margin systems. Springer, pp. 457-477.

Hinrichs, K.U., Hayes, J.M., Sylva, S.P., Brewer, P.G., DeLong, E.F., 1999. Methane-consuming archaebacteria in marine sediments. Nature 398, 802-805.

Hinrichs, K.U., Pancost, R.D., Summons, R.E., Sprott, G.D., Sylva, S.P., Sinninghe Damsté, J.S., Hayes, J.M., 2000. Mass spectra of sn-2 - hydroxyarchaeol, a polar lipid biomarker for anaerobic methanotrophy. Geochemistry, Geophysics, Geosystems 1, 2000GC000042.

Hoefs, M., Schouten, S., De Leeuw, J.W., King, L.L., Wakeham, S.G., Sinninghe Damsté, J.S., 1997. Ether lipids of planktonic archaea in the marine water column. Applied and Environmental Microbiology 63, 3090-3095.

Hopmans, E.C., Schouten, S., Pancost, R.D., van der Meer, M.T., Sinninghe Damsté, J.S., 2000. Analysis of intact tetraether lipids in archaeal cell material and sediments by high performance liquid chromatography/atmospheric pressure chemical ionization mass spectrometry. Rapid Communications in Mass Spectrometry 14, 585-589.

Hopmans, E.C., Weijers, J.W.H., Schefuss, E., Herfort, L., Sinninghe Damsté, J.S., Schouten, S., 2004. A novel proxy for terrestrial organic matter in sediments based on branched and isoprenoid tetraether lipids. Earth and Planetary Science Letters 224, 107-116.

Hoshino, T., Inagaki, F., 2019. Abundance and distribution of Archaea in the subseafloor sedimentary biosphere. The ISME Journal 13, 227-231.

House, C.H., Schopf, J.W., Stetter, K.O., 2003. Carbon isotopic fractionation by Archaeans and other thermophilic prokaryotes. Organic Geochemistry 34, 345-356.

Huber, H., Gallenberger, M., Jahn, U., Eylert, E., Berg, I.A., Kockelkorn, D., Eisenreich, W., Fuchs, G., 2008. A dicarboxylate/4-hydroxybutyrate autotrophic carbon assimilation cycle in the hyperthermophilic Archaeum Ignicoccus hospitalis. Proceedings of the National Academy of Sciences of the United States of America 105, 7851-7856.

Huber, H., Stetter, K.O., 2006. Thermoplasmatales. The Prokaryotes: Volume 3: Archaea. Bacteria: Firmicutes, Actinomycetes, 101-112.

Hug, L.A., Baker, B.J., Anantharaman, K., Brown, C.T., Probst, A.J., Castelle, C.J., Butterfield, C.N., Hernsdorf, A.W., Amano, Y., Ise, K., Suzuki, Y., Dudek, N., Relman, D.A., Finstad, K.M., Amundson, R., Thomas, B.C., Banfield, J.F., 2016. A new view of the tree of life. Nature Microbiology 1, 16048.

Hugler, M., Sievert, S.M., 2011. Beyond the Calvin cycle: autotrophic carbon fixation in the ocean. Annual Review of Marine Science 3, 261-289.

Huguet, C., Smittenberg, R.H., Boer, W., Sinninghe Damsté, J.S., Schouten, S., 2007. Twentieth century proxy records of temperature and soil organic matter input in the Drammensfjord, southern Norway. Organic Geochemistry 38, 1838-1849.

Imachi, H., Nobu, M.K., Nakahara, N., Morono, Y., Ogawara, M., Takaki, Y., Takano, Y., Uematsu, K., Ikuta, T., Ito, M., Matsui, Y., Miyazaki, M., Murata, K., Saito, Y., Sakai, S., Song, C., Tasumi, E., Yamanaka, Y., Yamaguchi, T., Kamagata, Y., Tamaki, H., Takai, K., 2019. Isolation of an archaeon at the prokaryote-eukaryote interface. bioRxiv, 726976.

Inagaki, F., Hinrichs, K.U., Kubo, Y., Bowles, M.W., Heuer, V.B., Hong, W.L., Hoshino, T., Ijiri, A., Imachi, H., Ito, M., Kaneko, M., Lever, M.A., Lin, Y.S., Methe, B.A., Morita, S., Morono, Y., Tanikawa, W., Bihan, M., Bowden, S.A., Elvert, M., Glombitza, C., Gross, D., Harrington, G.J., Hori, T., Li, K., Limmer, D., Liu, C.H., Murayama, M., Ohkouchi, N., Ono, S., Park, Y.S., Phillips, S.C., Prieto-Mollar, X., Purkey, M., Riedinger, N., Sanada, Y., Sauvage, J., Snyder, G., Susilawati, R., Takano, Y., Tasumi, E., Terada, T., Tomaru, H., Trembath-Reichert, E., Wang, D.T., Yamada, Y., 2015. DEEP BIOSPHERE. Exploring deep microbial life in coal-bearing sediment down to ~2.5 km below the ocean floor. Science 349, 420-424.

Ingalls, A.E., Shah, S.R., Hansman, R.L., Aluwihare, L.I., Santos, G.M., Druffel, E.R., Pearson, A., 2006. Quantifying archaeal community autotrophy in the mesopelagic ocean using natural radiocarbon. Proceedings of the National Academy of Sciences of the United States of America 103, 6442-6447.

Iversen, N., Jorgensen, B.B., 1985. Anaerobic methane oxidation rates at the sulfate-methane transition in marine sediments from Kattegat and Skagerrak (Denmark) 1. Limnology and Oceanography 30, 944-955.

Iverson, V., Morris, R.M., Frazar, C.D., Berthiaume, C.T., Morales, R.L., Armbrust, E.V., 2012. Untangling genomes from metagenomes: revealing an uncultured class of marine Euryarchaeota. Science 335, 587-590.

Jahn, U., Summons, R., Sturt, H., Grosjean, E., Huber, H., 2004. Composition of the lipids of Nanoarchaeum equitans and their origin from its host Ignicoccus sp. strain KIN4/I. Archives of Microbiology 182, 404-413.

Jehmlich, N., Vogt, C., Lunsmann, V., Richnow, H.H., von Bergen, M., 2016. Protein-SIP in environmental studies. Current Opinion in Biotechnology 41, 26-33.

Jennings, R.M., Whitmore, L.M., Moran, J.J., Kreuzer, H.W., Inskeep, W.P., 2014. Carbon dioxide fixation by Metallosphaera yellowstonensis and acidothermophilic iron-oxidizing microbial communities from Yellowstone National Park. Applied and Environmental Microbiology 80, 2665-2671.

Jørgensen, B.B., 2000. Bacteria and marine biogeochemistry, Marine Geochemistry. Springer, pp. 173-207.

Jørgensen, B.B., Kasten, S., 2006. Sulfur cycling and methane oxidation, Marine Geochemistry. Springer, pp. 271-309.

Kallmeyer, J., Pockalny, R., Adhikari, R.R., Smith, D.C., D'Hondt, S., 2012. Global distribution of microbial abundance and biomass in subseafloor sediment. Proceedings of the National Academy of Sciences of the United States of America 109, 16213-16216.

Kaneda, T., 1963. Biosynthesis of branched chain fatty acids II. Microbial synthesis of branched long chain fatty acids from certain short chain fatty acid substrates. Journal of Biological Chemistry 238, 1229-1235.

Kaneda, T., 1991. Iso-and anteiso-fatty acids in bacteria: biosynthesis, function, and taxonomic significance. Microbiology and Molecular Biology Reviews 55, 288-302.

Karl, D., Knauer, G., Martin, J., Ward, B., 1984. Bacterial chemolithotrophy in the ocean is associated with sinking particles. Nature 309, 54.

Karner, M.B., DeLong, E.F., Karl, D.M., 2001. Archaeal dominance in the mesopelagic zone of the Pacific Ocean. Nature 409, 507.

Kate, M., 1993. Membrane Lipids of archaea, in``The Biochemistry of Archaea (Archaebacteria),"ed by M. Kates, DJ Kushner, and AT Matheson. Elsevier, Amsterdam.

Keeling, R.F., Körtzinger, A., Gruber, N., 2010. Ocean deoxygenation in a warming world. Annual Review of Marine Science 2, 199-229.

Kellermann, M., 2012. Lipid biomolecules reveal patterns of microbial metabolism in extreme environments. Ph. D. thesis, Universität Bremen (Germany). Available online at http://elib. suub. uni-bremen. de/edocs/00102577-1. pdf.

Kellermann, M.Y., Wegener, G., Elvert, M., Yoshinaga, M.Y., Lin, Y.S., Holler, T., Mollar, X.P., Knittel, K., Hinrichs, K.U., 2012. Autotrophy as a predominant mode of carbon fixation in anaerobic methane-oxidizing microbial communities. Proceedings of the National Academy of Sciences of the United States of America 109, 19321-19326.

Kirchman, D., K'nees, E., Hodson, R., 1985. Leucine incorporation and its potential as a measure of protein synthesis by bacteria in natural aquatic systems. Applied and Environmental Microbiology 49, 599-607.

Knappy, C.S., Barilla, D., de Blaquiere, J.P., Morgan, H.W., Nunn, C.E., Suleman, M., Tan, C.H., Keely, B.J., 2012. Structural complexity in isoprenoid glycerol dialkyl glycerol tetraether lipid cores of Sulfolobus and other archaea revealed by liquid chromatography-tandem mass spectrometry. Chemistry and Physics of Lipids 165, 648-655.

Knittel, K., Wegener, G., Boetius, A., 2018. Anaerobic Methane Oxidizers, in: McGenity, T.J. (Ed.), Microbial Communities Utilizing Hydrocarbons and Lipids: Members, Metagenomics and Ecophysiology. Springer International Publishing, Cham, pp. 1-21.

Koga, Y., Akagawa-Matsushita, M., Ohga, M., Nishihara, M., 1993. Taxonomic significance of the distribution of component parts of polar ether lipids in methanogens. Systematic and Applied Microbiology 16, 342-351.

Koga, Y., Morii, H., 2005. Recent advances in structural research on ether lipids from archaea including comparative and physiological aspects. Bioscience, Biotechnology, and Biochemistry 69, 2019-2034.

Koga, Y., Morii, H., 2007. Biosynthesis of ether-type polar lipids in archaea and evolutionary considerations. Microbiology and Molecular Biology Reviews 71, 97-120.

Koga, Y., Nakano, M., 2008. A dendrogram of archaea based on lipid component parts composition and its relationship to rRNA phylogeny. Systematic and Applied Microbiology 31, 169-182.

Kohn, M.J., 1999. You are what you eat. Science 283, 335-336.

Kolber, Z.S., Van Dover, C., Niederman, R., Falkowski, P., 2000. Bacterial photosynthesis in surface waters of the open ocean. Nature 407, 177.

Könneke, M., Lipp, J.S., Hinrichs, K.U., 2012. Carbon isotope fractionation by the marine ammonia-oxidizing archaeon Nitrosopumilus maritimus. Organic Geochemistry 48, 21-24.

Könneke, M., Schubert, D.M., Brown, P.C., Hugler, M., Standfest, S., Schwander, T., Schada von Borzyskowski, L., Erb, T.J., Stahl, D.A., Berg, I.A., 2014. Ammonia-oxidizing archaea use the most energy-efficient aerobic pathway for CO_2 fixation. Proceedings of the National Academy of Sciences of the United States of America 111, 8239-8244.

Kopf, S.H., Sessions, A.L., Cowley, E.S., Reyes, C., Van Sambeek, L., Hu, Y., Orphan, V.J., Kato, R., Newman, D.K., 2016. Trace incorporation of heavy water reveals slow and heterogeneous pathogen growth rates in cystic fibrosis sputum. Proceedings of the National Academy of Sciences of the United States of America 113, E110-116.

Krukenberg, V., Harding, K., Richter, M., Glockner, F.O., Gruber-Vodicka, H.R., Adam, B., Berg, J.S., Knittel, K., Tegetmeyer, H.E., Boetius, A., Wegener, G., 2016. Candidatus Desulfofervidus auxilii, a hydrogenotrophic sulfate-reducing bacterium involved in the thermophilic anaerobic oxidation of methane. Environmental Microbiology 18, 3073-3091.

Kümmel, S., Herbst, F.-A., Bahr, A., Duarte, M., Pieper, D.H., Jehmlich, N., Seifert, J., von Bergen, M., Bombach, P., Richnow, H.H., 2015. Anaerobic naphthalene degradation by sulfate-reducing Desulfobacteraceae from various anoxic aquifers. FEMS Microbiology Ecology 91.

Kuypers, M.M., Blokker, P., Erbacher, J., Kinkel, H., Pancost, R.D., Schouten, S., Sinninghe Damsté, J.S., 2001. Massive expansion of marine archaea during a mid-Cretaceous oceanic anoxic event. Science 293, 92-95.

Kuypers, M.M., Sliekers, A.O., Lavik, G., Schmid, M., Jorgensen, B.B., Kuenen, J.G., Sinninghe Damsté, J.S., Strous, M., Jetten, M.S., 2003. Anaerobic ammonium oxidation by anammox bacteria in the Black Sea. Nature 422, 608-611.

Lam, P., Kuypers, M.M., 2011. Microbial nitrogen cycling processes in oxygen minimum zones. Annual Review of Marine Science 3, 317-345.

Langworthy, T.A., 1977. Long-chain diglycerol tetraethers from Thermoplasma acidophilum. Biochimica et Biophysica Acta (BBA)-Lipids and Lipid Metabolism 487, 37-50.

Laso-Perez, R., Krukenberg, V., Musat, F., Wegener, G., 2018. Establishing anaerobic hydrocarbon-degrading enrichment cultures of microorganisms under strictly anoxic conditions. Nature Protocols 13, 1310-1330.

Lengger, S.K., Hopmans, E.C., Sinninghe Damsté, J.S., Schouten, S., 2014. Fossilization and degradation of archaeal intact polar tetraether lipids in deeply buried marine sediments (Peru Margin). Geobiology 12, 212-220.

Lengger, S.K., Kraaij, M., Tjallingii, R., Baas, M., Stuut, J.-B., Hopmans, E.C., Sinninghe Damsté, J.S., Schouten, S., 2013. Differential degradation of intact polar and core glycerol dialkyl glycerol tetraether lipids upon post-depositional oxidation. Organic Geochemistry 65, 83-93.

Lengger, S.K., Sutton, P.A., Rowland, S.J., Hurley, S.J., Pearson, A., Naafs, B.D.A., Dang, X.Y., Inglis, G.N., Pancost, R.D., 2018. Archaeal and bacterial glycerol dialkyl glycerol tetraether (GDGT) lipids in environmental samples by high temperature-gas chromatography with flame ionisation and time-of-flight mass spectrometry detection. Organic Geochemistry 121, 10-21.

Liang, B., Wang, L.-Y., Zhou, Z., Mbadinga, S.M., Zhou, L., Liu, J.-F., Yang, S.-Z., Gu, J.-D., Mu, B.-Z., 2016. High frequency of Thermodesulfovibrio spp. and Anaerolineaceae in association with Methanoculleus spp. in a long-term incubation of n-alkanes-degrading methanogenic enrichment culture. Frontiers in Microbiology 7, 1431.

Lin, Y.S., Lipp, J.S., Elvert, M., Holler, T., Hinrichs, K.U., 2013. Assessing production of the ubiquitous archaeal diglycosyl tetraether lipids in marine subsurface sediment using intramolecular stable isotope probing. Environmental Microbiology 15, 1634-1646.

Lincoln, S.A., Wai, B., Eppley, J.M., Church, M.J., Summons, R.E., DeLong, E.F., 2014. Planktonic Euryarchaeota are a significant source of archaeal tetraether lipids in the ocean. Proceedings of the National Academy of Sciences of the United States of America 111, 9858-9863.

Lipp, J.S., Hinrichs, K.-U., 2009. Structural diversity and fate of intact polar lipids in marine sediments. Geochimica et Cosmochimica Acta 73, 6816-6833.

Lipp, J.S., Morono, Y., Inagaki, F., Hinrichs, K.U., 2008. Significant contribution of Archaea to extant biomass in marine subsurface sediments. Nature 454, 991-994.

Lipsewers, Y.A., Hopmans, E.C., Sinninghe Damsté, J.S., Villanueva, L., 2018. Potential recycling of thaumarchaeotal lipids by DPANN Archaea in seasonally hypoxic surface marine sediments. Organic Geochemistry 119, 101-109.

Liu, X.L., Lipp, J.S., Hinrichs, K.U., 2011. Distribution of intact and core GDGTs in marine sediments. Organic Geochemistry 42, 368-375.

Liu, X.L., Summons, R.E., Hinrichs, K.U., 2012. Extending the known range of glycerol ether lipids in the environment: structural assignments based on tandem mass spectral fragmentation patterns. Rapid Communications in Mass Spectrometry 26, 2295-2302.

Lloyd, K.G., Alperin, M.J., Teske, A., 2011. Environmental evidence for net methane production and oxidation in putative ANaerobic MEthanotrophic (ANME) archaea. Environmental Microbiology 13, 2548-2564.

Lloyd, K.G., Schreiber, L., Petersen, D.G., Kjeldsen, K.U., Lever, M.A., Steen, A.D., Stepanauskas, R., Richter, M., Kleindienst, S., Lenk, S., Schramm, A., Jorgensen, B.B., 2013. Predominant archaea in marine sediments degrade detrital proteins. Nature 496, 215-218.

Logemann, J., Graue, J., Koster, J., Engelen, B., Rullkotter, J., Cypionka, H., 2011. A laboratory experiment of intact polar lipid degradation in sandy sediments. Biogeosciences (Online) 8, 2547-2560.

Londry, K.L., Dawson, K.G., Grover, H.D., Summons, R.E., Bradley, A.S., 2008. Stable carbon isotope fractionation between substrates and products of Methanosarcina barkeri. Organic Geochemistry 39, 608-621.

Lu, H., Liu, W., Wang, H., Zhang, C.L., 2013. Carbon isotopic composition of isoprenoid tetraether in surface sediments of Lake Qinghai and surrounding soils. Organic Geochemistry 60, 54-61.

Macalady, J.L., Vestling, M.M., Baumler, D., Boekelheide, N., Kaspar, C.W., Banfield, J.F., 2004. Tetraether-linked membrane monolayers in Ferroplasma spp: a key to survival in acid. Extremophiles 8, 411-419.

Madigan, M.T., Martinko, J.M., Parker, J., 1997. Brock biology of microorganisms. Prentice hall Upper Saddle River, NJ.

Manefield, M., Whiteley, A.S., Griffiths, R.I., Bailey, M.J., 2002. RNA stable isotope probing, a novel means of linking microbial community function to phylogeny. Applied and Environmental Microbiology 68, 5367-5373.

Mårdén, P., Nyström, T., Kjelleberg, S., 1987. Uptake of leucine by a marine Gram-negative heterotrophic bacterium during exposure to starvation conditions. FEMS Microbiology Ecology 3, 233-241.

Marion, C., Dufois, F., Arnaud, M., Vella, C., 2010. In situ record of sedimentary processes near the Rhône River mouth during winter events (Gulf of Lions, Mediterranean Sea). Continental Shelf Research 30, 1095-1107.

Meador, T.B., Bowles, M., Lazar, C.S., Zhu, C., Teske, A., Hinrichs, K.U., 2015. The archaeal lipidome in estuarine sediment dominated by members of the Miscellaneous Crenarchaeotal Group. Environmental Microbiology 17, 2441-2458.

Meador, T.B., Zhu, C., Elling, F.J., Konneke, M., Hinrichs, K.U., 2014. Identification of isoprenoid glycosidic glycerol dibiphytanol diethers and indications for their biosynthetic origin. Organic Geochemistry 69, 70-75.

Michaelis, W., Seifert, R., Nauhaus, K., Treude, T., Thiel, V., Blumenberg, M., Knittel, K., Gieseke, A., Peterknecht, K., Pape, T., Boetius, A., Amann, R., Jorgensen, B.B., Widdel, F., Peckmann, J., Pimenov, N.V., Gulin, M.B., 2002. Microbial reefs in the Black Sea fueled by anaerobic oxidation of methane. Science 297, 1013-1015.

Middelburg, J.J., 2019. Marine Carbon Biogeochemistry: A Primer for Earth System Scientists. Springer.

Middelburg, J.J., Barranguet, C., Boschker, H.T., Herman, P.M., Moens, T., Heip, C.H., 2000. The fate of intertidal microphytobenthos carbon: An in situ ^{13}C-labeling study. Limnology and Oceanography 45, 1224-1234.

Miralles, J., Radakovitch, O., Aloisi, J.-C., 2005. ^{210}Pb sedimentation rates from the Northwestern Mediterranean margin. Marine Geology 216, 155-167.

Mitterer, R.M., 2010. Methanogenesis and sulfate reduction in marine sediments: a new model. Earth and Planetary Science Letters 295, 358-366.

Nguyen, T.B., Topçuoğlu, B.D., Holden, J.F., LaRowe, D.E., Lang, S.Q., 2019. Low fuel leads to large carbon isotopic fractionation of methane and biomarkers during hydrogenotrophic methanogenesis. Geochimica et Cosmochimica Acta.

Nichols, P.D., Shaw, P.M., Mancuso, C.A., Franzmann, P.D., 1993. Analysis of archaeal phospholipid-derived di-and tetraether lipids by high temperature capillary gas chromatography. Journal of Microbiological Methods 18, 1-9.

Nicolson, G.L., 2014. The Fluid-Mosaic Model of Membrane Structure: still relevant to understanding the structure, function and dynamics of biological membranes after more than 40 years. Biochimica et Biophysica Acta 1838, 1451-1466.

Niemann, H., Elvert, M., 2008. Diagnostic lipid biomarker and stable carbon isotope signatures of microbial communities mediating the anaerobic oxidation of methane with sulphate. Organic Geochemistry 39, 1668-1677.

Niemann, H., Lösekann, T., De Beer, D., Elvert, M., Nadalig, T., Knittel, K., Amann, R., Sauter, E.J., Schlüter, M., Klages, M., 2006. Novel microbial communities of the Haakon Mosby mud volcano and their role as a methane sink. Nature 443, 854.

Nunoura, T., Hirai, M., Miyazaki, M., Kazama, H., Makita, H., Hirayama, H., Furushima, Y., Yamamoto, H., Imachi, H., Takai, K., 2013. Isolation and characterization of a thermophilic, obligately anaerobic and heterotrophic marine Chloroflexi bacterium from a Chloroflexi-dominated microbial community associated with a Japanese shallow hydrothermal system, and proposal for Thermomarinilinea lacunofontalis gen. nov., sp. nov. Microbes and Environments 28, 228-235.

Offre, P., Spang, A., Schleper, C., 2013. Archaea in biogeochemical cycles. Annual Review of Microbiology 67, 437-457.

Oremland, R.S., Taylor, B.F., 1978. Sulfate reduction and methanogenesis in marine sediments. Geochimica et Cosmochimica Acta 42, 209-214.

Orphan, V.J., House, C.H., Hinrichs, K.U., McKeegan, K.D., DeLong, E.F., 2002. Multiple archaeal groups mediate methane oxidation in anoxic cold seep sediments. Proceedings of the National Academy of Sciences of the United States of America 99, 7663-7668.

Orsi, W.D., Smith, J.M., Liu, S., Liu, Z., Sakamoto, C.M., Wilken, S., Poirier, C., Richards, T.A., Keeling, P.J., Worden, A.Z., Santoro, A.E., 2016. Diverse, uncultivated bacteria and archaea underlying the cycling of dissolved protein in the ocean. The ISME Journal 10, 2158-2173.

Pachiadaki, M.G., Sintes, E., Bergauer, K., Brown, J.M., Record, N.R., Swan, B.K., Mathyer, M.E., Hallam, S.J., Lopez-Garcia, P., Takaki, Y., 2017. Major role of nitrite-oxidizing bacteria in dark ocean carbon fixation. Science 358, 1046-1051.

Palanques, A., Durrieu de Madron, X., Puig, P., Fabres, J., Guillén, J., Calafat, A., Canals, M., Heussner, S., Bonnin, J., 2006. Suspended sediment fluxes and transport processes in the Gulf of Lions submarine canyons. The role of storms and dense water cascading. Marine Geology 234, 43-61.

Pancost, R.D., Coleman, J.M., Love, G.D., Chatzi, A., Bouloubassi, I., Snape, C.E., 2008. Kerogen-bound glycerol dialkyl tetraether lipids released by hydropyrolysis of marine sediments: A bias against incorporation of sedimentary organisms? Organic Geochemistry 39, 1359-1371.

Parkes, R.J., Cragg, B., Roussel, E., Webster, G., Weightman, A., Sass, H., 2014. A review of prokaryotic populations and processes in sub-seafloor sediments, including biosphere:geosphere interactions. Marine Geology 352, 409-425.

Paster, B.J., 2010. Phylum XV. Spirochaetes Garrity and Holt 2001, Bergey's Manual® of Systematic Bacteriology. Springer, pp. 471-566.

Pearson, A., Hurley, S.J., Elling, F.J., Wilkes, E.B., 2019. CO_2-dependent carbon isotope fractionation in Archaea, Part I: Modeling the 3HP/4HB pathway. Geochimica et Cosmochimica Acta 261, 368-382.

Pearson, A., Hurley, S.J., Walter, S.R.S., Kusch, S., Lichtin, S., Zhang, Y.G., 2016. Stable carbon isotope ratios of intact GDGTs indicate heterogeneous sources to marine sediments. Geochimica et Cosmochimica Acta 181, 18-35.

Pearson, A., Ingalls, A.E., 2013. Assessing the Use of Archaeal Lipids as Marine Environmental Proxies. Annual Review of Earth and Planetary Sciences 41, 359-384.

Penger, J., Conrad, R., Blaser, M., 2012. Stable carbon isotope fractionation by methylotrophic methanogenic archaea. Applied and Environmental Microbiology 78, 7596-7602.

Pitcher, A., Hopmans, E.C., Mosier, A.C., Park, S.J., Rhee, S.K., Francis, C.A., Schouten, S., Sinninghe Damsté, J.S., 2011. Core and intact polar glycerol dibiphytanyl glycerol tetraether lipids of ammonia-oxidizing archaea enriched from marine and estuarine sediments. Applied and Environmental Microbiology 77, 3468-3477.

Platt, T., Rao, D.S., Irwin, B., 1983. Photosynthesis of picoplankton in the oligotrophic ocean. Nature 301, 702.

Polik, C.A., Elling, F.J., Pearson, A., 2018. Impacts of Paleoecology on the TEX_{86} Sea Surface Temperature Proxy in the Pliocene-Pleistocene Mediterranean Sea. Paleoceanography and Paleoclimatology 33, 1472-1489.

Ragsdale, S.W., Pierce, E., 2008. Acetogenesis and the Wood–Ljungdahl pathway of CO_2 fixation. Biochimica et Biophysica Acta (BBA)-Proteins and Proteomics 1784, 1873-1898.

Raven, J.A., 2009. Contributions of anoxygenic and oxygenic phototrophy and chemolithotrophy to carbon and oxygen fluxes in aquatic environments. Aquatic Microbial Ecology 56, 177-192.

Reeburgh, W.S., 2007. Oceanic methane biogeochemistry. Chemical Reviews 107, 486-513.

Ren, M., Feng, X., Huang, Y., Wang, H., Hu, Z., Clingenpeel, S., Swan, B.K., Fonseca, M.M., Posada, D., Stepanauskas, R., 2019. Phylogenomics suggests oxygen availability as a driving force in Thaumarchaeota evolution. The ISME Journal 13, 1.

Rinke, C., Rubino, F., Messer, L.F., Youssef, N., Parks, D.H., Chuvochina, M., Brown, M., Jeffries, T., Tyson, G.W., Seymour, J.R., Hugenholtz, P., 2019. A phylogenomic and ecological analysis of the globally abundant Marine Group II archaea (Ca. Poseidoniales ord. nov.). The ISME Journal 13, 663-675.

Rosenkranz, F., Cabrol, L., Carballa, M., Donoso-Bravo, A., Cruz, L., Ruiz-Filippi, G., Chamy, R., Lema, J., 2013. Relationship between phenol degradation efficiency and microbial community structure in an anaerobic SBR. Water Research 47, 6739-6749.

Rossel, P.E., Elvert, M., Ramette, A., Boetius, A., Hinrichs, K.U., 2011. Factors controlling the distribution of anaerobic methanotrophic communities in marine environments: Evidence from intact polar membrane lipids. Geochimica et Cosmochimica Acta 75, 164-184.

Rossel, P.E., Lipp, J.S., Fredricks, H.F., Arnds, J., Boetius, A., Elvert, M., Hinrichs, K.U., 2008. Intact polar lipids of anaerobic methanotrophic archaea and associated bacteria. Organic Geochemistry 39, 992-999.

Rütters, H., Sass, H., Cypionka, H., Rullkötter, J., 2002. Phospholipid analysis as a tool to study complex microbial communities in marine sediments. Journal of Microbiological Methods 48, 149-160.

Scandellari, F., Hobbie, E.A., Ouimette, A.P., Stucker, V.K., 2009. Tracing metabolic pathways of lipid biosynthesis in ectomycorrhizal fungi from position-specific ^{13}C-labelling in glucose. Environmental Microbiology 11, 3087-3095.

Schattenhofer, M., Fuchs, B.M., Amann, R., Zubkov, M.V., Tarran, G.A., Pernthaler, J., 2009. Latitudinal distribution of prokaryotic picoplankton populations in the Atlantic Ocean. Environmental Microbiology 11, 2078-2093.

Schmid, M.C., Risgaard-Petersen, N., Van De Vossenberg, J., Kuypers, M.M., Lavik, G., Petersen, J., Hulth, S., Thamdrup, B., Canfield, D., Dalsgaard, T., 2007. Anaerobic ammonium-oxidizing bacteria in marine environments: widespread occurrence but low diversity. Environmental Microbiology 9, 1476-1484.

Schmidt, F., Koch, B.P., Goldhammer, T., Elvert, M., Witt, M., Lin, Y.S., Wendt, J., Zabel, M., Heuer, V.B., Hinrichs, K.U., 2017. Unraveling signatures of biogeochemical processes and the depositional setting in the molecular composition of pore water DOM across different marine environments. Geochimica et Cosmochimica Acta 207, 57-80.

Schoon, P.L., Heilmann-Clausen, C., Schultz, B.P., Sluijs, A., Sinninghe Damsté, J.S., Schouten, S., 2013. Recognition of Early Eocene global carbon isotope excursions using lipids of marine Thaumarchaeota. Earth and Planetary Science Letters 373, 160-168.

Schouten, S., Hopmans, E.C., Baas, M., Boumann, H., Standfest, S., Könneke, M., Stahl, D.A., Sinninghe Damsté, J.S., 2008. Intact membrane lipids of "Candidatus Nitrosopumilus maritimus," a cultivated representative of the cosmopolitan mesophilic group I crenarchaeota. Applied and Environmental Microbiology 74, 2433-2440.

Schouten, S., Hopmans, E.C., Schefuß, E., Sinninghe Damsté, J.S., 2002. Distributional variations in marine crenarchaeotal membrane lipids: a new tool for reconstructing ancient sea water temperatures? Earth and Planetary Science Letters 204, 265-274.

Schouten, S., Hopmans, E.C., Sinninghe Damsté, J.S., 2013. The organic geochemistry of glycerol dialkyl glycerol tetraether lipids: A review. Organic Geochemistry 54, 19-61.

Schouten, S., Middelburg, J.J., Hopmans, E.C., Sinninghe Damsté, J.S., 2010. Fossilization and degradation of intact polar lipids in deep subsurface sediments: A theoretical approach. Geochimica et Cosmochimica Acta 74, 3806-3814.

Schouten, S., Strous, M., Kuypers, M.M., Rijpstra, W.I.C., Baas, M., Schubert, C.J., Jetten, M.S., Sinninghe Damsté, J.S., 2004. Stable carbon isotopic fractionations associated with inorganic carbon fixation by anaerobic ammonium-oxidizing bacteria. Applied and Environmental Microbiology 70, 3785-3788.

Schouten, S., Wakeham, S.G., Sinninghe Damsté, J.S., 2001. Evidence for anaerobic methane oxidation by archaea in euxinic waters of the Black Sea. Organic Geochemistry 32, 1277-1281.

Schröder, J.M., 2015. Intact polar lipids in marine sediments: improving analytical protocols and assessing planktonic and benthic sources. Bremen, Universität Bremen, Diss., 2015.

Schubert, C.J., Coolen, M.J., Neretin, L.N., Schippers, A., Abbas, B., Durisch-Kaiser, E., Wehrli, B., Hopmans, E.C., Sinninghe Damsté, J.S., Wakeham, S., Kuypers, M.M., 2006. Aerobic and anaerobic methanotrophs in the Black Sea water column. Environmental Microbiology 8, 1844-1856.

Schubotz, F., Lipp, J.S., Elvert, M., Hinrichs, K.U., 2011. Stable carbon isotopic compositions of intact polar lipids reveal complex carbon flow patterns among hydrocarbon degrading microbial communities at the Chapopote asphalt volcano. Geochimica et Cosmochimica Acta 75, 4399-4415.

Segarra, K.E., Schubotz, F., Samarkin, V., Yoshinaga, M.Y., Hinrichs, K.U., Joye, S.B., 2015. High rates of anaerobic methane oxidation in freshwater wetlands reduce potential atmospheric methane emissions. Nature Communications 6, 7477.

Sinninghe Damsté, J.S., Rijpstra, W.I., Hopmans, E.C., Jung, M.Y., Kim, J.G., Rhee, S.K., Stieglmeier, M., Schleper, C., 2012. Intact polar and core glycerol dibiphytanyl glycerol tetraether lipids of group I.1a and I.1b thaumarchaeota in soil. Applied and Environmental Microbiology 78, 6866-6874.

Sinninghe Damsté, J.S., Schouten, S., Hopmans, E.C., van Duin, A.C., Geenevasen, J.A., 2002. Crenarchaeol: the characteristic core glycerol dibiphytanyl glycerol tetraether membrane lipid of cosmopolitan pelagic crenarchaeota. Journal of Lipid Research 43, 1641-1651.

Sollai, M., Villanueva, L., Hopmans, E.C., Reichart, G.J., Sinninghe Damsté, J.S., 2019. A combined lipidomic and 16S rRNA gene amplicon sequencing approach reveals archaeal sources of intact polar lipids in the stratified Black Sea water column. Geobiology 17, 91-109.

Sørensen, J., Christensen, D., Jørgensen, B.B., 1981. Volatile Fatty Acids and Hydrogen as Substrates for Sulfate-Reducing Bacteria in Anaerobic Marine Sediment. Applied and Environmental Microbiology 42, 5-11.

Sorensen, K.B., Teske, A., 2006. Stratified communities of active Archaea in deep marine subsurface sediments. Applied and Environmental Microbiology 72, 4596-4603.

Spang, A., Caceres, E.F., Ettema, T.J.G., 2017. Genomic exploration of the diversity, ecology, and evolution of the archaeal domain of life. Science 357, 3883.

Spang, A., Saw, J.H., Jorgensen, S.L., Zaremba-Niedzwiedzka, K., Martijn, J., Lind, A.E., van Eijk, R., Schleper, C., Guy, L., Ettema, T.J.G., 2015. Complex archaea that bridge the gap between prokaryotes and eukaryotes. Nature 521, 173-179.

Sprott, G.D., Dicaire, C.J., Choquet, C.G., Patel, G.B., Ekiel, I., 1993. Hydroxydiether Lipid Structures in Methanosarcina spp. and Methanococcus voltae. Applied and Environmental Microbiology 59, 912-914.

Stadnitskaia, A., Ivanov, M., Sinninghe Damsté, J.S., 2008. Application of lipid biomarkers to detect sources of organic matter in mud volcano deposits and post-eruptional methanotrophic processes in the Gulf of Cadiz, NE Atlantic. Marine Geology 255, 1-14.

Stahl, D.A., de la Torre, J.R., 2012. Physiology and diversity of ammonia-oxidizing archaea. Annual Review of Microbiology 66, 83-101.

Steen, A.D., Crits-Christoph, A., Carini, P., DeAngelis, K.M., Fierer, N., Lloyd, K.G., Thrash, J.C., 2019. High proportions of bacteria and archaea across most biomes remain uncultured. The ISME Journal, 1-5.

Stieglmeier, M., Klingl, A., Alves, R.J., Rittmann, S.K., Melcher, M., Leisch, N., Schleper, C., 2014. Nitrososphaera viennensis gen. nov., sp. nov., an aerobic and mesophilic, ammonia-oxidizing archaeon from soil and a member of the archaeal phylum Thaumarchaeota. International Journal of Systematic and Evolutionary Microbiology 64, 2738-2752.

Stookey, L.L., 1970. Ferrozine - a new spectrophotometric reagent for iron. Analytical Chemistry 42, 779.

Sturt, H.F., Summons, R.E., Smith, K., Elvert, M., Hinrichs, K.U., 2004. Intact polar membrane lipids in prokaryotes and sediments deciphered by high-performance liquid chromatography/electrospray ionization multistage mass spectrometry--new biomarkers for biogeochemistry and microbial ecology. Rapid Communications in Mass Spectrometry 18, 617-628.

Summons, R.E., Franzmann, P.D., Nichols, P.D., 1998. Carbon isotopic fractionation associated with methylotrophic methanogenesis. Organic Geochemistry 28, 465-475.

Swan, B.K., Martinez-Garcia, M., Preston, C.M., Sczyrba, A., Woyke, T., Lamy, D., Reinthaler, T., Poulton, N.J., Masland, E.D.P., Gomez, M.L., 2011. Potential for chemolithoautotrophy among ubiquitous bacteria lineages in the dark ocean. Science 333, 1296-1300.

Swiatczak, P., Cydzik-Kwiatkowska, A., Rusanowska, P., 2017. Microbiota of anaerobic digesters in a full-scale wastewater treatment plant. Archives of Environmental Protection 43, 53-60.

Takai, K., Nakamura, K., Toki, T., Tsunogai, U., Miyazaki, M., Miyazaki, J., Hirayama, H., Nakagawa, S., Nunoura, T., Horikoshi, K., 2008. Cell proliferation at 122℃ and isotopically heavy CH_4 production by a hyperthermophilic methanogen under high-pressure cultivation. Proceedings of the National Academy of Sciences of the United States of America 105, 10949-10954.

Takano, Y., Chikaraishi, Y., Ogawa, N.O., Nomaki, H., Morono, Y., Inagaki, F., Kitazato, H., Hinrichs, K.-U., Ohkouchi, N., 2010. Sedimentary membrane lipids recycled by deep-sea benthic archaea. Nature Geoscience 3, 858-861.

Thomas, C., Grossi, V., Antheaume, I., Ariztegui, D., 2019. Recycling of archaeal biomass as a new strategy for extreme life in Dead Sea deep sediments. Geology 47 479-482.

Trembath-Reichert, E., Morono, Y., Ijiri, A., Hoshino, T., Dawson, K.S., Inagaki, F., Orphan, V.J., 2017. Methyl-compound use and slow growth characterize microbial life in 2-km-deep subseafloor coal and shale beds. Proceedings of the National Academy of Sciences of the United States of America 114, E9206-E9215.

Tully, B.J., 2019. Metabolic diversity within the globally abundant Marine Group II Euryarchaea offers insight into ecological patterns. Nature Communications 10, 271.

Uda, I., Sugai, A., Itoh, Y.H., Itoh, T., 2001. Variation in molecular species of polar lipids from Thermoplasma acidophilum depends on growth temperature. Lipids 36, 103-105.

van der Meer, M.T., Schouten, S., Rijpstra, W.I.C., Fuchs, G., Sinninghe Damsté, J.S., 2001. Stable carbon isotope fractionations of the hyperthermophilic crenarchaeon Metallosphaera sedula. FEMS Microbiology Letters 196, 67-70.

Varela, M.M., van Aken, H.M., Sintes, E., Reinthaler, T., Herndl, G.J., 2011. Contribution of Crenarchaeota and Bacteria to autotrophy in the North Atlantic interior. Environmental Microbiology 13, 1524-1533.

Veuger, B., van Oevelen, D., Middelburg, J.J., 2012. Fate of microbial nitrogen, carbon, hydrolysable amino acids, monosaccharides, and fatty acids in sediment. Geochimica et Cosmochimica Acta 83, 217-233.

Villanueva, L., Sinninghe Damsté, J.S., Schouten, S., 2014. A re-evaluation of the archaeal membrane lipid biosynthetic pathway. Nature Reviews Microbiology 12, 438-448.

Volkman, J.K., Barrett, S.M., Blackburn, S.I., Mansour, M.P., Sikes, E.L., Gelin, F., 1998. Microalgal biomarkers: a review of recent research developments. Organic Geochemistry 29, 1163-1179.

Vuillemin, A., Wankel, S.D., Coskun, Ö.K., Magritsch, T., Vargas, S., Estes, E.R., Spivack, A.J., Smith, D.C., Pockalny, R., Murray, R.W., D'Hondt, S., Orsi, W.D., 2019. Archaea dominate oxic subseafloor communities over multimillion-year time scales. Science Advances 5, eaaw4108.

Wakeham, S.G., Lewis, C.M., Hopmans, E.C., Schouten, S., Sinninghe Damsté, J.S., 2003. Archaea mediate anaerobic oxidation of methane in deep euxinic waters of the Black Sea. Geochimica et Cosmochimica Acta 67, 1359-1374.

Wegener, G., Kellermann, M.Y., Elvert, M., 2016a. Tracking activity and function of microorganisms by stable isotope probing of membrane lipids. Current Opinion in Biotechnology 41, 43-52.

Wegener, G., Krukenberg, V., Riedel, D., Tegetmeyer, H.E., Boetius, A., 2015. Intercellular wiring enables electron transfer between methanotrophic archaea and bacteria. Nature 526, 587-590.

Wegener, G., Krukenberg, V., Ruff, S.E., Kellermann, M.Y., Knittel, K., 2016b. Metabolic Capabilities of Microorganisms Involved in and Associated with the Anaerobic Oxidation of Methane. Frontiers in Microbiology 7, 46.

Wegener, G., Niemann, H., Elvert, M., Hinrichs, K.U., Boetius, A., 2008. Assimilation of methane and inorganic carbon by microbial communities mediating the anaerobic oxidation of methane. Environmental Microbiology 10, 2287-2298.

Weijers, J.W., Lim, K.L., Aquilina, A., Sinninghe Damsté, J.S., Pancost, R.D., 2011. Biogeochemical controls on glycerol dialkyl glycerol tetraether lipid distributions in sediments characterized by diffusive methane flux. Geochemistry, Geophysics, Geosystems 12.

Weijers, J.W., Schouten, S., Hopmans, E.C., Geenevasen, J.A., David, O.R., Coleman, J.M., Pancost, R.D., Sinninghe Damsté, J.S., 2006. Membrane lipids of mesophilic anaerobic bacteria thriving in peats have typical archaeal traits. Environmental Microbiology 8, 648-657.

Weijers, J.W.H., Wiesenberg, G.L.B., Bol, R., Hopmans, E.C., Pancost, R.D., 2010. Carbon isotopic composition of branched tetraether membrane lipids in soils suggest a rapid turnover and a heterotrophic life style of their source organism(s). Biogeosciences (Online) 7, 2959-2973.

Whitman, W.B., Coleman, D.C., Wiebe, W.J., 1998. Prokaryotes: the unseen majority. Proceedings of the National Academy of Sciences of the United States of America 95, 6578-6583.

Widdel, F., Bak, F., 1992. Gram-negative mesophilic sulfate-reducing bacteria, The prokaryotes. Springer, pp. 3352-3378.

Woese, C.R., Fox, G.E., 1977. Phylogenetic structure of the prokaryotic domain: the primary kingdoms. Proceedings of the National Academy of Sciences of the United States of America 74, 5088-5090.

Woese, C.R., Kandler, O., Wheelis, M.L., 1990. Towards a natural system of organisms: proposal for the domains Archaea, Bacteria, and Eucarya. Proceedings of the National Academy of Sciences of the United States of America 87, 4576-4579.

Wörmer, L., Elvert, M., Fuchser, J., Lipp, J.S., Buttigieg, P.L., Zabel, M., Hinrichs, K.U., 2014. Ultra-high-resolution paleoenvironmental records via direct laser-based analysis of lipid biomarkers in sediment core samples. Proceedings of the National Academy of Sciences of the United States of America 111, 15669-15674.

Wörmer, L., Lipp, J.S., Schröder, J.M., Hinrichs, K.-U., 2013. Application of two new LC–ESI–MS methods for improved detection of intact polar lipids (IPLs) in environmental samples. Organic Geochemistry 59, 10-21.

Xie, S., Lipp, J.S., Wegener, G., Ferdelman, T.G., Hinrichs, K.U., 2013. Turnover of microbial lipids in the deep biosphere and growth of benthic archaeal populations. Proceedings of the National Academy of Sciences of the United States of America 110, 6010-6014.

Yamada, T., Sekiguchi, Y., Hanada, S., Imachi, H., Ohashi, A., Harada, H., Kamagata, Y., 2006. Anaerolinea thermolimosa sp. nov., Levilinea saccharolytica gen. nov., sp. nov. and Leptolinea tardivitalis gen. nov., sp. nov., novel filamentous anaerobes, and description of the new classes Anaerolineae classis nov. and Caldilineae classis nov. in the bacterial phylum Chloroflexi. International Journal of Systematic and Evolutionary Microbiology 56, 1331-1340.

Yamauchi, N., 2010. The pathway of leucine to mevalonate in halophilic archaea: efficient incorporation of leucine into isoprenoidal lipid with the involvement of isovaleryl-CoA dehydrogenase in Halobacterium salinarum. Biosci Biotechnol Biochem 74, 443-446.

Yoshinaga, M.Y., Holler, T., Goldhammer, T., Wegener, G., Pohlman, J.W., Brunner, B., Kuypers, M.M., Hinrichs, K.-U., Elvert, M., 2014. Carbon isotope equilibration during sulphate-limited anaerobic oxidation of methane. Nature Geoscience 7, 190-194.

Yoshinaga, M.Y., Lazar, C.S., Elvert, M., Lin, Y.S., Zhu, C., Heuer, V.B., Teske, A., Hinrichs, K.U., 2015. Possible roles of uncultured archaea in carbon cycling in methane-seep sediments. Geochimica et Cosmochimica Acta 164, 35-52.

Yu, T., Liang, Q., Niu, M., Wang, F., 2017. High occurrence of Bathyarchaeota (MCG) in the deep-sea sediments of South China Sea quantified using newly designed PCR primers. Environmental Microbiology Reports 9, 374-382.

Yu, T., Wu, W., Liang, W., Lever, M.A., Hinrichs, K.U., Wang, F., 2018. Growth of sedimentary Bathyarchaeota on lignin as an energy source. Proceedings of the National Academy of Sciences of the United States of America 115, 6022-6027.

Zabel, M., Aiello, I., Becker, K., Braum, S., Broda, N., Dibke, C., Elvert, M., Gagen, E., Goldhammer, T., Heuer, V., 2011. Biogeochemistry and methane hydrates of the Black Sea; Oceanography of the Mediterranean; Shelf sedimentation and cold water carbonates.

Zarzycki, J., Brecht, V., Müller, M., Fuchs, G., 2009. Identifying the missing steps of the autotrophic 3-hydroxypropionate CO_2 fixation cycle in Chloroflexus aurantiacus. Proceedings of the National Academy of Sciences of the United States of America 106, 21317-21322.

Zhou, Z., Pan, J., Wang, F., Gu, J.D., Li, M., 2018. Bathyarchaeota: globally distributed metabolic generalists in anoxic environments. FEMS Microbiology Reviews 42, 639-655.

Zhu, C., Lipp, J.S., Wörmer, L., Becker, K.W., Schröder, J., Hinrichs, K.-U., 2013. Comprehensive glycerol ether lipid fingerprints through a novel reversed phase liquid chromatography–mass spectrometry protocol. Organic Geochemistry 65, 53-62.

Zhuang, G.C., Elling, F.J., Nigro, L.M., Samarkin, V., Joye, S.B., Teske, A., Hinrichs, K.U., 2016. Multiple evidence for methylotrophic methanogenesis as the dominant methanogenic pathway in hypersaline sediments from the Orca Basin, Gulf of Mexico. Geochimica et Cosmochimica Acta 187, 1-20.

Zhuang, G.C., Heuer, V.B., Lazar, C.S., Goldhammer, T., Wendt, J., Samarkin, V.A., Elvert, M., Teske, A.P., Joye, S.B., Hinrichs, K.U., 2018. Relative importance of methylotrophic methanogenesis in sediments of the Western Mediterranean Sea. Geochimica et Cosmochimica Acta 224, 171-186.